The Nelson Mandela AFrican Institution of Science and Technology

NM-AIST Repository **https://dspace.mm-aist.ac.tz**

Computational and Communication Science Engineering PhD Theses and Dissertations [CoCSE]

2016

Analysis and Simulations of Nanofluid Flow and Heat Transfer in a Porous Pipe

Khamis, Sara

The Nelson Mandela African Institution of Science and Technology

http://dspace.nm-aist.ac.tz/handle/123456789/59

Provided with love from The Nelson Mandela African Institution of Science and Technology

ANALYSIS AND SIMULATION OF NANOFLUID FLOW AND HEAT TRANSFER IN A POROUS PIPE

Sara Abdalla Khamis

A Dissertation Submitted in Partial Fulfillment of the Requirements for the Degree of Doctor of Philosophy in Mathematical and Computer Sciences and Engineering of the Nelson Mandela African Institution of Science and Technology

Arusha, Tanzania

April, 2016

ABSTRACT

The study of fluid flow and heat transfer through a cylindrical pipe and channel with porous boundaries are important research area due to its wide range of applications in engineering and industrial processes. Some practical applications include problems dealing with transpiration cooling, gaseous diffusion in order to produce fuel for nuclear reactors, controlling boundary layer flow over aircraft wings by injection or suction of fluid out of or into the wing, lubrication of porous bearings, petroleum technology, ground water hydrology, seepage of water in river beds, purification and filtration processes. A nanofluid is the suspension of nanoparticles in a base fluid. Nanofluids are promising for heat transfer enhancement due to their high thermal conductivity. For practical applications of nanofluids research in nanofluids convection are important. Owing to their enhanced properties, nanofluids can be used in a plethora of technical and biomedical applications such as nanofluid coolant which include electronics cooling, vehicle cooling, transformer cooling, computers cooling and other electronic devices cooling. Other applications are medical applications which include magnetic drug targeting, cancer therapy and safer surgery by cooling.

This study considered the detailed analysis of laminar flow behavior and heat transfer using this innovative fluid as working fluid through a pipe and channel with porous boundaries for both steady and unsteady scenarios. We considered water-based nanofluids where copper and alumina were used as nanoparticles. The appropriate mathematical models for the problems were derived from the laws of conservation of mass, momentum and energy balance. The governing nonlinear Partial Differential Equations (PDE) and boundary conditions were converted into nonlinear Ordinary Differential Equations (ODE) using appropriate similarity transformations for the case of steady state formulated model and method of lines when unsteady situation was considered. These equations were solved analytically by regular perturbation methods with series improvement technique and numerically using an efficient Runge-Kutta-Fehlberg integration technique coupled with shooting scheme and multidimensional Newton-Raphson root finding technique.

In chapter 1, the key concepts and derivations related to fluid flow, the statement of the problem, the objectives of the study, Significance of the study and the methodology are given. In chapter 2, the heat transfer characteristics of Berman flow of water-based nanofluids in a porous channel with Navier slip, viscous dissipation and convective cooling is investigated. Chapter 3 the combined effect of variable viscosity, Brownian motion, thermophoresis and convective cooling

on unsteady flow of nanofluid in a cylindrical pipe with permeable wall are analysed. In chapter 4 we investigates the effects of buoyancy force and variable viscosity on unsteady flow and heat transfer of water-based nanofluid containing Copper and Alumina as nanoparticles. Analysis of unsteady water-based nanofluid flow in a permeable cylindrical pipe through saturated porous medium with the effect of buoyancy-driven force, variable viscosity and Navier slip are examined. The useful results for the velocity, temperature, nanoparticles concentration profiles, pressure gradient, skin friction and Nusselt number were obtained and discussed quantitatively. The effects of important governing flow parameters on the entire flow structure were examined. The conclusion remarks are carried out in chapter 6.

DECLARATION

I, **SARA ABDALLA KHAMIS** do hereby declare to the Senate of Nelson Mandela African Institution of Science and Technology that this dissertation is my own original work and that it has neither been submitted nor being concurrently submitted for degree award in any other institution.

Sara Abdalla Khamis — 13th April,2016

Name and signature of candidate — **Date**

The above declaration is confirmed

Prof. Oluwole Daniel Makinde — 15th April, 2015

Name and signature of supervisor 1 — **Date**

Dr. Yaw Nkansah-Gyekye — 15th April, 2016

Name and signature of supervisor 2 — **Date**

COPYRIGHT

This dissertation is copyright material protected under the Berne Convention, the Copyright Act of 1999 and other international and national enactments, in that behalf, on intellectual property. It must not be reproduced by any means, in full or in part, except for short extracts in fair dealing; for researcher private study, critical scholarly review or discourse with an acknowledgement, without the written permission of the office of Deputy Vice Chancellor for Academics, Research and Innovations, on behalf of both the author and the Nelson Mandela African Institution of Science and Technology.

CERTIFICATION

The undersigned certify that have read and found the dissertation acceptable by the Nelson Mandela African Institution of Science and Technology.

Prof. Oluwole Daniel Makinde  15th April, 2016

Name and signature of supervisor 1 **Date**

Dr. Yaw Nkansah-Gyekye  15th April, 2016

Name and signature of supervisor 2 **Date**

ACKNOWLEDGEMENT

I would like to express my sincere gratitude to my principal supervisor Prof. Oluwole Daniel Makinde for his patient, intellectual guidance and encouragement throughout my research work. I have experienced an excellent level of supervision, invaluable recommendations, support and opportunity to gain from his wealth of knowledge. His supervision has enhanced my knowledge in the field of computational fluid dynamics.

I would like to give my special thanks to my internal supervisor Dr. Yaw Nkansah-Gyekye for his helpful comments, invaluable support and encouragement. His inspiration kept me motivated during the completion of this work.

I highly appreciate the financial support from the Nelson Mandela African Institution of Science and Technology. I am also highly indebted to the State University of Zanzibar for offering me a three years study leave.

My special thank to the School of Computational and Communication Science and Engineering, Head of Department of Applied Mathematics and Computational Science, Prof. Dmitry Kuznetov and all other members of staff for their great support in one way or another.

I express my deep sense of indebtedness to my parents for their unconditional love, continuous patience and blessings at every stage throughout my life.

I would especially like to thank my lovely husband, my daughter and my sons for their love, continuous support and most of all their patience during my absence.

My sincere thanks also to my classmates for their encouragement and support throughout our studies.

Despite all the support, I remain solely responsible for all deficiencies in this work.

DEDICATION

I dedicate this work to my parents and all my family members.

TABLE OF CONTENTS

ABSTRACT i

DECLARATION iii

COPYRIGHT iv

CERTIFICATION v

ACKNOWLEDGEMENT vi

DEDICATION vii

LIST OF TABLES xii

LIST OF FIGURES xvi

CHAPTER ONE: Introduction 1

1.1 Background Information 1

1.1.1 Heat transfer 3

1.1.2 Flow in pipes 6

1.1.3 Laminar and turbulent flows 7

1.1.4 Porous pipe/channel 8

1.1.5 Porous media 8

1.1.6 Nanofluids 8

1.1.7 Materials for nanoparticles and base fluids 9

1.1.8 Nanofluids synthesis 10

1.1.9 Characteristic features of nanofluids 11

1.1.10 Thermophysical characteristics of nanofluids 11

1.1.11 Finite control volume 14

1.1.12 Gauss divergence theorem 15

1.1.13 Streamline 15

1.1.14 Material derivative 15

1.1.15 Reynold's transport theorem 15

1.1.16 Basic Governing equations for the problem 16

1.1.17 Continuity equation 16

1.1.18 Momentum Equation (Navier-Stokes equation) 19
1.1.19 Energy equation 23
1.1.20 Well-posedness 24
1.2 Statement of the Problem 25
1.3 Research Objectives 25
1.3.1 General objective 25
1.3.2 The specific objectives 25
1.4 Significance of the Research 26
1.5 Research Methodology 26
1.5.1 Numerical approach 27
1.5.2 Analytical approach 30
1.6 Dissertation Outline 30

CHAPTER TWO: Analysis of Heat Transfer in Berman Flow of Nanofluids with Navier Slip, Viscous Dissipation and Convective Cooling[1] **32**
2.1 Introduction 32
2.2 Problem Formulation 34
2.3 Perturbation Method 37
2.4 Numerical Procedure 39
2.5 Results and Discussion 40
2.5.1 Velocity profiles with parameter variation 42
2.5.2 Temperature profiles with parameter variation 46
2.5.3 Skin Friction, Pressure Gradient and Nusselt Number 50
2.6 Conclusion 54

CHAPTER THREE: Modelling the Effects of Variable Viscosity in Unsteady Flow of Nanofluids in a Pipe with Permeable Wall and Convective cooling [2] **56**
3.1 Introduction 56
3.2 Mathematical Model 58
3.3 Numerical Procedure 61
3.4 Results and Discussion 62
3.4.1 Non-Dimensional Velocity Profiles with Parameter Variation 62
3.4.2 Non- Dimensional Temperature Profiles with Parameter Variations . . . 66

3.4.3 Non-Dimensional Nanoparticles Volume Concentration Profiles with Parameter Variations . . . 71
3.4.4 Skin Friction and Local Nusselt Number with Parameters Variation . . 75
3.5 Conclusion . . . 78

CHAPTER FOUR: Unsteady flow of variable viscosity Cu-water and Al_2O_3-water nanofluids in a porous pipe with buoyancy force[3] 80
4.1 Introduction . . . 80
4.2 Mathematical Model . . . 82
4.3 Numerical Procedure . . . 85
4.4 Results and Discussion . . . 86
4.4.1 Transient and steady flow analysis . . . 86
4.4.2 Dimensionless velocity profile with parameters variations . . . 90
4.4.3 Dimensionless temperature profile with parameters variations . . . 93
4.4.4 Wall shear stress and heat transfer rate . . . 96
4.5 Conclusion . . . 99

CHAPTER FIVE: Buoyancy-Driven Heat Transfer of Water-Based Nanofluid in a Permeable Cylindrical Pipe with Navier Slip Through Saturated Porous Medium[4] 100
5.1 Introduction . . . 100
5.2 Problem Formulation . . . 102
5.3 Numerical Procedure . . . 105
5.4 Results and Discussion . . . 106
5.4.1 Velocity Profile with Parameters Variation . . . 107
5.4.2 Temperature Profiles with Parameters Variation . . . 111
5.4.3 Skin Friction and Nusselt Number with Parameters variation . . . 115
5.5 Conclusion . . . 119

CHAPTER SIX: General Discussion, Conclusion and Recommendation 121
6.1 General Discussion . . . 121
6.2 Conclusion . . . 122
6.3 Recommendations . . . 124

REFERENCES **125**

LIST OF TABLES

1.1 Typical values of heat transfer coefficients (W/m^2K) (John, 2008) 6

1.2 Thermal conductivity of selected typical materials (Choi, 1995; Eastman *et al.*, 2004) 9

2.1 Thermophysical properties of the water and nanoparticles (Kakac and Pramuanjaroenkij, 2009; Xuan and Li, 2003; Wen and Ding, 2005; Wang et al., 2013; Oztop and Abu-Nada, 2008) 41

2.2 Computation showing the normal velocity profiles for $Re = 1$ 41

2.3 Computation showing the axial velocity profiles for $Re = 1,\ \lambda = 0.05,\ X = 1,\ \eta = 0$ 42

3.1 computation showing the skin friction and Nusselt number $Pr = 6.2$, $Sc = 1$. . 76

4.1 Thermophysical properties of the fluid phase (water) and nanoparticles (Kuznetsov and Nield, 2010) 86

5.1 Thermophysical properties of the water and nanoparticles (Oztop and Abu-Nada, 2008) 106

5.2 Computation showing the C_f and Nu for various values of embedded parameters for $t = 2,\ \varphi = 0.3$ 116

LIST OF FIGURES

1.1 Heat transfer modes 4
1.2 Convection heat transfer process (a) Forced convection (b) Natural convection . 5
1.3 Laminar and Turbulent flows 8
1.4 Nanoparticles and base fluid illustration 10
1.5 Nanoparticles produced by single step and two step methods 11
1.6 Finite control volume 14
1.7 An arbitrary differential volume element 17
1.8 An arbitrary macroscopic control volume 18
1.9 Cylindrical Coordinate system 18
1.10 Stresses acting on a fluid element 19
2.1 Schematic diagram of the physical system 34
2.2 Nanofluids axial velocity profiles 43
2.3 Axial velocity profiles with increasing φ 43
2.4 Axial velocity profiles with increasing Re 44
2.5 Axial velocity profiles with increasing λ 44
2.6 Nanofluids normal velocity profiles 45
2.7 Normal velocity profiles with increasing φ 45
2.8 Normal velocity profiles with increasing Re 46
2.9 Normal velocity profiles with increasing λ 46
2.10 Nanofluids temperature profiles 47
2.11 Temperature profiles with increasing φ 48
2.12 Temperature profiles with increasing Bi 48
2.13 Temperature profiles with increasing Re 49
2.14 Temperature profiles with increasing λ 49
2.15 Temperature profiles with increasing Ec 50
2.16 Temperature profiles with increasing X 50
2.17 Skin friction with increasing φ 51
2.18 Skin friction with increasing Re and λ 52
2.19 Axial pressure gradient with increasing φ 52
2.20 Axial pressure gradient with increasing Re and λ. 53
2.21 Nusselt number with increasing φ 53
2.22 Nusselt number with increasing Re and λ. 54

2.23 Nusselt number with increasing X, Bi and Ec. 54
3.1 Schematic diagram of the problem 58
3.2 Velocity profiles with increasing distance 63
3.3 Velocity profiles with increasing distance 63
3.4 Velocity profiles with increasing time 64
3.5 Velocity profiles with increasing β 64
3.6 Velocity profiles with increasing Ec 65
3.7 Velocity profiles with increasing G 65
3.8 Velocity profiles with increasing Bi 66
3.9 Velocity profiles with increasing distance suction and injection Re 66
3.10 Temperature profiles with increasing distance 67
3.11 Temperature profiles with increasing distance 68
3.12 Temperature profiles with increasing Time 68
3.13 Temperature profiles with increasing Ec 69
3.14 Temperature profiles with increasing β 69
3.15 Temperature profiles with increasing Bi 70
3.16 Temperature profiles with increasing suction and injection Reynolds number . . 70
3.17 Nanoparticles distribution profiles with increasing distance 71
3.18 Nanoparticles distribution profiles with increasing time 72
3.19 Nanoparticles distribution profiles with increasing β 72
3.20 Nanoparticles distribution profiles with increasing Ec 73
3.21 Nanoparticles distribution profiles with increasing Nt 73
3.22 Nanoparticles distribution profiles with increasing Nb 74
3.23 Nanoparticles distribution profiles with increasing Bi 74
3.24 Nanoparticles distribution profiles with increasing Re 75
3.25 Nanoparticles distribution profiles with increasing Re 77
3.26 Nanoparticles distribution profiles with increasing Re 77
3.27 Nanoparticles distribution profiles with increasing Re 78
3.28 Nanoparticles distribution profiles with increasing Re 78
4.1 Physical geometry and coordinate system 82
4.2 Transient and steady state velocity profiles 87
4.3 Transient and steady state temperature profiles 88

4.4 Nanofluids velocity profiles with increasing distance 88
4.5 Nanofluids temperature profiles with increasing distance 89
4.6 Nanofluid velocity solution from shooting method and method of lines 89
4.7 Nanofluid Temperature solution from shooting method and method of lines . . 90
4.8 Nanofluids velocity profiles with increasing φ 91
4.9 Nanofluids velocity profiles with increasing β 91
4.10 Nanofluids velocity profiles with increasing A 92
4.11 Nanofluids velocity profiles with increasing Gr 92
4.12 Nanofluids velocity profiles with increasing Re 93
4.13 Nanofluid temperature profiles with increasing φ 94
4.14 Nanofluid temperature profiles with increasing Ec 94
4.15 Nanofluid temperature profiles with increasing Gr 95
4.16 Nanofluid temperature profiles with increasing β 95
4.17 Nanofluid temperature profiles with increasing suction Re 96
4.18 Skin friction profiles for both nanofluids 97
4.19 Skin friction profiles with increasing φ and Re 97
4.20 Skin friction profiles with increasing φ, Gr and β 98
4.21 Nusselt number profiles with increasing φ for both nanofluids 98
4.22 Nusselt number profiles with increasing φ, β. Ec and Gr 99
5.1 Schematic diagram of the physical system 102
5.2 Transient and steady state non-dimensional velocity evolutions for Cu-water and Al_2O_3-water nanofluids 108
5.3 Non-dimensional velocity evolutions with increasing nanoparticles volume fraction φ 108
5.4 Non-dimensional velocity evolutions with increasing β 109
5.5 Non-dimensional velocity evolutions with increasing Gr 109
5.6 Non-dimensional velocity evolutions with increasing λ 110
5.7 Non-dimensional velocity evolutions with increasing M 110
5.8 Non-dimensional velocity evolutions with increasing S 111
5.9 Transient and steady state non-dimensional temperature evolutions for Cu-water and Al_2O_3-water nanofluids 112
5.10 Non-dimensional temperature evolutions with increasing φ 112

5.11 Non-dimensional temperature evolutions with increasing Gr 113
5.12 Non-dimensional temperature evolutions with increasing β 113
5.13 Non- dimensional temperature evolution with increasing λ 114
5.14 Non-dimensional velocity evolutions with increasing M 114
5.15 Non-dimensional temperature evolution with increasing S 115
5.16 Skin friction profiles for Cu-water and Al_2O_3-water nanofluids 117
5.17 Skin fiction profiles with increasing φ,β and λ 117
5.18 Skin fiction profiles with increasing M, S and λ 118
5.19 Nusselt number profiles for Cu-water and Al_2O_3-water nanofluids 118
5.20 Nusselt number profiles with increasing φ, β, and λ 119
5.21 Nusselt number profiles with increasing M, S and λ 119

LIST OF APPENDICES

Appendix A. 133
Appendix B. 133
Appendix C. 134
Appendix D. 139

LIST OF SYMBOLS

Symbols

a	Channel half width	t	Dimensionless time
A	Pressure gradient	Re	Reynolds number
m	variable viscosity parameter	q_w	heat flux
Bi	Local Biot number	V	Wall suction velocity
C_f	Skin friction	(u, v)	Velocity components
g	Acceleration due to gravity	F	Dimensionless stream function
Ec	Eckert number	$\bar{t}$	time
P	Dimensionless pressure	Pr	Prandtl number
Gr	Grashof number	Nu	Nusselt number
k	Thermal conductivity	ρc_p	heat capacitance
r	Dimensional normal coordinate	T	Temperature
X	Dimensionless axial coordinate	x	Dimensional axial coordinate
Z	Dimensionless axial coordinate	z	Dimensional axial coordinate
c_p	Specific heat at a constant pressure	h	Heat transfer coefficient
W	Dimensionless axial velocity	Da	Darcy number
M	Porous media resistance parameter	Sc	Schmidt number
H	Dimensionless temperature	$\bar{P}$	Pressure
(x, y)	Cartesian coordinates	(z, r)	Cylindrical coordinates

Greek Symbols

	Stream function
$\bar{\psi}$	Dimensionless stream function
θ	Dimensionless temperature
Ω	Vorticity
$\bar{\Omega}$	Dimensionless vorticity
Φ	Dimensionless temperature
μ	Dynamic viscosity
α	Thermal diffusivity
η	Dimensionless normal coordinate
ρ	Density
ν	Kinematic viscosity
φ	Solid volume fraction parameter
β	variable viscosity parameter
γ	volumetric expansion coefficient
λ	Navier slip parameter
τ_w	wall shear stress
τ	nanoparticles heat capacity ratio

Superscripts and subscripts

a	ambient
$_0$	Initial
w	Wall
nf	Nanofluid
f	Base fluid
s	Solid fraction

CHAPTER ONE

Introduction

This chapter describes the general introduction of the study. It mainly focuses on the background information of the study. The main terminologies and mathematical equations used in this dissertation are defined and derived. The statement of the problem and research justification, aims and objectives of the study, significance of the study and the research methodology are also explained.

1.1 Background Information

Fluid flow and heat transfer continues to be a field of major interest to engineering and scientific researchers, designers, developers as well as manufacturers. Considerable effort has been devoted to research in traditional applications such as chemical processing, general manufacturing, and energy devices, including general power systems, heat exchangers and high performance gas turbines. In addition, a significant number of papers, address topics that are at the frontiers of both fundamental research and important emerging applications, such as microchannel flows, bio-heat transfer, electronics cooling, semiconductors and a number of natural phenomena ranging from upwelling currents in the oceans to heat transport in stellar atmospheres (Senthilkumar *et al.,* 2012).

Heat transfer fluids such as water, mineral oil and ethylene glycol play a vital role in many industrial processes, but the heat transfer properties of these common fluids are low when compared to most of the solids and it becomes a primary obstacle to the high compactness and effectiveness of heat exchangers. The essential initiative is to seek the solid particles having thermal conductivities several hundred times higher than those of conventional fluids (Kumar *et al.*, 2013).

The conventional method for increasing heat dissipation is to increase the area available for exchanging heat with a heat transfer fluid but this approach requires an undesirable increase in the size of thermal management system. Therefore an urgent need for new and innovative coolants with improved performance (Pawel *et al.*, 2008). From the 1990s, researchers began to apply nanomaterial technology to heat transfer and have achieved many meaningful results on heat transfer enhancement. Choi (1995) firstly proposed the concept of nanofluid, which is a fluid with some kinds of nanometer-sized particles suspended into a base liquid.

Nanofluids can be considered to be the next generation heat transfer fluids because they offer exciting new possibilities to enhance heat transfer performance compared to pure liquids. The thermo-physical and transport properties of the conventional fluids are improved by adding the nanoparticles in base fluid. The effective thermal conductivity of nanofluids increases with increase in temperature. The heat transfer coefficient depends not only on the thermal conductivity but also on other properties, such as the specific heat capacity, density, and dynamic viscosity of a nanofluid. At low volume fractions, the density and specific heat of nanofluids looks to be very similar to those characterizing the base fluid (Senthilkumar *et al.*, 2012). The two most important features of nanofluids are Brownian motion and thermophoresis (Xuan and Li, 2003). Brownian motion describes the random movement of nanoparticles in the base fluid. This random movement is due to collision of particles into each other. The collision passes on the kinetic energy of the particles to the molecules. The impact of particles upon other particles is negligible because the concentration of particles in nanofluids is normally low, whereas thermophoresis describes the nanoparticle dispersion in the base fluid due to temperature gradient (Motsumi and Makinde, 2012). As a new kind of heat transfer fluid, the nanofluid is a new technology attempt to use the special properties of this functional fluid to enhance the heat transfer systems. It has wide application prospects such as combustion induced gas motion inside a solid rocket motor, flow filtration, isotope separation, surface ablation, pulmonary circulation etc. Moreover, the instance of laminar flow through a pipe or channel with porous walls is an idealisation of the flow behaviour that occurs in the real world in corresponding geometries. It can be used to model processes such as transpiration cooling, where the walls of a pipe or channel containing heated fluid are protected from overheating by passing cooler fluid over the exterior surface of the pipe or channel; another application is to model the fluid flow occurring during the separation of isotopes of Uranium-235 and Uranium-238 by gaseous diffusion in order to produce fuel for nuclear reactors; controlling boundary layer flow over aircraft wings by injection or suction of fluid out of or into the wing, or as part of a model for flow past a membrane or filter; lubrication of porous bearings; petroleum technology; ground water hydrology; seepage of water in river beds; purification and filtration processes etc. Furthermore, continuous and rapid nano-technological advances in industrial processing require design and operation problems to be resolved as quickly as possible in order to keep companies competitive, particularly in terms of energy efficiency and low costs. For many years, experiments and empirical analysis have been the preferred solution tools for industrial analysis. Despite the strongness and

reliable nature of experimental methodology, certain factors limit its applicability scope. Thus, mathematical modeling and analysis of fluid flow and heat transfer is quickly becoming a quick tool in solving many challenges problems in engineering and applied sciences. Normally, it is the fastest and least expensive way, given that it minimises the number of experiments that need to be conducted to determine the influence of several parameters on the performance and efficiency of the process related to cooling and heating phenomena.

In this study, we consider the analysis of rectilinear axisymmetric laminar incompressible nanofluid flow models of heat transfer with some variable parameters governing the flow. To describe the behavior of flow dynamics the equations governing flow are solved numerically. This is what is known as computational simulation. Results of this simulation include the velocity distribution, distribution of temperature and pressure in the entire flow domain, the heat transfer rate and skin friction in the walls are also presented.

1.1.1 Heat transfer

Heat transfer is defined as thermal energy-in-transit due to spatial temperature difference. Heat transfer takes place whenever there exist a temperature gradient within a system or whenever two systems at different temperatures are brought into thermal contact. Heat, which is energy-in-transit cannot be measured or observed directly, but the effects produced by it can be observed and measured (Paul and Gorazo, 2007). Since heat transfer involves transfer and/or conversion of energy, all heat transfer processes must obey the first and second laws of thermodynamics.

Modes of Heat Transfer:

The different types of heat transfer are usually referred as 'mode of heat transfer'. Generally heat transfer takes place in three modes: conduction, convection and radiation (Figure 1.1).

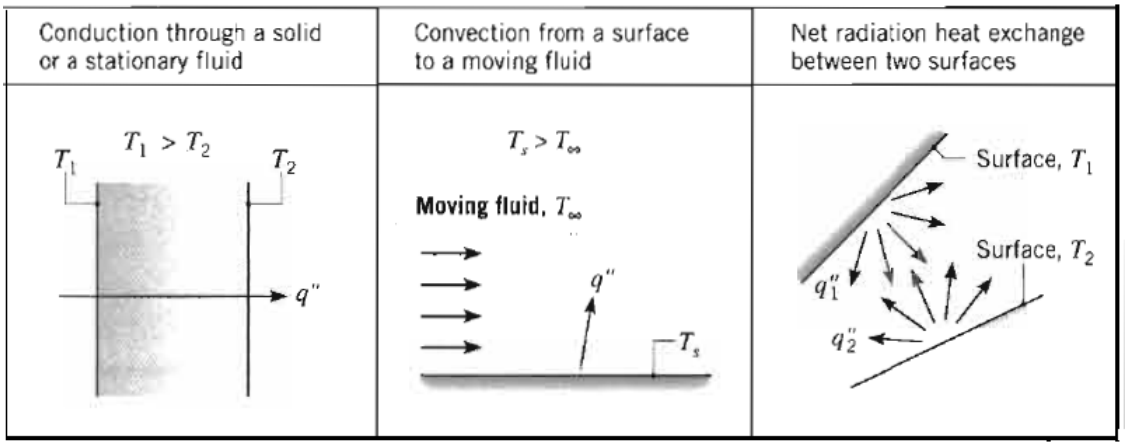

Figure 1.1: Heat transfer modes

Conduction

This is energy transfer across a system boundary due to a temperature difference by the mechanism of inter-molecular interactions. Conduction needs matter and does not require any bulk motion of matter (Raju, 2011). The conduction rate equation is described by the Fourier law:

$$Q = -kA\nabla T \quad \text{(Blazeki, 2005)} \tag{1.1}$$

where Q is the heat flow vector (W)

k is the thermal conductivity (Wm/K)

A is the cross-sectional area in direction of heat flow (m^2)

∇T is the gradient of the temperature (K/m).

Convection

This heat transfer mode is comprised of two mechanisms: random molecular motion which is termed diffusion and the bulk motion of the fluid. This fluid motion is associated with the fact, at any instant, large numbers of molecules are moving collectively or as aggregates. In the presence of a temperature gradient, such motion contributes to the heat transfer. Because the molecules in the aggregate retain their random motion, the total heat is then due to super-position of energy transport by the random motion of molecules and by the bulk motion of the fluid (Blazeki, 2005). We use the term convective when referring to cumulative transport and advection when referring to transport due to bulk fluid motion.

Convection heat transfer is classified according to the nature of the flow: Forced convection

when the flow is caused by external means, such as fan, pump, atmospheric winds. In contrast, free (natural) convection the flow is induced by buoyancy forces, which is due to the density differences caused by temperature variations in the fluid (refer to Figure 1.2). Regardless of

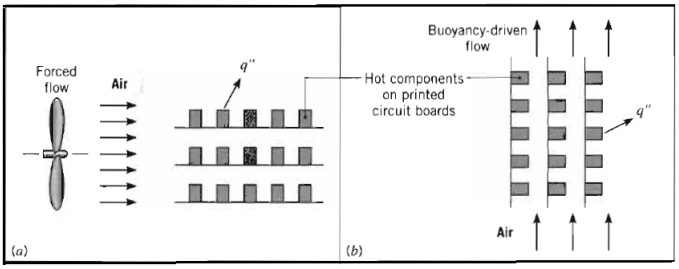

Figure 1.2: Convection heat transfer process (a) Forced convection (b) Natural convection

the particular nature of the convection heat transfer process. The rate of transfer is given by *Newton's Law of Cooling*.

$$q^{''} = h(T_W - T_\infty) \tag{1.2}$$

where

h is the convective heat transfer coefficient (M/m^2K)

T_w is the surface temperatures of the wall (^0C)

T_∞ is the bulk fluid temperature (^0C)

The temperature gradient near the wall depends on the rate at which the fluid near the wall can transport energy into the mainstream. The temperature gradient depends on the flow field, higher velocities leads to higher temperature gradients and hence higher heat transfer rates. Thus determination of convection heat transfer requires the application of laws of fluid mechanics in addition to the laws of heat transfer. The typical values of heat transfer coefficient are shown in Table 1.1.

Table 1.1: Typical values of heat transfer coefficients (W/m^2K) (John, 2008)

Free convection	air	$6 - 30$
	water	$20 - 100$
Forced convection	air	$30 - 300$
	water	$300 - 18,000$
	oil	$60 - 1,800$
Boiling	Synthetic refrigerant	$500 - 300$
	water	$3,000 - 60,000$
condensation	Synthetic refrigerant	$1,500 - 5,000$
	water	$6,000 - 120,000$

Radiation

This occurs where heat energy is transferred by electromagnetic radiation that arises due to temperature of the body. The intensity of such energy flux depends upon the temperature of the body and the nature of its surface (John, 2008). The rate of radiation heat exchange between a small surface and a large surrounding is given by the expression,

$$Q = \varepsilon\sigma A(T_s^4 - T_{sur}^4) \tag{1.3}$$

where

ε= surface emissivity

A= surface area

T_s = absolute temperature

T_{sur} =absolute temperature of the surroundings

σ = Stefan-Boltzmann constant

1.1.2 Flow in pipes

Pipe flow is a type of flow within a closed conduit. This is an internal flow where as fluid is completely confined by inner surfaces of the tubes and there is a limit on how much the boundary layer grows. Flow through pipes is commonly used in heating and cooling applications and

fluid distribution networks. The fluid velocity in a pipe changes from zero at the surface due to no-slip condition to a maximum velocity at the center of the pipe. A boundary layer developed at the entrance. Eventually the boundary layer fills the entire pipe, and the flow is said to be fully developed. If the flow is laminar a parabolic velocity profile is experienced.

1.1.3 Laminar and turbulent flows

Fluid flow can be grouped into two categories, laminar or turbulent flow. Laminar flow implies that the fluid moves in sheets that slip relative to each other and it occurs at very low velocities where there are only small disturbances and little or no local velocity variations. In laminar flow, the motion of the fluid particles is very orderly and can be characterized by high momentum diffusion and low momentum convection. The Reynolds number is used to characterize the flow regime.

The Reynolds number, Re, is a dimensionless number that represents the ratio of inertial forces to viscous forces; and is defined as:

$$Re = \frac{intertial\ forces}{viscous forces} = \frac{VL}{\nu}, \tag{1.4}$$

where,

V is a mean velocity (m/s),

L is a characteristic linear dimension(m),

$\nu = \frac{\mu}{\rho}$ is a kinematics viscosity (m^2/s).

The Reynolds number helps quantify the relative importance of inertial and viscous forces for given flow conditions. For internal flow, such as within a pipe, laminar flow occurs at a Reynolds number less than 2300.

Opposite of laminar, turbulence is a flow regime characterized by chaotic and stochastic changes. Turbulent flows involve large Reynolds numbers and contain three dimensional vorticity fluctuations. The flow is considered as laminar if ($Re < 2000$) and Turbulent if $Re > 4000$ (Blazeki, 2005). The laminar and turbulent flow in a fluid is illustrated in Figure 1.3.

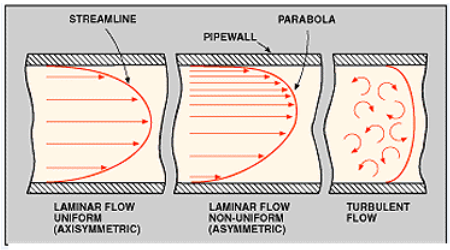

source: http://www.omega.com/techref/flowcontrol.html

Figure 1.3: Laminar and Turbulent flows

1.1.4 Porous pipe/channel

This consists of pipe/channel with permeable walls. The walls are made up of a solid matrix with void space filled with the fluids. The walls are interconnected in such a way that fluid can flow through medium.

1.1.5 Porous media

A porous medium can be defined as a solid body which contains void spaces or pores that are distributed randomly; without any conceivable pattern throughout the structure of the solid body. Extremely small voids are called molecular interstices and very large ones are called caverns. Pores are intermediate between caverns and molecular interstices. Fluid flow can only take place in the inter-connected pore space of the porous media this pore is called the effective pore space.

1.1.6 Nanofluids

The heat rejection requirements are continually increasing due to trends toward faster speeds and smaller features for microelectronic devices, more power output for engines, and brighter beams for optical devices. Cooling becomes one of the top technical challenges facing high-tech industries such as microelectronics, transportation, manufacturing, and metrology. The conventional methods for increase cooling rates are extended surfaces such as fins and increasing flow rates. However, current design solutions already push available technology to its limits (Eastman *et al.,* 2004).

New technologies and new advanced fluids with potential to improve flow and thermal characteristics are of critical importance. Nanofluids are a new class of advanced heat-transfer

fluids engineered by dispersing nanoparticles smaller than $100nm$ (nanometer) in diameter and fibres in conventional heat transfer fluids.

The key incentive to utilize this new type of fluid in engineering devices is its capability of enhancing heat transfer and having the same Newtonian behavior of other fluids in spite of containing solid particles. This is due to fact that solids materials have thermal conductivities several times larger than those of conventional heat transfer fluids (see Table1.2). Since the introduction of the term nanofluid, there have been remarkable experiments done to shed some light on the behavior of this novel fluid. (Kamyar *et al.*, 2012; Wen and Ding, 2005).

Table 1.2: Thermal conductivity of selected typical materials (Choi, 1995; Eastman *et al.*, 2004)

Materials		Thermal conductivity (W/mK)
Carbon	Diamond	2300
	Carbon nanotubes	~ 2000
	Graphite	110-190
Metallic materials	Silver	429
	copper	401
	Aluminum	237
Non-metallic materials	Silicon	148
	Silicon Carbide	120
	Alumina	40
Heat transfer fluid	Water	0.613
	Ethylene glycol	0.253
	Engine oil	0.145

1.1.7 Materials for nanoparticles and base fluids

The common materials used for nanoparticles and base fluids are:

1. Nanoparticle materials including:

   - Oxides (e.g. Al_2O_3, CuO, TiO_2, SiO_2).

- Metals (e.g. Al, Ag, Au, Cu, Fe).
- Nitrides (e.g. AlN, SiN).
- Nonmetals (e.g., graphite, carbon, nanotubes).
- Layered (e.g. $Al + Al_2O_3$, $Cu + C$).

2. The base fluid which is usually a conductive fluid includes: water; ethylene or tri-ethylene-glycols and other coolants; oil and other lubricants; bio-fluids; polymer solutions and other common fluids.

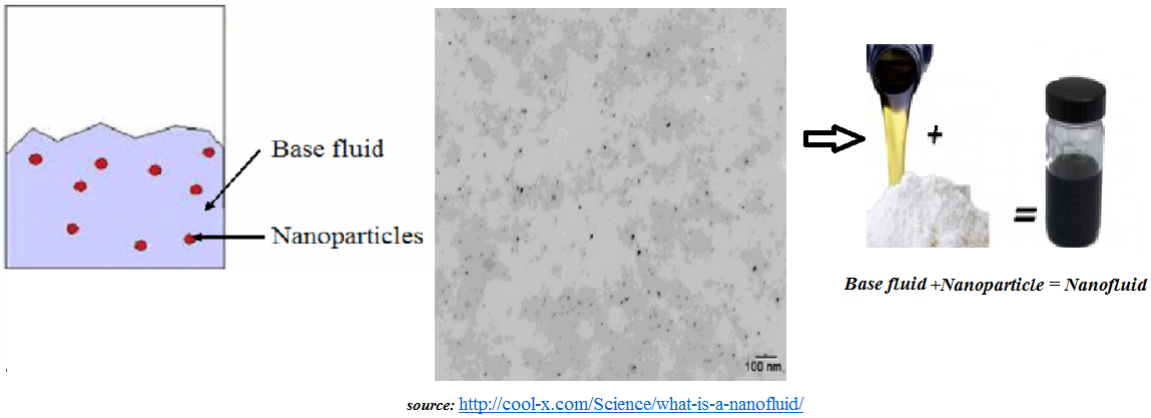

Figure 1.4: Nanoparticles and base fluid illustration

1.1.8 Nanofluids synthesis

In general, there are two methodologies used to produce nanofluids, namely:

Single-step method, where nanoparticles are produced and dispersed simultaneously into the base fluid. The single-step method is a process combining the preparation of nanoparticles with the synthesis of nanofluids, for which the nanoparticles are directly prepared by physical vapor deposition technique or a liquid chemical method. This process is best for metallic nanofluids (Wang and Mujumdar, 2007)

Two-step Process, nanoparticles are produced by evaporation and inert-gas condensation processing, and then dispersed (mixed, including mechanical agitation and sonification) in base fluid, this is method is best for oxide nanoparticles. Figure 1.5 illustrates the nanoparticles produced using single step and two step methods.

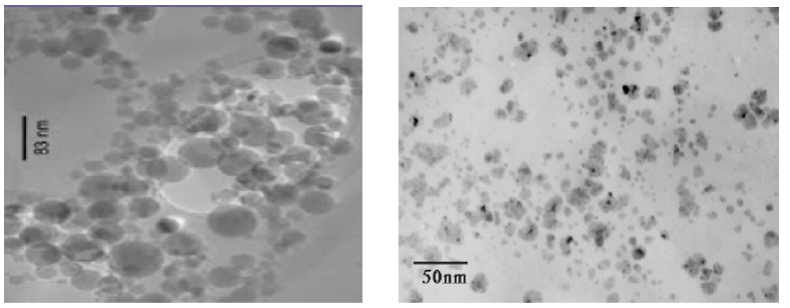

(a) ZrO_2 in water produced with two step method (b) Cu produced by direct evaporation in to ethylene glycol

source: http://www.slideshare.net/jalisantosh/nanofluids

Figure 1.5: Nanoparticles produced by single step and two step methods

1.1.9 Characteristic features of nanofluids

Nanofluids have an unprecedented combination of characteristic features desired in fluid and heat transfer systems which make them suitable for next generation flow and heat transfer fluids. These features are:

- Increased thermal conductivity at low nanoparticles concentrations.
- Strongly temperature-dependent and size dependent.
- Nonlinear increase in conductivity with nanoparticles concentrations.
- Increase in boiling critical heat flux.

Detailed explanation of these features can be seen from (Wen and Ding, 2005; Das *et al.*, 2003b,a; You *et al.*, 2003; Yang and Han, 2003)

1.1.10 Thermophysical characteristics of nanofluids

Density

The density of any fluid is defined as the mass per unit volume. The density of nanofluid is based on the physical principle of the mixture rule. As such it can be represented as (Khanafer and Vafai, 2011):

$$\rho_{eff} = \left(\frac{M}{V}\right)_{eff} = \frac{M_f + M_s}{V_f + V_s} = \frac{\rho_f V_f + \rho_s V_s}{V_f + V_s} = (1-\varphi)\rho_f + \varphi\rho_s. \tag{1.5}$$

To examine the validity of equation (1.5), a number of experiments have been done and excellent agreement results has been obtained (Pak and Cho, 1998; Ho *et al.*, 2010).

Heat capacity

We can determine the effective specific heat of nanofluid by assuming thermal equilibrium between the nanoparticles and the base fluid phase as follows:

$$\begin{aligned}(\rho c_p)_{eff} &= \rho_{eff}\left(\frac{Q}{M\Delta T}\right)_{eff} = \rho_{eff}\frac{Q_f + Q_s}{(M_f + M_s)\Delta T} \\ &= \rho_{eff}\frac{(Mc_p)_f\Delta T + (Mc_p)_s\Delta T}{(M_f + M_s)\Delta T} = \rho_{eff}\frac{(\rho c_p)_f V_f + (\rho c_p)_s V_s}{\rho_f V_f + \rho_s V_s} \\ &= (1-\varphi)(\rho c_p)_f + \varphi(\rho c_p)_s \Rightarrow (c_p)_{eff} = \frac{(1-\varphi)(\rho c_p)_f + \varphi(\rho c_p)_s}{(1-\varphi)\rho_f + \varphi\rho c_f},\end{aligned} \tag{1.6}$$

where, f and s refer to the base fluid and solid nanoparticle respectively and $\varphi = \frac{V_s}{V_f + V_s}$ is the volume fraction of the nanoparticles (Khanafer and Vafai, 2011).

Thermal expansion coefficient

The thermal expansion coefficient of nanofluids can be estimated utilizing the volume fraction of the nanoparticles on a weight basis as presented by (Khanafer *et al.*, 2003):

$$\gamma_{eff} = \frac{(1-\varphi)(\rho\gamma)_f + \varphi(\rho\gamma)_s}{\rho_{eff}} \tag{1.7}$$

However, Hwang *et al.* (2007) suggested a very simple model for the thermal expansion coefficient, the model equation is given by:

$$\gamma_{eff} = (1-\varphi)\gamma_f + \varphi\gamma_s, \tag{1.8}$$

where γ_f represents the thermal expansion coefficient of base fluid and γ_s represents the thermal expansion coefficient of nanoparticles.

Thermal conductivity

Several theoretical and experimental studies have been published in the literature to model thermal conductivity of nanofluids. However there are no existing theoretical studies that predicts accurately the thermal conductivity of the fluids. Maxwell's model (Maxwell, 1881) was one of the first models proposed for solid-liquid mixture. The model is based on the solution of heat conduction equation through a stationary random suspension of spheres. This model predicts thermal conductivity reasonably well for dilute mixtures of relatively large particles in fluids. The effective thermal conductivity is given by:

$$\begin{aligned}\frac{k_{eff}}{k_f} &= \frac{(k_s + 2k_f) + 2\varphi(k_s - k_f)}{(k_s + 2k_f) + 2\varphi(k_s - k_f)} \\ &= 1 + \frac{3\varphi(k_s - k_f)}{2k_f + k_s - \varphi(k_s - k_f)},\end{aligned} \tag{1.9}$$

where k_f and k_s represents the thermal conductivity of base fluid and nanoparticles respectively.

Viscosity

Generally, we can define viscosity as the ratio of shear stress to the velocity. It is regarded as the resistance that the fluid offer against deforming under influence of shear stress. viscosity transforms kinetic energy of (macroscopic) motion into heat energy. Regarding viscosity in nanofluid different analytical models have been presented by researcher to model the effective viscosity of nanofluid as a function of volume fraction. Einstein (1906) presented a simple model for fluids with a low concentration of spherical particles as follows:

$$\frac{\mu_{eff}}{\mu_f} = 1 + 2.5\varphi. \tag{1.10}$$

Brinkman (1952) generalized the Einstein correlation for higher concentrations:

$$\frac{\mu_{eff}}{\mu_f} = \frac{1}{(1-\varphi)^{2.5}} = 1 + 2.5\varphi + 4.375\varphi^2 + \ldots. \tag{1.11}$$

Batchelor (1977) studied the effect of the Brownian motion on the effective viscosity in a suspension of rigid and spherical particles and developed the following correlation:

$$\frac{\mu_{eff}}{\mu_f} = 1 + 2.5\varphi + 6.5\varphi^2. \tag{1.12}$$

Temperature dependent viscosity

When the viscosity of the fluid tends to decrease with the increase of temperature (and vice versa) then it is referred to as temperature dependence viscosity. When the temperature of the fluid increases, the the rate of molecular interchange moves faster and far away from other which causes the cohensive forces to decrease rapidly. As cohensive forces are decreasing, the shear stress will decrease as well. Similarly, as the rate of molecular interchange is increasing, there will be increase of shear stress. The temperature dependent viscosity considered in this study is an exponential function as presented by Klemp *et al.* (1990) as,

$$\mu_f(T) = \mu_0 exp\left(-m(T - T_a)\right). \tag{1.13}$$

1.1.11 Finite control volume

Consider a general flow field as represented by the streamlines in Figure 1.6. Let us imagine a closed volume drawn within a finite region of the flow. This volume defines a control volume, V, and a control surface, S, is defined as the closed surface which bounds the volume (Alexandre and Jerrold, 1992). The control volume may be fixed in space with the fluid moving through it, as shown on the left of Figure 1.6. Alternatively, the control volume may be moving with the fluid such that the same fluid particles are always inside it, as shown on the right of Figure 1.6. In either case, the control volume is a reasonably large, finite region of the flow. The fundamental physical principles are applied to the fluid inside the control volume, and to the fluid crossing the control surface (if the control volume is fixed in space). Therefore, instead of looking at the whole flow field at once, with the control volume model we use the fluid in the finite region of the volume itself.

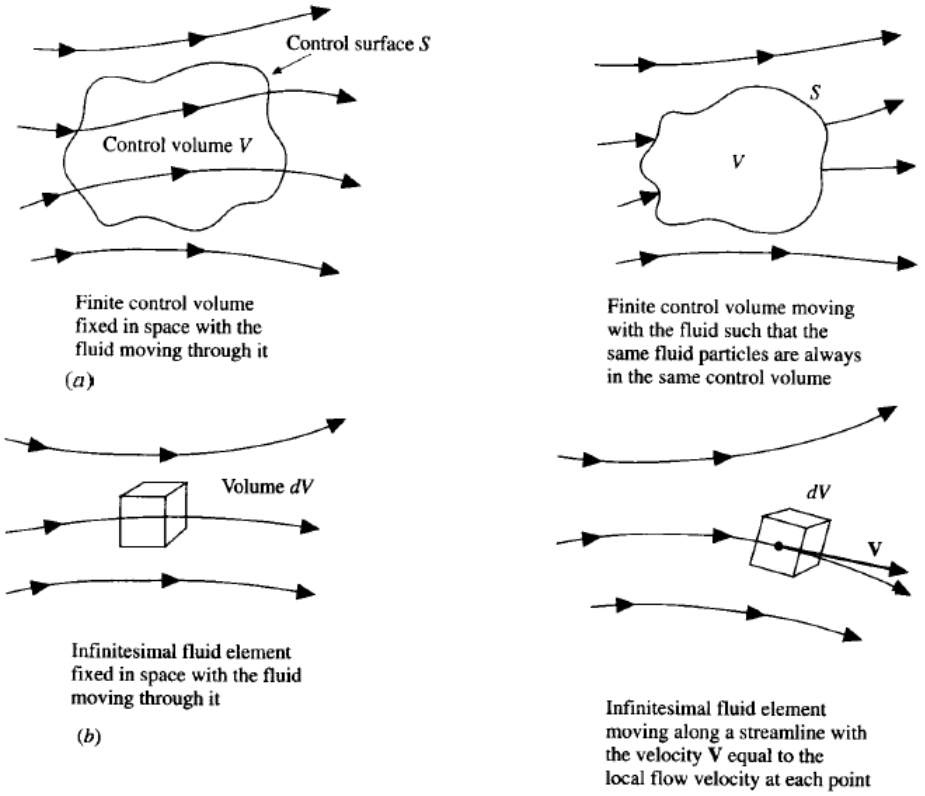

Figure 1.6: Finite control volume

1.1.12 Gauss divergence theorem

Let $\Omega \in \mathbb{R}^3$ and $\mathbf{n}$ be the outward unit normal to the boundary Γ. Then for any differentiable function $f(x)$

$$\int_{\Omega} \nabla \cdot \mathbf{f} dx = \int_{\Gamma} \mathbf{f} \cdot \mathbf{n} \qquad \text{(Alexandre and Jerrold, 1992)} \tag{1.14}$$

1.1.13 Streamline

A streamline is a curve which is tangent to the velocity vector $\mathbf{V} = (v_x, v_y, v_z)$ at every point. It is given by the relation

$$\frac{dx}{v_x} = \frac{dy}{v_y} = \frac{dz}{v_z} \qquad \text{(Alexandre and Jerrold, 1992)}$$

Streamlines can be visualized by injecting tracer particles into the flow field.

1.1.14 Material derivative

The continuity equation contains the time-derivative of the fluid density. For any physical quantity $f = f(x,t)$ (density, temperature, each velocity component, etc.), we must actually take care to distinguish two different time derivatives. $\frac{\partial f}{\partial t}$, we mean the rate of change of f at a particular point that is fixed in space. But the rate of change of f in a given element of fluid as it moves along its trajectory $x = x(t)$ in the flow defines the material (substantial) derivative

$$\begin{aligned} \frac{df}{dt} &= \frac{d}{dt} f(x(t), y(t), z(t), t) \\ &= \frac{\partial f}{\partial t} + \frac{dx}{dt}\frac{\partial f}{\partial x} + \frac{dy}{dt}\frac{\partial f}{\partial y} + \frac{dz}{dt}\frac{\partial f}{\partial z} \\ &= \frac{\partial f}{\partial x} + u\frac{\partial f}{\partial x} + v\frac{\partial f}{\partial y} + w\frac{\partial f}{\partial z} \\ \frac{df}{dt} &= \frac{\partial f}{\partial t} + \vec{q} \cdot \vec{\nabla} f \end{aligned} \tag{1.15}$$

$The\ substantial\ derivative\ =\ local\ derivative\ +\ convective\ derivative$

where, $\frac{\partial}{\partial t}$ is the local derivative, $\vec{q} \cdot \vec{\nabla}$ is the convective derivative and $\frac{d}{dt}$ is the material derivative.

1.1.15 Reynold's transport theorem

Let $u = u(x,t)$, where $x = x(x_0, t)$. The rate of change in a moving volume is equal to the rate of change in a fixed volume plus convective transfer through the surface. Mathematically this

can be written as (Alexandre and Jerrold, 1992):

$$\frac{d}{dt}\int_{V_t} u(x,t)dV = \int_{V\equiv V_t} \frac{\partial u(x,t)}{\partial t}dV + \int_{S\equiv S_t} u(x,t)\mathbf{q}\cdot\mathbf{n}dS$$

1.1.16 Basic Governing equations for the problem

The cornerstone of computational fluid dynamics is the fundamental governing equations of fluid dynamics viz; the continuity, momentum and energy equations. They are the mathematical statements of three fundamental physical principles upon which all of fluid dynamics is based:

(a) mass is conserved

(b) Newton's 2nd law ($\vec{F} = m\vec{a}$)

(c) energy is conserved

1.1.17 Continuity equation

The continuity equation represents the law of conservation of mass which states that mass cannot be created nor destroyed; that is

the total mass in the system = original mass + mass added - mass removed

or

the rate of increase of mass = net flux of mass.

We consider differential and integral approaches to derive the continuity equation.

Differential Approach

Consider a stationary differential volume element of length Δx, width Δy and height Δz in cartesian coordinates as shown in Figure 1.7. The conservation of mass for this control volume element $(\Delta x\Delta y\Delta z)$ can expressed as:

$$\left.\begin{array}{llll} Rate\ of\ change = Rate\ of\ mass & & & - Rate\ of\ mass \\ of\ mass\ in \Delta V & convected\ into\ \Delta V & & convected\ out\ of\ \Delta V \end{array}\right\}.$$

Mathematically this can be expressed as;

$$\Delta x\Delta y\Delta z\frac{\partial \rho}{\partial t} = \Delta y\Delta z\left[(\rho u)|_x - (\rho u)|_{x+\Delta x}\right] + \Delta x\Delta z\left[(\rho v)|_y - (\rho v)|_{y+\Delta y}\right] + \Delta x\Delta y\left[(\rho w)|_z - (\rho w)|_{z+\Delta z}\right] \quad (1.16)$$

where ρ is the fluid density in ΔV. Dividing both side of the equation (1.16) by ΔV, taking the limit $\lim \Delta V \to 0$ and invoking the definition of partial derivative we have;

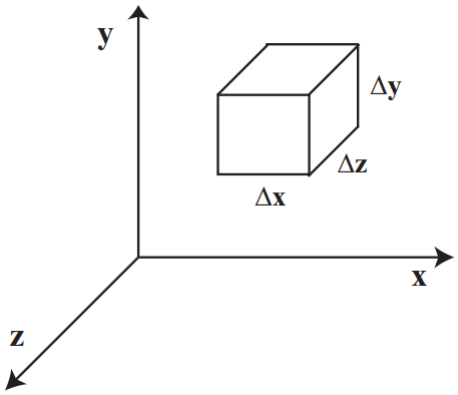

Figure 1.7: An arbitrary differential volume element

$$\frac{\partial \rho}{\partial t} = -\left[\frac{\partial}{\partial x}(\rho u) + \frac{\partial}{\partial y}(\rho v) + \frac{\partial}{\partial z}(\rho w)\right] \tag{1.17}$$

The term in the bracket in the equation (1.17) is simply $\nabla \cdot (\rho\vec{q})$. Thus equation (1.17) can written as;

$$\frac{\partial \rho}{\partial t} = -\vec{\nabla} \cdot (\rho\vec{q}) \tag{1.18}$$

where $\vec{q}$ is the velocity vector i.e. $\vec{q} = (u, v, w)$ and ∇ is called "del" or "gradient" operator. In rectangular coordinates $\nabla = \hat{i}\frac{\partial}{\partial x} + \hat{j}\frac{\partial}{\partial y} + \hat{k}\frac{\partial}{\partial z}$. Equation (1.18) is called the *differential form* of the continuity equation. For incompressible flow, i.e., the density of the flow is constant hence ρ is a function of neither time nor space. The continuity equation (1.18) is reduced to:

$$\frac{d\rho}{dt} = \vec{\nabla} \cdot \vec{q} = 0 \qquad \text{(Alexandre and Jerrold, 1992)} \tag{1.19}$$

Integral Approach

In similar manner, it is possible to derive the continuity equation over an arbitrary, spatially fixed region of microscopic size (see Figure 1.8). The closed volume is called control volume.

$$\frac{d}{dt}\int_V \rho dV = -\oint_s \rho\vec{q} \cdot \vec{n} dS \tag{1.20}$$

The equivalence of equations (1.16) and equation (1.20) are demonstrated through the divergence theorem. The divergence Gauss' theorem states that if V is a volume bounded by a closed surface S and $\vec{A}$ is a continuous vector field, then:

$$\int_V (\vec{\nabla} \cdot \vec{A}) dV = -\oint_s (\vec{A} \cdot \vec{n}) dS \tag{1.21}$$

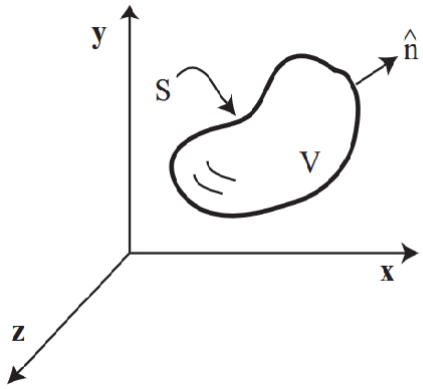

Figure 1.8: An arbitrary macroscopic control volume

Thus the surface integral in equation (1.20) may be converted to volume integral:

$$\frac{d}{dt}\int_V \rho dV = -\int_V (\vec{\nabla}\cdot\rho\vec{q})dV \tag{1.22}$$

Since the control volume is fixed in space, the ordinary derivative may be brought inside of the integral and changed into a partial derivative, allowing both sides of the equation to be consolidated within the integral:

$$\int_V \left[\frac{\partial\rho}{\partial t} + \vec{\nabla}\cdot(\rho\vec{q})dV\right] = 0 \quad \text{(Alexandre and Jerrold, 1992)} \tag{1.23}$$

Because this equation holds for an arbitrary volume V , the integrand must vanish, leading to the same expression which was derived from differential approach.

The equation of continuity may be equivalently obtained in any appropriate coordinate system.

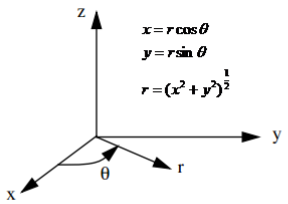

Figure 1.9: Cylindrical Coordinate system

Its expansion in cylindrical coordinate (r, θ, z) (see Figure 1.9) is given as:

$$\frac{\partial\rho}{\partial t} + \frac{1}{r}\frac{\partial}{\partial r}(\rho r u) + \frac{1}{r}\frac{\partial}{\partial\theta}(\rho v) + \frac{\partial}{\partial z}(\rho w) = 0 \tag{1.24}$$

For incompressible flow the equation becomes:

$$\frac{1}{r}\frac{\partial}{\partial r}(ru) + \frac{1}{r}\frac{\partial v}{\partial \theta} + \frac{\partial w}{\partial z} = 0 \quad \text{(Alexandre and Jerrold, 1992)} \tag{1.25}$$

1.1.18 Momentum Equation (Navier-Stokes equation)

The Navier-Stokes equations, developed by Claude-Louis Navier and George Gabriel Stokes in 1822, are equations which can be used to determine the velocity vector field that applies to a fluid, given some initial conditions. They arise from the application of Newton's second law in combination with a fluid stress (due to viscosity) and a pressure term. For almost all real situations, they result in a system of nonlinear PDE which makes them difficult or impossible to solve.

Physical principle: $\vec{F} = m\vec{a}$ (Newton's second law).

Consider the forces acting on a small element of sides δx, δy and δz, Figure 1.10. When the

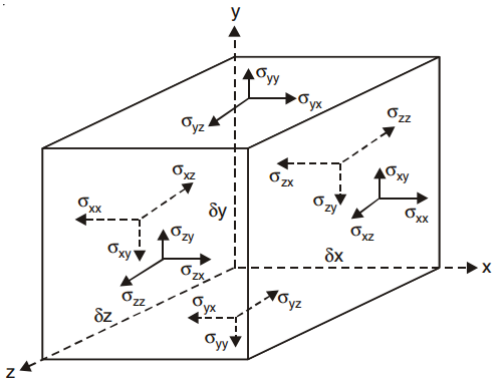

Figure 1.10: Stresses acting on a fluid element

fluid is at rest, the forces acting on the element will be only normal to the surface and will be in the form of pressure. When the real fluid is in motion, in additional to the normal stresses, shear stresses will also act on the surfaces as shown in the Figure 1.10. Calling our Newton's second law of motion

$$\vec{F} = m\vec{a} \tag{1.26}$$

The total force $\vec{F}$ is composed in two forces namely:

- Body forces, which act directly on the volumetric mass of the fluid element. Examples are gravitational, electromagnetic forces.

- Surface forces, which act directly on the surface of the fluid element. They are due to two sources viz: the pressure distribution acting on the surface and viscous stress.

Allowing for the total force $\vec{F} = \vec{b}$ and substituting density for mass, we get a similar equation

$$\vec{b} = \rho \frac{dq}{dt}(x, y, z, t). \tag{1.27}$$

We substitute density for mass because we are operating with a fixed control volume and infinitesimal fluid parcels. The force b is a force that acts throughout the body of fluid (as opposed a shear force, which acts parallel to a plane). Now applying chain rule of the derivative of velocity we get

$$\vec{b} = \rho \left(\frac{\partial \vec{q}}{\partial t} + \frac{\partial \vec{q}}{\partial x}\frac{\partial x}{\partial t} + \frac{\partial \vec{q}}{\partial y}\frac{\partial y}{\partial t} + + \frac{\partial \vec{q}}{\partial z}\frac{\partial z}{\partial t} \right) \tag{1.28}$$

$$= \rho(\frac{\partial \vec{q}}{\partial t} + \vec{q} \cdot \nabla \vec{q}) \tag{1.29}$$

We assumed that the body force on the fluid parcels is due to two components, fluid stresses and other external forces, that is:

$$\vec{b} = \nabla \cdot \sigma + \vec{f_b}, \tag{1.30}$$

where σ represents stress tensor and $\vec{f_b}$ represents external forces. The fluid stress is represented as the divergence of the stress tensor because the divergence is the extent to which the tensor acts like a sink or source. The tensor can be represented as (Alexandre and Jerrold, 1992):

$$\sigma = \begin{pmatrix} \sigma_{xx} & \tau_{xy} & \tau_{xz} \\ \tau_{yx} & \sigma_{yy} & \tau_{yz} \\ \tau_{zx} & \tau_{zy} & \sigma_{zz}, \end{pmatrix}$$

The stress tensor σ denoted above is often divided into two terms of interest in the general form of the Navier-Stokes equation. The two terms are the volumetric stress tensor, which tends to change the volume of the body, and the stress deviator tensor, which tends to deform the body (see Figure 1.10). The volumetric stress tensor represents the force which sets the volume of the body (namely, the pressure forces). The stress deviator tensor represents the forces which determine body deformation and movement, and is composed of the shear stresses on the fluid.

Thus, σ is broken down into

$$\sigma = \begin{pmatrix} \sigma_{xx} & \tau_{xy} & \tau_{xz} \\ \tau_{yx} & \sigma_{yy} & \tau_{yz} \\ \tau_{zx} & \tau_{zy} & \sigma_{zz} \end{pmatrix} \tag{1.31}$$

$$= -\begin{pmatrix} p & 0 & 0 \\ 0 & p & 0 \\ 0 & 0 & p \end{pmatrix} + \begin{pmatrix} \sigma_{xx}+p & \tau_{xy} & \tau_{xz} \\ \tau_{yx} & \sigma_{yy}+p & \tau_{yz} \\ \tau_{zx} & \tau_{zy} & \sigma_{zz}+p \end{pmatrix} \tag{1.32}$$

Denoting the stress deviator tensor as Υ, we can make the substitution in equation (1.32)

$$\sigma = -pI + \Upsilon \tag{1.33}$$

Substituting this into equation (1.30), we arrive at the most general form of the Navier-Stokes equation:

$$\rho(\frac{\partial \vec{q}}{\partial t} + \vec{q} \cdot \nabla \vec{q}) = -\nabla p + \nabla \cdot \Upsilon + f_b \tag{1.34}$$

If we assume the fluid is Newtonian and incompressible. The basis for the Newtonian fluid equations is the assumption about the nature of the stress tensor. For a Newtonian fluid, the stress is proportional to the rate of deformation (the change in velocity in the directions of the stress). In other words,

$$\tau_{ij} = \mu \left(\frac{\partial u_i}{\partial x_j} + \frac{\partial u_j}{\partial x_i} \right) \quad \text{(Alexandre and Jerrold, 1992)} \tag{1.35}$$

where μ is the the viscosity of the fluid which defines how easily the fluid flows when subjected to body forces. The Navier-Stokes equation uses the divergence of stress, $\nabla \cdot \Upsilon$. We can calculate the stress term

$$\nabla \cdot \sigma = \mu \nabla \cdot \begin{pmatrix} \sigma_{xx} & \tau_{xy} & \tau_{xz} \\ \tau_{yx} & \sigma_{yy} & \tau_{yz} \\ \tau_{zx} & \tau_{zy} & \sigma_{zz} \end{pmatrix}$$

$$= \mu \begin{pmatrix} 2\frac{\partial u}{\partial x} & \frac{\partial u}{\partial y} + \frac{\partial v}{\partial x} & \frac{\partial u}{\partial z} + \frac{\partial w}{\partial x} \\ \frac{\partial u}{\partial y} + \frac{\partial v}{\partial x} & 2\frac{\partial v}{\partial y} & \frac{\partial v}{\partial z} + \frac{\partial w}{\partial y} \\ \frac{\partial u}{\partial z} + \frac{\partial w}{\partial x} & \frac{\partial v}{\partial z} + \frac{\partial w}{\partial y} & 2\frac{\partial w}{\partial z} \end{pmatrix} \tag{1.36}$$

Calculating the x term of the divergence:

$$\begin{aligned}(\nabla \cdot \sigma)_i &= \mu \frac{\partial}{\partial x}(2\frac{\partial u}{\partial x}) + \frac{\partial}{\partial y}\left(\frac{\partial u}{\partial y} + \frac{\partial v}{\partial x}\right) \\ &= \mu \frac{\partial^2 u}{\partial x^2} + \frac{\partial^2 u}{\partial y^2} + \frac{\partial^2 u}{\partial z^2} + \frac{\partial^2 u}{\partial x^2} + \frac{\partial^2 v}{\partial x \partial y} + \frac{\partial^2 w}{\partial x \partial z} \\ &= \mu \nabla^2 u + \mu \frac{\partial}{\partial x}\left(\frac{\partial u}{\partial x} + \frac{\partial v}{\partial y} + \frac{\partial w}{\partial z}\right) \\ &= \mu \nabla^2 u + \mu \frac{\partial}{\partial x}(\nabla \cdot q) \\ &= \mu \nabla^2 u + \mu \frac{\partial}{\partial x}(0) \\ &= \mu \nabla^2 u\end{aligned}$$

Extending this to the other divergence terms, we can replace the divergence with a vector Laplacian:

$$\nabla \cdot \Upsilon = \mu \nabla^2 q \tag{1.37}$$

Substituting equation (1.37) into equation (1.34), the final momentum equation for an incompressible fluid in vector form is as follows:

$$\rho\left(\frac{\partial \vec{q}}{\partial t} + \vec{q} \cdot \nabla \vec{q}\right) = -\nabla p + \mu \nabla^2 q + \vec{f_b} \text{ (Alexandre and Jerrold, 1992; Raju, 2011)}$$

The Navier-Stokes equation for each of the three components in cartesian coordinates are:

x-component

$$\rho\left(\frac{\partial u}{\partial t} + u\frac{\partial u}{\partial x} + v\frac{\partial u}{\partial y} + w\frac{\partial u}{\partial z}\right) = \frac{\partial p}{\partial x} + \mu\left(\frac{\partial^2 u}{\partial x^2} + \frac{\partial^2 u}{\partial y^2} + \frac{\partial^2 u}{\partial z^2}\right) + f_{b_x} \tag{1.38}$$

y-Component

$$\rho\left(\frac{\partial v}{\partial t} + u\frac{\partial v}{\partial x} + v\frac{\partial v}{\partial y} + w\frac{\partial v}{\partial z}\right) = \frac{\partial p}{\partial y} + \mu\left(\frac{\partial^2 v}{\partial x^2} + \frac{\partial^2 v}{\partial y^2} + \frac{\partial^2 v}{\partial z^2}\right) + f_{b_y} \tag{1.39}$$

z-Component

$$\rho\left(\frac{\partial w}{\partial t} + u\frac{\partial w}{\partial x} + v\frac{\partial w}{\partial y} + w\frac{\partial w}{\partial z}\right) = \frac{\partial p}{\partial z} + \mu\left(\frac{\partial^2 w}{\partial x^2} + \frac{\partial^2 w}{\partial y^2} + \frac{\partial^2 w}{\partial z^2}\right) + f_{b_z} \tag{1.40}$$

Corresponding equations of conservation of momentum in the cylindrical co-ordinate system are

r- Component

$$\begin{aligned}\rho\left(\frac{\partial u}{\partial t} + u\frac{\partial u}{\partial r} + \frac{v}{r}\frac{\partial u}{\partial \theta} - \frac{v^2}{r} + w\frac{\partial u}{\partial z}\right) &= -\frac{\partial p}{\partial r} + \mu\left(\frac{\partial}{\partial r}\left(\frac{1}{r}\frac{\partial (ru)}{\partial r}\right)\right) \\ &+ \mu\left(\frac{1}{r^2}\frac{\partial^2 u}{\partial \theta^2} - \frac{2}{r^2}\frac{\partial v}{\partial \theta} + \frac{\partial^2 u}{\partial z^2}\right) + f_{b_r},\end{aligned} \tag{1.41}$$

θ- Component

$$\rho\left(\frac{\partial v}{\partial t}+u\frac{\partial v}{\partial r}+\frac{v}{r}\frac{\partial v}{\partial \theta}+\frac{uv}{r}+w\frac{\partial v}{\partial z}\right) = -\frac{\partial p}{\partial \theta}+\mu\left(\frac{\partial}{\partial r}\left(\frac{1}{r}\frac{\partial (rv)}{\partial r}\right)\right) + \mu\left(\frac{1}{r^2}\frac{\partial^2 v}{\partial \theta^2}+\frac{2}{r^2}\frac{\partial u}{\partial \theta}+\frac{\partial^2 v}{\partial z^2}\right)+f_{b_\theta}, \tag{1.42}$$

z- Component

$$\rho\left(\frac{\partial w}{\partial t}+u\frac{\partial w}{\partial r}+\frac{v}{r}\frac{\partial w}{\partial \theta}+w\frac{\partial w}{\partial z}\right) = -\frac{\partial p}{\partial z}+\mu\left(\frac{\partial}{\partial r}\left(\frac{1}{r}\frac{\partial (rw)}{\partial r}\right)+\frac{1}{r^2}\frac{\partial^2 w}{\partial \theta^2}+\frac{\partial^2 w}{\partial z^2}\right)+f_{b_z}. \tag{1.43}$$

1.1.19 Energy equation

To complete the system of equation, we require the third physical principle which states that energy is conserved. A statement of this physical principle is the first law of thermodynamics. When applied to the flow model of a fluid element moving with flow, the first law of thermodynamics states that the the accumulation of internal energy inside the system is equal to sum of heat transmitted to the fluid particle and rate of work done by external forces, i.e.,

$$E_t = Q + W \Rightarrow \frac{dE_t}{dt} = \frac{dQ}{dt} = \frac{dW}{dt} \text{ (Alexandre and Jerrold, 1992)} \tag{1.44}$$

Using the Fourier's law of heat conduction which states that: the heat flux is proportional to the local temperature gradients. Mathematically this can be written as:

$$Q = -k\nabla T, \tag{1.45}$$

where k is the thermal conductivity. The quantity E_t consists of kinetic energy and potential energy given by

$$\frac{dE_t}{dt} = \rho\delta V(\frac{de}{dt}+\frac{1}{2}q^2). \tag{1.46}$$

Using Fourier's law equation (1.45) we can find the rate of heat transmitted from the system as follows:

$$\frac{dQ}{dt} = \delta V\left(\frac{\partial}{\partial x}(k\frac{\partial T}{\partial x})+\frac{\partial}{\partial y}(k\frac{\partial T}{\partial y})+\frac{\partial}{\partial z}(k\frac{\partial T}{\partial z})\right). \tag{1.47}$$

Also we can find the rate of work done by external forces as:

$$\frac{dW}{dt} = \rho\delta V\left(\frac{1}{2}q^2+\nu\Phi\right) \tag{1.48}$$

Now combining equations (1.46), (1.47) and (1.48) we obtain,

$$\rho\delta V(\frac{de}{dt}+\frac{1}{2}q^2) = \delta V\left(\frac{\partial}{\partial x}(k\frac{\partial T}{\partial x})+\frac{\partial}{\partial y}(k\frac{\partial T}{\partial y})+\frac{\partial}{\partial z}(k\frac{\partial T}{\partial z})\right)+\rho\delta V\left(\frac{1}{2}q^2+\nu\Phi\right), \tag{1.49}$$

if k is constant equation (1.49) can be simplified to

$$\rho\frac{de}{dt} = k\nabla^2 T + \rho\nu\Phi. \tag{1.50}$$

If we define $e = c_p T$ where c_P is the specific heat capacity at constant pressure and applying the definition of material derivative then we have

$$\rho c_p\left(\frac{\partial T}{\partial t} + q\cdot\nabla T\right) = \underbrace{k\nabla^2 T}_{\text{heat conduction}} + \underbrace{\rho\nu\Phi}_{\text{viscous dissipation}} \quad \text{(Alexandre and Jerrold, 1992)}, \tag{1.51}$$

where Φ is the viscous dissipation function. This gives the rate at which mechanical energy is converted into thermal energy. For laminar flow of an incompressible fluid this be can defined in cartesian coordinates as:

$$\begin{aligned}\Phi &= \frac{1}{2}\left(\frac{\partial u_i}{\partial x_j} + \frac{\partial u_j}{\partial x_i}\right)\\ &= 2\left[\left(\frac{\partial u}{\partial x}\right)^2 + \left(\frac{\partial v}{\partial y}\right)^2 + \left(\frac{\partial w}{\partial z}\right)^2\right]\\ &+ \left(\frac{\partial v}{\partial x} + \frac{\partial u}{\partial y}\right)^2 + \left(\frac{\partial w}{\partial y} + \frac{\partial v}{\partial z}\right)^2 + \left(\frac{\partial u}{\partial z} + \frac{\partial w}{\partial x}\right)^2.\end{aligned} \tag{1.52}$$

Equation (1.51) is called energy equation and can be written in various forms.

The corresponding equation of conservation of energy in cylindrical coordinate system (r, θ, z) is given by:

$$\rho c_p\left(\frac{\partial T}{\partial t} + q\cdot\nabla T\right) = \frac{k}{r}\frac{\partial}{\partial r}\left(r\frac{\partial T}{\partial r}\right) + \frac{k}{r^2}\frac{\partial^2 T}{\partial\theta^2} + k\frac{\partial^2 T}{\partial z^2} + \mu\Phi, \tag{1.53}$$

where, the dissipation function Φ is given by:

$$\begin{aligned}\Phi &= 2\left[\left(\frac{\partial u}{\partial r}\right)^2 + \left(\frac{1}{r}\frac{\partial v}{\partial\theta} + \frac{u}{r}\right)^2 + \left(\frac{\partial w}{\partial z}\right)^2\right]\\ &+ \left(r\frac{\partial}{\partial r}(\frac{v}{r}) + \frac{1}{r}\frac{\partial u}{\partial\theta}\right)^2 + \left(\frac{\partial u}{\partial z} + \frac{\partial w}{\partial r}\right)^2 + \left(\frac{1}{r}\frac{\partial w}{\partial\theta} + \frac{\partial v}{\partial w}\right)^2.\end{aligned} \tag{1.54}$$

The energy equation must be solved together with the momentum and the continuity equations.

1.1.20 Well-posedness

According to Hadamard (1902), a mathematical models of physical phenomena is well-posed if it satisfies the following conditions:

1. A solution exists
2. The solution is unique
3. The solution's behavior changes continuously with the initial conditions.

1.2 Statement of the Problem

Currently, a large number of industries use the cooling system with traditional heat transfer fluids such as water, oils, glycol and fluorocarbons. However they inherently poor heat transfer performance due to their low thermal conductivities. Several researches have been carried out to improve the heat transport properties of fluids. Solid metallic materials, such as silver, copper and iron, and non-metallic materials, such as alumina, Copper oxide, Silicon carbide and carbon nanotubes, have much higher thermal conductivities than base fluids. Therefore, the thermal conductivities of fluids can be increased by adding solid particles into the base fluids. Furthermore, modeling of the dynamics of flows through porous channel and cylindrical pipe walls are useful for industrial, agriculture, medical and domestic applications such as cooling systems, gaseous diffusion technology, mechanized irrigation and filtration, isotope separation, surface ablation as well as pulmonary circulation. Using a mathematical model, it is therefore necessary to examine the combined effect of the nanoparticles and other embedded parameters on the entire flow structure for the purpose of maximizing the nanofluid convection heat transfer applications.

1.3 Research Objectives

1.3.1 General objective

The general objective of this research is to model and analyze the laminar incompressible flow of nanofluids and heat transfer in a cylindrical pipe and channel with permeable wall for both transient and steady state flow problems.

1.3.2 The specific objectives

The specific objectives of this study are as follows:

1. To formulate mathematical models of nanofluids flow through a cylindrical pipe or channel with porous walls under various physical situation.

2. To investigate the effects of Navier slip, viscous dissipation and other flow parameters on heat transfer in Berman flow of nanofluids.

3. To investigate the combined effects of thermophoresis and Brownian motion of particles in the nanofluids flow.

4. To investigate the effects of embedded flow parameters on the skin friction and heat transfer characteristics due to nanofluids compared to base fluids.

5. To investigate the differences in flow behavior of convectional fluids and nanofluids.

1.4 Significance of the Research

The mathematical modelling and analysis of non-linear flow in a porous channel and cylindrical cylinder are quickly becoming a tool for solving many challenging problems in engineering, medicine, irrigation and applied sciences. The following are among the significance of this research work:

- The findings and knowledge gained will provide useful information to engineers in designing smallest heat exchanger systems which works with high efficiency and low cost.
- The study provides insight into solutions for practical problems related to mass and heat transfer through porous wall and porous media geometries.
- The research adds scientific advancement knowledge to the researchers and other interested people working with computational fluid dynamics.
- The study will serve as a useful tool for heat transfer prediction.
- The findings from this study illuminate known discrepancy in analysis and help to ratify a fundamental source of uncertainty in the models.
- The study provide some clarification and insight for understanding several pertinent aspects of modeling transport phenomena in porous channel and cylindrical pipe.
- Opportunity of extending the research.

1.5 Research Methodology

In this study, both numerical and analytical approaches are employed in solving the models equations which are nonlinear Boundary Value Problems (BVP) and Initial Boundary Value Problems (IBVP). Concerning numerical methods, shooting method, Newton's Raphsons method, method of lines and Runge-Kutta method are employed. Shooting method is employed to solve a nonlinear BVP while method of line is employed to the nonlinear IBVP. Shooting

method is a combination of Newton-Raphson and fourth order Runge-Kutta method, also the method of line involve the use of fourth order Runge-Kutta method. For nanofluid flow in a porous channel considered, Berman similarity is employed to transform 2D PDE to ODE and shooting method is employed to tackle the problem numerically, while in other problems considered, method of line is employed to tackle the PDE which then solved using Runge-Kutta-Fehlberg iteration scheme. With the analytical method, regular perturbation methods with series improvement technique are employed. The computational algorithms were implemented in a computer using MATLAB and MAPLE symbolic package. In the following subsection, the brief explanation of these methods are given.

1.5.1 Numerical approach

Shooting method

The shooting method is an iterative algorithm that reformulates the original boundary value problem in to a set of initial value problem with its appropriate initial conditions. The new problem requires the solution of the IVP with the initial conditions arbitrary chosen to approximate the boundary conditions at the end points. If these boundary conditions are not satisfied to the required accuracy, then the procedure is repeated again with a new set of initial conditions until the required accuracy is acquired or a limit to the iteration is reached. The resultant IVP is solved numerically using any appropriate technique for solving the linear ordinary differential equations. In our case we use the 4^{th} order Runge-Kutta method, which provides high accuracy results. The solution of the IVP should converge to that of the BVP. The algorithm for the above procedure is implemented on a computer using MATLAB and MAPLE symbolic package. The computed results are presented in graphical form. Consider a two-point boundary value problem

$$y'' = f(x, y, y'), \quad y(a) = \alpha, \quad y(b) = \beta. \tag{1.55}$$

where $a < b$ and $x \in [a, b]$. By making initial guess s for $y'(a)$ and denoted by $y(x, s)$. The initial value problem becomes:

$$y'' = f(x, y.y'), \;\; y(a) = \alpha, \;\; y'(a) = s. \tag{1.56}$$

Introducing the notation $u(x; s), \quad v(x; s) = \frac{\partial}{\partial x} y(x; s)$ equation (1.55) can be written as:

$$\frac{\partial}{\partial}u(x;s) = v(x;s), \quad u(a;s) = \alpha$$
$$\frac{\partial}{\partial}v(x;s) = f(x, u(x;s), v(x;s)), \quad v(a;s) = \beta. \quad (1.57)$$

The solution $u(x;s)$ of the initial value problem in equation (1.57), will coincide with the solution $y(x)$ of the boundary value problem in equation (1.55), we can find a value δ such that:

$$\psi(s) = u(b;s) - \beta = 0. \quad (1.58)$$

Equation (1.58) can be solved if and only if there exist $s \in \Re$, such that $\psi(s) = 0$.

Newton-Raphson Method

The Newton-Raphson method is an efficient and powerful method for finding function roots. The method produce faster convergence when good initial guess is provided. Consider a sequence $\{S_n\}_{n=1}^{\infty}$ generated by:

$$s_{n+1} = s_n - \frac{\psi(s_n)}{\psi'(s_n)}. \quad (1.59)$$

Starting by arbitrary chosen s_0. To calculate $\psi'(s_n)$ we introduce new independent variable $\xi(x;s) = \frac{\partial u(x;s)}{\partial x}$, $\varsigma(x;s) = \frac{\partial v(x;s)}{\partial x}$ and differentiate the initial value problem (1.57) with respect to s to obtain second IVP.

$$\frac{\partial \xi(x;s)}{\partial x} = \varsigma(x;s), \quad \xi(a;s) = 0$$
$$\frac{\partial \varsigma(x;s)}{\partial x} = p(x;s)\xi(x;s) + q(x;s)\varsigma(x;s), \quad \varsigma(a;s) = 1, \quad (1.60)$$

where,

$$p(x;s) = \frac{\partial f(x, u(x;s), v(x;s))}{\partial u}, \quad q(x;s) = \frac{\partial f(x, u(x;s), v(x;s))}{\partial v}. \quad (1.61)$$

We assign the value s_n to s, $n \geq 0$, then the IVP (1.57) and (1.60) were solved using an numerical method for IVPs such as Runge-Kutta in the interval $[a, b]$.

Thus an approximation of $u(b;s)$ is obtained to calculte $\psi(s_n) = u(b;s_n) - \beta$ and we also obtain an approximation $\xi(b;s) = \psi'(s_n)$. The values $\psi(s_n)$ and $\psi'(s_n)$ gives the next Newton-Raphson iterate s_{n+1} from equation (1.60). The procedure is repeated until the iterate s_n settle to a fixed number of digits.

Runge-Kutta-Fehlberg Method

One way to guarantee accuracy in solution of IVPs is to solve the problem twice using step size h and $h/2$ and compare answers at mesh points corresponding to the large step size. But this requires a significant amount of computation for the smaller step size and must be repeated if it is determined that the agrement is not good enough.

Runge-Kutta-Fehlberge method is one way try to resolve this problem. It has a procedure to determine if the proper step size h is being used. At each step two different approximation is accepted. If the two answers do not agree to a specified accuracy, the step size is reduced. If the answers agree to more significant digits than required, the step size is increased.

Each step requires the following six values:

$$\left.\begin{aligned}
k_1 &= hf(t_n,\ y_n),\\
k_2 &= hf(t_n + \tfrac{1}{4}h,\ y_n + \tfrac{1}{4}k_1),\\
k_3 &= hf(t_n + \tfrac{3}{8}h,\ y_n + \tfrac{3}{32}k_1 + \tfrac{9}{32}k_2),\\
k_4 &= hf(t_n + \tfrac{12}{13}h,\ y_n + \tfrac{1932}{2197}k_1 - \tfrac{7200}{2197}k_2 + \tfrac{7296}{2197}k_3),\\
k_5 &= hf(t_n + h,\ y_n + \tfrac{439}{216}k_1 - 8k_2 + \tfrac{3680}{513}k_3 - \tfrac{845}{4104}k_4),\\
k_6 &= hf(t_n + \tfrac{1}{2}h,\ y_n - \tfrac{8}{27}k_1 + 2k_2 - \tfrac{3544}{2565}k_3 + \tfrac{1859}{4104}k_4 - \tfrac{11}{40}k_5)
\end{aligned}\right\}, \tag{1.62}$$

Then the approximation to the solution of the IVP is made using a Runge-Kutta method of order 4:

$$y_{n+1} = y_n + \frac{25}{216}k_1 + \frac{1408}{2565}k_3 + \frac{2197}{4101}k_4 - \frac{1}{5}k_5. \tag{1.63}$$

Runge-Kutta-Fehlberg method with shooting technique

The proposed methods have been used extensively by several researchers in dealing with the problems of convective boundary layer flows (Ishak, 2009; Deswita *et al.*, 2010; Singh *et al.*, 2010). The solution procedure is much simpler and effective and the obtained result is of high accuracy. The numerical code that incorporate the methods described above, using either MATLAB (for unsteady models) or MAPLE (steady formulated model) was developed to tackle the problems.

Method of line

The method of lines is a general technique for solving partial differential equations by typically using finite difference relationships for the spatial derivatives and ordinary differential equations

for the time derivative. This is a technique that enables conversion of PDEs into sets of ODEs, which is in some sense, are equivalent to the former partial differential equations. The basic idea behind is to discretized along the spatial coordinates only; this approximation is called semi-discretization. If discretize in space and leave time continuous, a system of ODEs obtained. The focus of the method of line is its merits of both the finite difference method and analytical method. Thus, one of the salient features of this method is the use of existing and generally well established numerical methods for ODEs.

1.5.2 Analytical approach

Perturbation theory

Perturbation theory comprises mathematical methods for finding an approximate solution to a problem, by starting from the exact solution of a related problem. Perturbation theory is applicable if the problem at hand cannot be solved exactly, but can be formulated by adding a small term to the mathematical description of the exactly solvable problem. The theory leads to an expression for the desired solution in terms of power series in some small parameter known as a perturbation series. The leading term in this power series is the solution of the exactly solvable problem, while further terms describe the deviation in the solution, due to the deviation from the initial problem. Because of the nonlinear nature of model equations of our problem, it is convenient to apply perturbation theory. We form a perturbation series of the parameter ϵ:

$$\psi(\varsigma) = \sum_{j=1}^{\infty} \psi_j \epsilon^j,$$

substituting the power series expansion in to the problem equations and collecting the coefficients of the likes power of ξ and then solve the equations for the coefficients of solution series iteratively to get the solution ϵ.

1.6 Dissertation Outline

This dissertation is divided into six chapters, of which chapters 2, 3, 4 and 5 comprise the main body. The chapters are organized as follows:

Chapter 1 provides a general overview of the research context with a description of the background of the research, the problem statement, research objectives, significance of the research, research methodology. The chapter also includes a derivation of the basic fluids models related

to our topic.

Chapter 2 presents an analysis of heat transfer in Berman flow of nanofluids with Navier slip, viscous dissipation and convective Cooling.

Chapter 3 is about an analysis to study the combined effect of variable viscosity, Brownian motion and thermophoresis on unsteady flow of nanofluids in a pipe with permeable wall and convective cooling.

Chapter 4 presents the analysis on unsteady flow of variable viscosity Cu-water and Al_2O_3-water nanofluids in a porous pipe with buoyancy force.

Chapter 5 presents an analysis to study the Buoyancy-Driven heat transfer characteristics of water based nanofluid past permeable cylindrical pipe with Navier slip through saturated porous medium.

Chapter 6 concludes the dissertation with a general discussion of research findings, recommendation and suggestions for continued research on this topic.

CHAPTER TWO

Analysis of Heat Transfer in Berman Flow of Nanofluids with Navier Slip, Viscous Dissipation and Convective Cooling[1]

Summary: In this chapter, heat transfer characteristics of a Berman flow of water based nanofluids containing copper (Cu) and alumina (Al_2O_3) as nanoparticles in a porous channel with Navier slip, viscous dissipation and convective cooling is investigated. It is assumed that the exchange of heat with the ambient surrounding takes place at the channel walls following the Newton's law of cooling. The governing partial differential equations and boundary conditions are converted into a set of nonlinear ordinary differential equations using appropriate similarity transformations. These equations are solved analytically by regular perturbation methods with series improvement technique and numerically using an efficient Runge-Kutta-Fehlberg integration technique coupled with shooting scheme. The effects of the governing parameters on the dimensionless velocity, temperature, skin friction, pressure drop and Nusselt numbers are presented graphically and discussed quantitatively. Our results reveal that both velocity, temperature and heat transfer coefficient (Nu) are increasing with the increase of suction Reynolds number and Navier slip parameter and the effects of increasing Biot number and nanoparticles volume fraction is to decrease the nanofluid temperature.

2.1 Introduction

The study of fluid flow and heat transfer between two porous boundaries has gained tremendous attention of researchers due to its wide applications in engineering and industrial processes. Some of the practical interests include problems dealing with transpiration cooling - where the walls of a channel containing heated fluid are protected from overheating by passing cooler fluid over the exterior surface of the channel; fluid flow occurring during the separation of isotopes of Uranium-235 and Uranium-238 by gaseous diffusion in order to produce fuel for nuclear reactors; controlling boundary layer flow over aircraft wings by injection or suction of fluid out of or into the wing; lubrication of porous bearings; petroleum technology; ground water hydrology; seepage of water in river beds; purification and filtration processes; methods of decreasing rates of heat transfer in combustion chambers exhaust nozzles and porous walled flow reactors etc. In a pioneering work, Berman (1953) presented an exact solution of the

[1] This chapter is based on the paper:

O. D. Makinde, S. Khamis, M. S. Tshehla, and O. Franks (2014). Analysis of Heat Transfer in Berman Flow of Nanofluids with Navier Slip, Viscous Dissipation, and Convective Cooling. *Advances in Mathematical Physics*, 13 pages.

Navier-Stokes equations that describes the steady two-dimensional flow of an incompressible viscous fluid along a channel with parallel rigid porous walls, the flow being driven by uniform suction or injection at the walls. Sellars (1955) extended Bermans work to high suction Reynolds number. Yuan (1956) considered the flow in a channel with porous walls. He obtained solutions for small suction and injection values and asymptotic solution valid at large injection values.

Terrill (1982, 1983), gave an exact series solution for the fully developed laminar flow in a pipe of circular cross section with porous wall driven by a spatially variable though time independent suction and/or injection. Studies on developing flow in porous-walled ducts with suction and injection effects were carried out by Sorour *et al.* (1987) and Zaturska *et al.* (1988). In view of the above interests, several researchers have also investigated the heat transfer problems between two permeable parallel walls under different physical situations (Pederson and Kinney, 1971; Raithby, 1971; Makinde, 1999).

Moreover, the applications of conventional heat transfer fluids such as water and glycol mixture in engineering flow processes are limited due to their low thermal properties. A potential solution to improve these thermal properties is to add nanoparticles into the conventional fluids, hence forming the nanofluids as coined by Choi (1995). Nanofluids contain thermally conducting submicron solid particles and have great potential as a high-energy carrier. The nanoparticles such as Copper, Alumina, Titania and Copper Oxide, unlike larger-sized particles, can be suspended stably within the conventional fluids without settling out of suspension. Nanofluids are free from numerous problems such as abrasion, clogging and high pressure loss, and are considered to be the next-generation working fluids in modern heat transfer technologies Pak and Cho (1998). Experimental results (Wen and Ding, 2005; Xuan and Li, 2003; Wang et al., 2013) have shown that even with small solid volume fraction of nanoparticles (usually less than 5%), the thermal conductivity of heat transfer fluids can be enhanced by $10 - 50\%$. Several authors (Oztop and Abu-Nada, 2008; Kakac and Pramuanjaroenkij, 2009; Makinde, 2013a) have also theoretically investigated the heat transfer enhancement of nanofluids under different physical conditions.

Meanwhile, advances in the manufacture of micro-devices has enabled experimental investigation of fluid flow in nano and microscale, and many experimental results have provided evidences to support the slip condition (Huang and Breuer, 2007; Martin and Boyd, 2006). In order to describe the slip characteristics of fluid on the solid surface, Navier (1823) introduced a more general boundary condition, namely the fluid velocity component tangential to the solid surface, relative to the solid surface, is proportional to the shear stress on the fluid$-$solid interface. The proportionality is called the slip length which describes the slipperiness of the surface. However, from the literature survey, it is found that no study has been conducted on the heat transfer characteristics of Berman flow of nanofluids with Navier slip, viscous dissipation and convective cooling at the walls. Hence the present study is an attempt in this direction. The flow of water base nanofluids containing copper (Cu) and alumina (Al_2O_3) as nanoparticles in a

uniformly porous wall channel with Navier slip, viscous dissipation and convective heat exchange with the ambient surrounding is investigated. Sections 2-4 give in more details the model nonlinear governing equations together with the analytical and numerical solution techniques employed to tackle the problem. In section 5, we present graphically and discuss the main features of the flow and heat transfer characteristics in a range of governing parameters. Final conclusions are drawn in section 6.

2.2 Problem Formulation

Consider a two dimensional steady flow of a viscous incompressible water based nanofluids containing copper (Cu) and alumina (Al_2O_3) as nanoparticles in a uniformly porous wall channel. The channel wall is subjected to Navier slip and convectively exchange heat with the ambient surrounding. We choose a Cartesian co-ordinates system in such a way that the x- axis is taken along the channel and the y-axis is normal to it as shown in Figure 2.1:

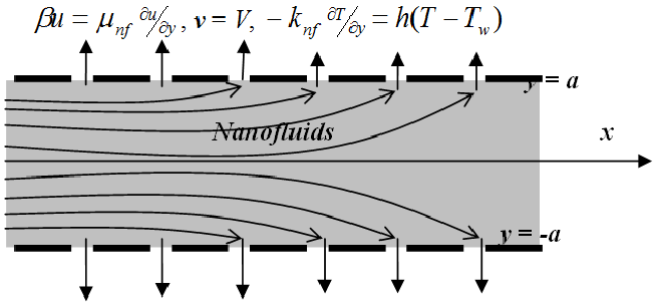

Figure 2.1: Schematic diagram of the physical system

The governing equations which are those of conservation of mass, momentum, and energy are:

$$\frac{\partial u}{\partial x} + \frac{\partial v}{\partial y} = 0, \tag{2.1}$$

$$\rho_{nf}\left(u\frac{\partial u}{\partial x} + v\frac{\partial u}{\partial y}\right) = -\frac{\partial p}{\partial x} + \mu_{nf}\left(\frac{\partial^2 u}{\partial x^2} + \frac{\partial^2 u}{\partial y^2}\right), \tag{2.2}$$

$$\rho_{nf}\left(u\frac{\partial v}{\partial x} + v\frac{\partial v}{\partial y}\right) = -\frac{\partial p}{\partial y} + \mu_{nf}\left(\frac{\partial^2 v}{\partial x^2} + \frac{\partial^2 v}{\partial y^2}\right), \tag{2.3}$$

$$\begin{aligned} u\frac{\partial T}{\partial x} + v\frac{\partial T}{\partial y} &= \frac{k_{nf}}{(\rho c_p)_{nf}}\left(\frac{\partial^2 T}{\partial x^2} + \frac{\partial^2 T}{\partial y^2}\right) + \frac{2\mu_{nf}}{(\rho c_p)_{nf}}\left[\left(\frac{\partial u}{\partial x}\right)^2 + \left(\frac{\partial v}{\partial y}\right)^2\right] \\ &+ \frac{\mu_{nf}}{(\rho c_p)_{nf}}\left(\frac{\partial v}{\partial x} + \frac{\partial v}{\partial y}\right)^2, \end{aligned} \tag{2.4}$$

where (u, v) are the velocity components of the nanofluid in the (x, y) directions respectively, $V(> 0)$ uniform wall suction velocity, p is the pressure, T is the nanofluid temperature, μ_{nf} is the effective

dynamic viscosity of the nanofluid (Brinkman, 1952), k_{nf} is the effective thermal conductivity of the nanofluid (Maxwell, 1904), ρ_{nf} is the nanofluid density and $(\rho c_p)_{nf}$ is the heat capacitance of the nanofluid which are given by (Xuan and Li, 2003; Wen and Ding, 2005; Oztop and Abu-Nada, 2008; Kakac and Pramuanjaroenkij, 2009; Wang *et al.*, 2013; Makinde, 2013a).

$$\mu_{nf} = \frac{\mu_f}{(1-\varphi)^{2.5}}, \quad \rho_{nf} = (1-\varphi)\rho_f + \varphi\rho_s, \quad \alpha_{nf} = \frac{k_{nf}}{(\rho c_p)_{nf}},$$
$$\frac{k_{nf}}{k_f} = \frac{(k_s+2k_f)-2\varphi(k_f-k_s)}{(k_s+2k_f)+\varphi(k_f-k_s)}, \quad (\rho c_p)_{nf} = (1-\varphi)(\rho c_p)_f + \varphi(\rho c_p)_s. \quad (2.5)$$

In equation (2.5), φ is the nanoparticles solid volume fraction, ρ_f is the reference density of the fluid fraction, ρ_s is the reference density of the solid fraction, μ_f is the viscosity of the fluid fraction, k_f is the thermal conductivity of the fluid fraction, c_p is the specific heat at constant pressure and k_s is the thermal conductivity of the solid volume fraction. Due to the symmetric nature of the flow, the boundary conditions at the channel centreline and at the porous wall may be written as (Berman, 1953; Sellars, 1955; Yuan, 1956; Terrill, 1982)

$$\frac{\partial u}{\partial y}(x,0) = 0, \quad \frac{\partial T}{\partial y}(x,0) = 0, \quad v(x,0) = 0, \quad (2.6)$$

$$\beta u(x,a) = \mu_{nf}\frac{\partial u}{\partial y}(x,a), \quad v(x,a) = V, \quad -k_{nf}\frac{\partial T}{\partial y}T(x,a) = h\left[T(x,a) - T_W\right], \quad (2.7)$$

where T_w is the ambient surrounding temperature, h is the coefficient of heat transfer and β is the Navier slip coefficient. Introducing the stream function ψ and vorticity Ω into the governing equations (2.1)-(2.5) as follows:

$$u = \frac{\partial \psi}{\partial y}, \quad v = -\frac{\partial \psi}{\partial x} \quad \Omega = \frac{\partial u}{\partial y} - \frac{\partial v}{\partial x} = \frac{\partial^2 \psi}{\partial y^2} + \frac{\partial^2 \psi}{\partial x^2}. \quad (2.8)$$

After eliminating the pressure P from equations (2.2) and (2.3), we obtain

$$\rho_{nf}\left(\frac{\partial \psi}{\partial y}\frac{\partial \Omega}{\partial x} - \frac{\partial \psi}{\partial x}\frac{\partial \Omega}{\partial y}\right) = \mu_{nf}\left(\frac{\partial^2 \Omega}{\partial x^2} + \frac{\partial^2 \Omega}{\partial y^2}\right), \quad (2.9)$$

$$\begin{aligned}\left(\frac{\partial \psi}{\partial y}\frac{\partial T}{\partial x} - \frac{\partial \psi}{\partial x}\frac{\partial T}{\partial y}\right) &= \frac{k_{nf}}{(\rho c_p)_{nf}}\left(\frac{\partial^2 T}{\partial x^2} + \frac{\partial^2 T}{\partial y^2}\right) + \frac{4\mu_{nf}}{(\rho c_p)_{nf}}\left(\frac{\partial^2 \psi}{\partial x \partial y}\right)^2 \\ &+ \frac{\mu_{nf}}{(\rho c_p)_{nf}}\left(-\frac{\partial^2 \psi}{\partial x^2} + \frac{\partial^2 \psi}{\partial y^2}\right)^2. \end{aligned} \quad (2.10)$$

The following dimensionless variables and parameters are introduced into equations (2.9)and (2.11) together with their corresponding boundary conditions:

$$\eta = \frac{y}{a}, \quad \bar{\psi} = \frac{\psi}{Va}, \quad \bar{\Omega} = \frac{\Omega a}{V}, \quad \Phi = \frac{T - T_w}{T_w}, \quad Re = \frac{Va}{\nu f}, \quad X = \frac{x}{a}, \quad \nu_f = \frac{\mu_f}{\rho_f},$$
$$Pr = \frac{\mu_f c_p}{k_f}, \quad m_1 = (1 - \varphi + \varphi\rho_s/\rho_f)(1-\varphi)^{2.5}, \quad \lambda = \frac{\mu_f}{\beta a}, \quad \bar{P} = \frac{aP}{V\mu_f},$$
$$m_2 = m_4\left(1 - \varphi + \varphi\frac{(\rho c_p)_s}{(\rho c_p)_f}\right), \quad Bi = \frac{ha}{k_f}, \quad Ec = \frac{V^2}{c_p T_w},$$
$$m_3 = \frac{m_4}{(1-\varphi)^{2.5}}, \quad m_4 = \frac{(k_s+2k_f)+\varphi(k_f-k_s)}{(k_s+2k_f)-2\varphi(k_f-k_s)}, \quad (2.11)$$

and we obtain

$$m_1 Re\left(\frac{\partial\bar{\psi}}{\partial\eta}\frac{\partial\bar{\Omega}}{\partial X}-\frac{\partial\bar{\psi}}{\partial X}\frac{\partial\bar{\Omega}}{\partial\eta}\right)=\left(\frac{\partial^2\bar{\Omega}}{\partial\eta^2}+\frac{\partial^2\bar{\Omega}}{\partial X^2}\right), \tag{2.12}$$

$$\begin{aligned} m_2 ReP_r\left(\frac{\partial\bar{\psi}}{\partial\eta}\frac{\partial\bar{\Phi}}{\partial X}-\frac{\partial\bar{\psi}}{\partial X}\frac{\partial\bar{\Phi}}{\partial\eta}\right) &= \left(\frac{\partial^2\bar{\phi}}{\partial\eta^2}+\frac{\partial^2\bar{\phi}}{\partial X^2}\right)+4m_3E_cP_r\left(\frac{\partial^2\bar{\psi}}{\partial X\partial\eta}\right)^2 \\ &+ m_3E_cP_r\left(-\frac{\partial^2\bar{\psi}}{\partial X^2}+\frac{\partial^2\bar{\psi}}{\partial\eta^2}\right)^2, \end{aligned} \tag{2.13}$$

with

$$\frac{\partial^2\bar{\psi}}{\partial\eta^2}(X,0)=0,\quad \frac{\partial\Phi}{\partial\eta}(X,0)=0,\quad \frac{\partial\bar{\psi}}{\partial X}(X,0)=0, \tag{2.14}$$

$$\frac{\partial\bar{\psi}}{\partial\eta}(X,1)=\frac{\lambda}{(1-\varphi)^{2.5}}\frac{\partial^2\bar{\psi}}{\partial\eta^2}(X,1),\ \ \frac{\partial\bar{\psi}}{\partial X}(x,a)=-1,\quad \frac{\partial\Phi}{\partial\eta}(X,1)=-m_4Bi\Phi(X,1), \tag{2.15}$$

where Re is the flow Reynolds number such that $Re>0$ represents wall suction and $Re<0$ represents wall injection; E_c is the Eckert number, Bi is the Biot number, P_r is the base fluid Prandtl number, m_1,m_2, m_3 and m_4 can be easily determined from the thermophysical properties of the base fluid and the nanoparticles, λ is the Navier slip parameter such that $\lambda=0$ corresponds to no slip, while full lubrication is described in the limit $\lambda\to\infty$. To transform 2D PDE to ODE, we seek a similarity form of solution as obtained by Berman (1953),

$$\bar{\psi}(X,\eta)=XF(\eta), W(X,\eta)=X\frac{dF}{d\eta},\ \ \Phi(X,\eta)=H(\eta)+X^2\theta(\eta). \tag{2.16}$$

Equations (2.12)-(2.14) together with the boundary conditions in (2.14)-(2.15) then become

$$\frac{d^4F}{d\eta^4}=m_1Re\left(\frac{dF}{d\eta}\frac{d^2F}{d\eta^2}-F\frac{d^3F}{d\eta^3}\right), \tag{2.17}$$

$$\frac{d^2\theta}{d\eta^2}=m_3E_cP_r\left(\frac{d^2F}{d\eta^2}\right)^2+m_2RePr\left(2\theta\frac{dF}{d\eta}-F\frac{d\theta}{d\eta}\right), \tag{2.18}$$

$$\frac{d^2H}{d\eta^2}=-2\theta-4m_3E_cP_r\left(\frac{dF}{d\eta}\right)^2-m_2RePrF\frac{dH}{d\eta}, \tag{2.19}$$

$$\frac{d^2F}{d\eta^2}(0)=0,\quad \frac{d\theta}{d\eta}(0)=0,\quad \frac{dH}{d\eta}(0)=0,\quad F(0)=0, \tag{2.20}$$

$$\frac{dF}{d\eta}(1)=b\frac{d^2F}{d\eta^2}(1),\ \ F(1)=-1\ \ \frac{d\theta}{d\eta}(1)=-m_4Bi\theta(1),\ \ \frac{dH}{d\eta}(1)=-m_4BiH(1), \tag{2.21}$$

where $b=\lambda(1-\varphi)^{2.5}$. The dimensionless fluid axial pressure gradient is given as:

$$-\frac{d\bar{P}}{dX}=XA, \tag{2.22}$$

where

$$(1-\varphi)^{2.5}A = -\frac{d^2F}{d\eta^2} + m_1 Re\left[\left(\frac{d^2F}{d\eta^2}\right)^2 - F\frac{d^2F}{d\eta^2}\right]. \tag{2.23}$$

Other quantities of practical interest in this study are the local skin friction coefficient C_f and the local Nusselt number Nu, which are defined as

$$C_f = \frac{a\tau_w}{\mu_f V}, \quad Nu = \frac{aq_w}{k_f T_w}, \tag{2.24}$$

where τ_w is the wall shear stress and q_w is the heat flux at the channel walls which are given by

$$\tau_w = \mu\frac{\partial u}{\partial y}\mid_{y=a}, \quad q_w = -k_{nf}\frac{\partial T}{\partial y}\mid_{y=a}. \tag{2.25}$$

Using equations (2.11) and (2.16), we substitute equation (2.25) into (2.24) and obtain

$$C_f = \frac{X}{(1-\varphi)^{2.5}}\frac{d^2F}{d\eta^2}(1), \quad Nu = -\frac{k_{nf}}{k_f}\left[\frac{dH}{d\eta}(1) + X^2\frac{d\theta}{d\eta}(1)\right]. \tag{2.26}$$

In the following section, the boundary value problem (2.17) - (2.21) was solved analytically using regular perturbation method and numerically by the Runge-Kutta-Fehlberg method with shooting technique (Na, 1979). The results are utilised to compute the fluid pressure gradient, local skin friction and local Nusselt number as highlighted in equations (2.24) and (2.26).

2.3 Perturbation Method

Due to the nonlinear nature of the model equations (2.17)-(2.21), it is convenient to form a power series expansion in the parameter R that is,

$$F(\eta) = \sum_{i=1}^{\infty} F_i Re^i, \quad \theta(\eta) = \sum_{i=1}^{\infty} \theta_i Re^i. \tag{2.27}$$

Substituting the solution series in (2.27) into (2.17)-(2.21) and collecting the coefficients of like powers of R, we obtain the following.

Zeroth Order. Consider

$$\frac{d^4F_0}{d\eta^4} = 0, \quad \frac{d^2F_0}{d\eta^2} = -m_3E_cP_r\left(\frac{d^2F_0}{d\eta^2}\right)^2, \quad \frac{d^2H_0}{d\eta^2} = -2\theta_0 - 4m_3E_cP_r\left(\frac{dF_0}{d\eta}\right)^2, \tag{2.28}$$

with

$$\frac{d^2F_0}{d\eta^2}(0) = 0, \quad \frac{d\theta_0}{d\eta}(0) = 0, \quad \frac{dH_0}{d\eta}(0) = 0, \quad F_0(0) = 0, \tag{2.29}$$

$$\frac{dF_0}{d\eta}(1) = b\frac{d^2F_0}{d\eta^2}(1), \quad F_0(1) = -1 \quad \frac{d\theta_0}{d\eta}(1) = -m_4Bi\theta_0(1), \quad \frac{dH_0}{d\eta}(1) = -m_4BiH_0(1). \tag{2.30}$$

Higher Order $n \geq 1$**.** Consider

$$\frac{d^4F_n}{d\eta^4} = m_1 Re \sum_{i=0}^{n-1} \left(\frac{dF_i}{d\eta} \frac{d^2F_{n-i-1}}{d\eta^2} - F_i \frac{d^3F_{n-i-1}}{d\eta^3} \right), \tag{2.31}$$

$$\frac{d^2\theta_n}{d\eta^2} = -m_3 E_c P_r \sum_{i=0}^{n} \left(\frac{d^2F_i}{d\eta^2} \frac{d^2F_{n-i}}{d\eta^2} \right) + m_2 RePr \sum_{i=0}^{n-1} \left(2\theta_i \frac{dF_{n-i-1}}{d\eta} - F_i \frac{d\theta_{n-i-1}}{d\eta} \right), \tag{2.32}$$

$$\frac{d^2H_n}{d\eta^2} = -2\theta_n - 4m_3 EcPr \sum_{i=0}^{n} \left(\frac{dF_i}{d\eta} \frac{dF_{n-i}}{d\eta} \right) - m_2 RePr \sum_{i=0}^{n-1} \left(F_i \frac{dH_{n-i-1}}{d\eta} \right), \tag{2.33}$$

with

$$\frac{d^2F_n}{d\eta^2}(0) = 0, \quad \frac{d\theta_n}{d\eta}(0) = 0, \qquad \frac{dH_n}{d\eta}(0) = 0, \quad F_n(0) = 0, \tag{2.34}$$

$$\frac{dF_n}{d\eta}(1) = b\frac{d^2F_n}{d\eta^2}(1), \;\; F_n(1) = 0 \;\; \frac{d\theta_n}{d\eta}(1) = -m_4 Bi\theta_n(1), \quad \frac{dH_n}{d\eta}(1) = -m_4 BiH_n(1). \tag{2.35}$$

The equations are solved iteratively and the series solutions for the velocity and temperature fields are given as:

$$F(\eta) = \frac{\eta(\eta^2 + 6b - 3)}{2 - 6b} + \frac{\eta Rem_1(\eta^2 - 1)}{280(3b-1)^3} \left(3\eta^4 b - \eta^4 + 3\eta^2 b - \eta^2 - 18b + 2 \right) + O(Re^2), \tag{2.36}$$

$$\theta(\eta) = \frac{3(4 + m_4 Bi + \eta^4 m_4 Bi) m_3 EcPr}{4m_4 Bi(3b-1)^2} + O(Re), \tag{2.37}$$

$$\begin{aligned} H(\eta) = -\frac{3m_3 EcPr}{2m_4 Bi(3b-1)^2} \Bigg(& 2\eta^2 + \frac{7}{2} m_4 Bi\eta^2 + \frac{1}{6}\eta^6 m_4 Bi + 2m_4 Bi\eta^4 b \\ & -\eta^4 m - 4Bi + 12m_4 Bib^2\eta^2 - 12m_4 Bib\eta^2 \Big) - \frac{3m_3 EcPr}{2m_4^3 Bi^3(3b-1)^2(9b^2 - 6b + 1)} (6 \\ & +9m_4 Bi - 24m_4 Bib + 36m_4 Bib^2 - 15m_4^2 Bi^2 b + 18m_4^2 Bi^2 b^2 \big) + O(Re), \end{aligned} \tag{2.38}$$

where $b = \lambda(1-\varphi)^{2.5}$. Note that if the parameters $\varphi = 0, \;\; b = 0$, in (2.36) we will recover the solution for the classical case of conventional fluid given in (Berman, 1953; Sellars, 1955; Yuan, 1956; Terrill, 1982). Using a computer symbolic algebra package (MAPLE), several terms of the above solution series in equations (2.36)-(2.38) are obtained. From equations (2.36)-(2.38) together with equations (2.23) and (2.26), we obtained the series solutions for the skin friction, Nusselt number and axial pressure gradient as follows:

$$\begin{aligned} C_f = \frac{X}{(1-\varphi)^{2.5}} \Bigg[& \frac{3}{1-3b} - \frac{3Rem_1}{35(3b-1)^3} \\ & - \frac{Re^2 m_1^2 (3465b^2 - 1743b + 394)}{40425(3b-1)^5} + O(Re^3) \Bigg], \end{aligned} \tag{2.39}$$

$$A = \frac{1}{(1-\varphi)^{2.5}}\left[\frac{3}{1-3b} - \frac{9Rem_1(105b^3-140b^2+63b-9)}{35(3b-1)^3} + \frac{Re^2m_1^2(1155b^3-1309b^2+364b-26)}{13475(3b-1)^5} + O(Re^3)\right], \quad (2.40)$$

$$\begin{aligned}\frac{k_f}{k_{nf}}Nu &= \frac{6m_3EcPrG_1}{m_4Bi(3b-1)^2} + \frac{2Rem_3EcPrG_2}{105m_4^2Bi^2(3b-1)^4} \\ &+ X^2\left(\frac{3m_3EcPr}{(3b-1)^2} + \frac{3Rem_3EcPrG_3}{35m_4Bi(3b-1)^4}\right) + O(R^2),\end{aligned} \quad (2.41)$$

where the expression for $G_i, i = 1, 2, 3$ are given in the appendix A. We are aware that these power series solutions are valid for very small parameter values of Re. However, using Hermite-Pade approximation technique see (Makinde, 1999) that is based on the series summation and improvement method; the usability of the extended solution series is improved beyond small parameter values of Re.

2.4 Numerical Procedure

An efficient finite difference approach based on Runge-Kutta-Fehlberg method with shooting technique (Na, 1979) has been employed to numerically solve the coupled nonlinear ordinary differential equations (2.17)- (2.19) subject to the boundary conditions (2.20)-(2.21) for different values of governing parameters. The boundary value problem is first transformed into an initial value problem (IVP). Let

$$z_1 = F,\ \ z_2 = \frac{dF}{d\eta},\ \ z_3 = \frac{d^F}{d\eta^2},\ \ z_4 = \frac{d^3F}{d\eta^3},\ \ z_5 = \theta,\ \ z_6 = \frac{d\theta}{d\eta},\ \ z_7 = H,\ \ z_8 = \frac{dH}{d\eta}. \quad (2.42)$$

Substituting equation (2.42) into equations (2.17)-(2.21), we obtain a system of first order differential equations respectively, as follows:

$$\begin{aligned}&\frac{dz_1}{d\eta} = z_2,\ \ \frac{dz_2}{d\eta} = z_3,\ \ \frac{dz_3}{d\eta} = z_4,\ \ \frac{dz_4}{d\eta} = m_1Re\left(z_2z_3 - z_1z_4\right), \\ &\frac{dz_5}{d\eta} = z_6,\ \ \frac{dz_6}{d\eta} = -m_3EcPrz_3^2 + m_2RePr\left(2z_5z_2 - z_1z_6\right), \\ &\frac{dz_7}{d\eta} = z_8,\ \ \frac{dz_8}{d\eta} = -2z_5 - 4m_3EcPrz_2^2 - m_2RePr\left(z_1z_8\right),\end{aligned} \quad (2.43)$$

subject to the initial conditions

$$\begin{aligned}z_1(0) &= 0,\ \ z_2(0) = s_1,\ \ z_3(0) = 0,\ \ z_4(0) = s_2, \\ z_5(0) &= s_3,\ \ z_6(0) = 0,\ \ z_7(0) = s_4,\ \ z_8(0) = 0.\end{aligned} \quad (2.44)$$

By applying the shooting method with the Newton-Raphson algorithm to guess the unspecified conditions $s_1,\ s_2,\ s_3$ and s_4 in equation (2.44), the resulting initial value problem is then integrated numerically until the boundary conditions at $\eta = 1$ are achieved. The step size is taken as $\Delta\eta = 0.001$ and the convergence criteria were set to 10^{-7}.

2.5 Results and Discussion

The flow of water base nanofluids containing Cu and Al_2O_3 as nanoparticles and their heat transfer characteristics in a symmetrically porous channel with Navier slip and convective cooling at the surface are investigated. The governing partial differential equations and the corresponding boundary conditions are converted into a set of nonlinear ordinary differential equations and tackled both analytically using the perturbation method coupled with series improvement technique and numerically using Runge-Kutta-Fehlberg integration technique coupled with shooting scheme. Thermophysical properties of base fluid and nanoparticles are presented in Table 2.1. For pure water, the momentum diffusivity is dominant and convection is very effective in transferring within the fluid in comparison to pure conduction. Following Kakac and Pramuanjaroenkij (2009); Oztop and Abu-Nada (2008); Makinde (2013a), we take $Pr = 6.2$ in the numerical computation. Note that when $\varphi = 0$, no nanoparticle is present in the based fluid (water). The solid volume fraction in the base fluid is taken as $\varphi = 0$ to 0.3 (i.e., ranging from 0 to 30 percent). In order to get a clear insight into the entire flow structure and thermal development, we have assigned numerical values to other parameters encountered in the problem. Numerical solutions are displayed in Tables 2.2-2.3 together with Figures 2.2-2.23. The numerical values of suction driven normal velocity profile ($Re = 1$) is displayed in Table 2.2. In the absence of nanoparticles ($\varphi = 0$) and Navier slip λ at the channel walls, the results agreed well with the one already in the literature see (Berman, 1953; Sellars, 1955; Yuan, 1956) for the flow of conventional fluid in a symmetrical porous wall channel. However, Cu-water nanofluid is affected more by the combined effects of suction and Navier slip at wall in comparison to Al_2O_3-water nanofluid. Table 2.3 shows the perfect agreement between the series solution and the numerical solution for the axial velocity profiles along the channel centreline with increasing concentration of nanoparticles for both Cu-water and Al_2O_3-water nanofluids.

Table 2.1: Thermophysical properties of the water and nanoparticles (Kakac and Pramuan-jaroenkij, 2009; Xuan and Li, 2003; Wen and Ding, 2005; Wang *et al.*, 2013; Oztop and Abu-Nada, 2008)

Physical properties	**Fluid phase (water)**	**Cu**	Al_2O_3
$C_p(J/kgK)$	4179	385	765
$\rho(kg/m^3)$	997.1	8933	3970
k(W/mK)	0.613	400	40

Table 2.2: Computation showing the normal velocity profiles for $Re = 1$

η	$-F(\eta)$ $\lambda = 0,\ \varphi = 0$ Ref.(Berman, 1953; Sellars, 1955; Yuan, 1956)	$-F(\eta)$ $\lambda = 0,\ \varphi = 0$ Present	$-F(\eta)$ $\lambda = 0.05, \varphi = 0.1$ Cu-water	$-F(\eta)$ $\lambda = 0.05, \varphi = 0.1$ Al_2O_3-water
0.0	0.00000	0.000000	0.000000	0.000000
0.1	0.14874	0.148739	0.160680	0.160920
0.2	0.29455	0.294548	0.317732	0.318184
0.3	0.43449	0.434493	0.467527	0.468132
0.4	0.56564	0.565639	0.606428	0.607103
0.5	0.68504	0.685042	0.730781	0.731419
0.6	0.78974	0.789739	0.836887	0.837373
0.7	0.87672	0.876724	0.920958	0.921192
0.8	0.94292	0.942920	0.979045	0.978994
0.9	0.98514	0.985137	1.006937	1.006713
1.0	1.00000	1.000000	1.000000	1.000000

Table 2.3: Computation showing the axial velocity profiles for $Re = 1,\ \lambda = 0.05,\ X = 1,\ \eta = 0$

φ	$W(1,0)$ Cu-Water (Series)	$W(1,0)$ Cu-Water (Numerical)	$W(1,0)$ Al_2O_3-Water (Series)	$W(1,0)$ Al_2O_3-Water (Numerical)
0.00	1.581405	1.581405	1.581405	1.581405
0.01	1.583733	1.583733	1.584084	1.584084
0.05	1.594688	1.594688	1.596218	1.596218
0.10	1.612850	1.612850	1.615303	1.615303
0.15	1.637660	1.637660	1.640343	1.640343
0.20	1.672037	1.672037	1.674097	1.674097
0.25	1.721196	1.721196	1.721395	1.721395
0.30	1.795420	1.795420	1.791485	1.791485

2.5.1 Velocity profiles with parameter variation

The effects of parameter variation on both the axial and normal velocity components are displayed in Figures 2.2-2.9. Generally, it is interesting to note that the effect of Navier slip causes flow reversal at the channel walls. In Figure 2.2, the profiles shows that Cu-water moves faster along the channel centreline region and subjected to higher flow reversal at the wall as compared to Al_2O_3-water in the presence of suction. With Cu-water as the working nanofluid, increasing nanoparticles volume fraction concentration from 0-30% increases both the axial velocity along the centreline region and the flow reversal at the channel walls as shown in Figure 2.3. Similar trend is observed in Figure 2.4 and Figure2.5 with a growing suction parameter and Navier slip parameter. Figures 2.6-2.9 show that the nanofluids normal velocity profiles. With suction and Navier slip, the Cu-water moves faster to the wall as compared to Al_2O_3-water as illustrated in Figure 2.6. A further increase in normal velocity towards the walls is observed with a growing in suction parameter, Navier slip parameter and nanoparticles volume fraction as shown in Figures 2.7-2.9.

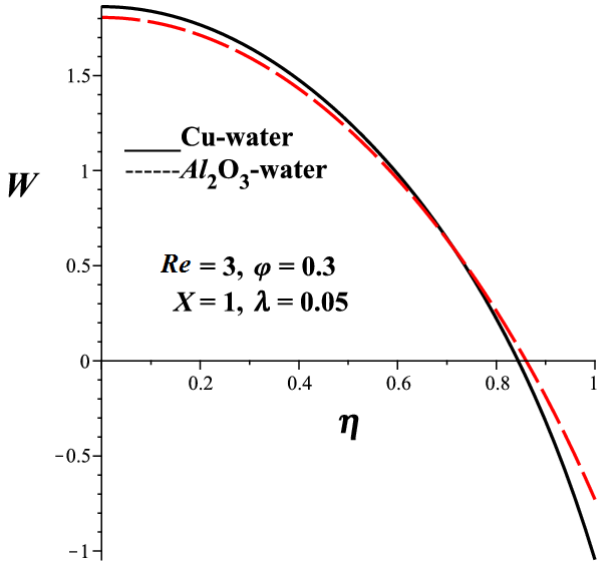

Figure 2.2: Nanofluids axial velocity profiles

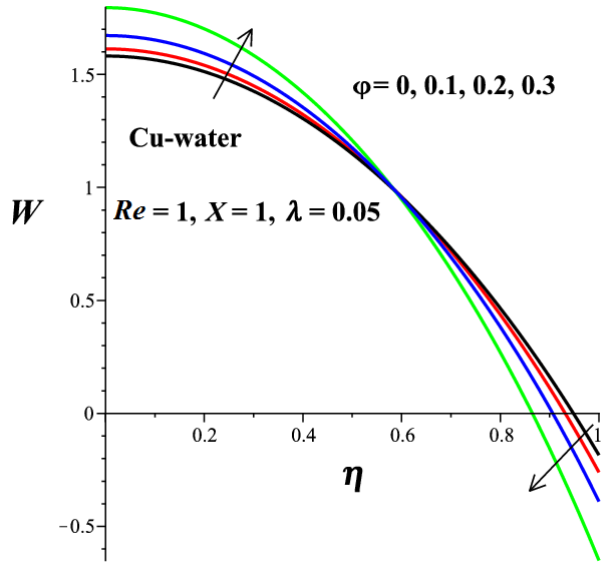

Figure 2.3: Axial velocity profiles with increasing φ

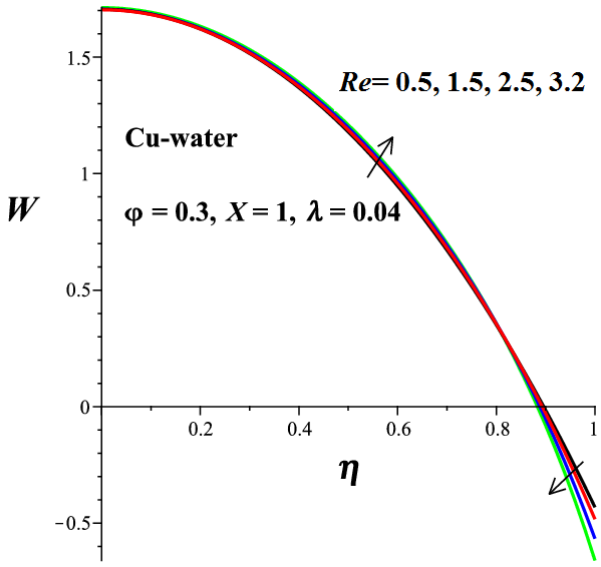

Figure 2.4: Axial velocity profiles with increasing Re

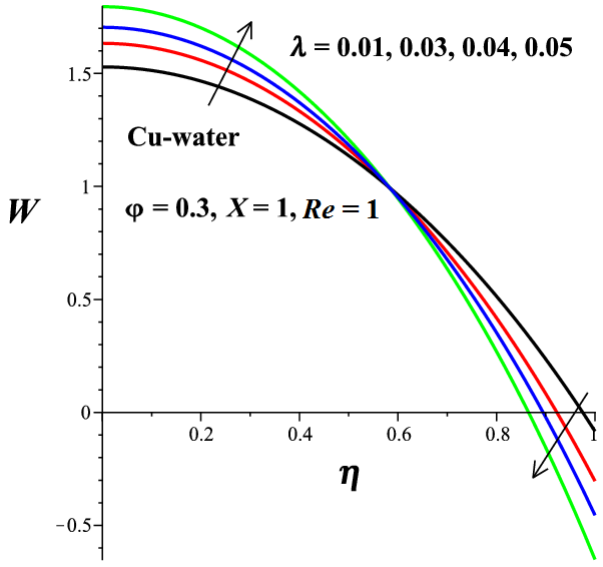

Figure 2.5: Axial velocity profiles with increasing λ

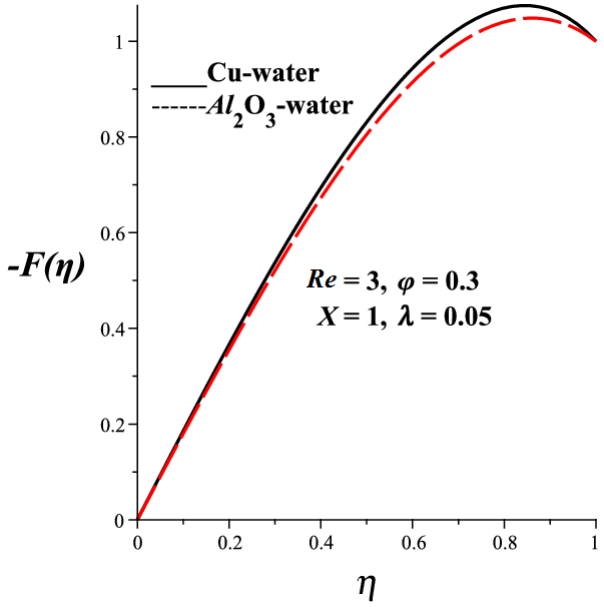

Figure 2.6: Nanofluids normal velocity profiles

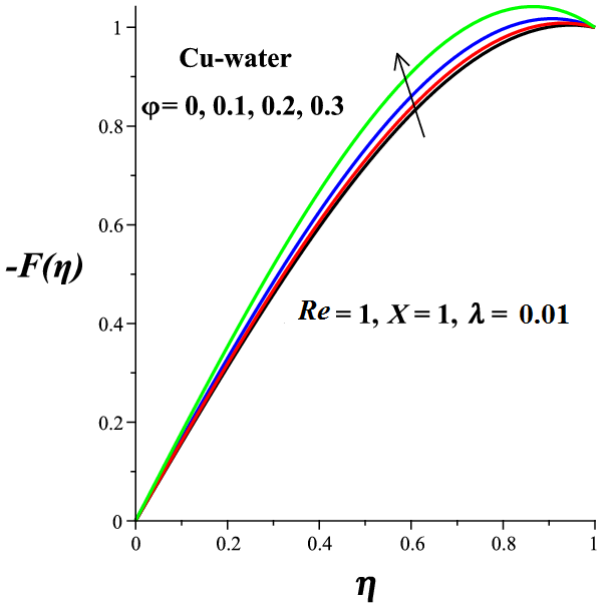

Figure 2.7: Normal velocity profiles with increasing φ

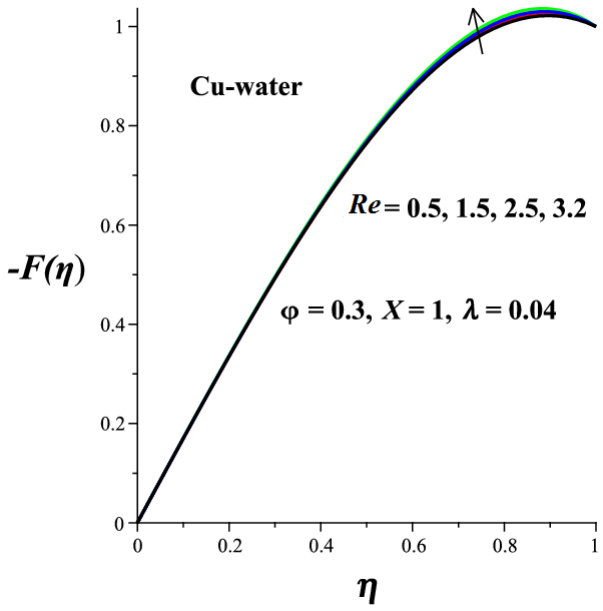

Figure 2.8: Normal velocity profiles with increasing Re

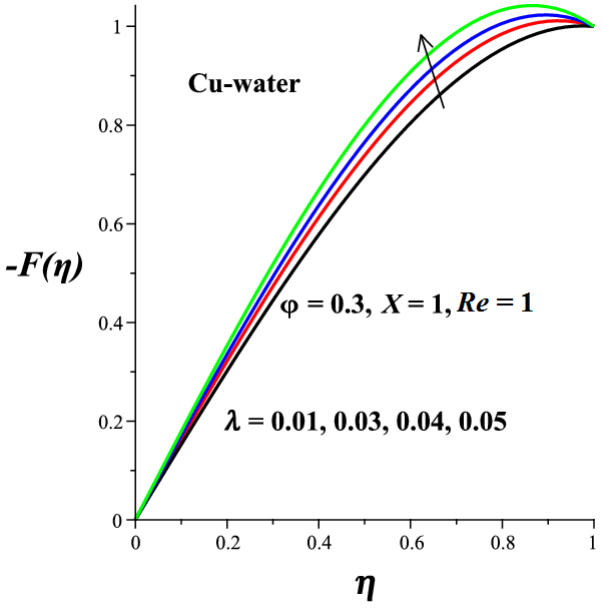

Figure 2.9: Normal velocity profiles with increasing λ

2.5.2 Temperature profiles with parameter variation

Figures 2.10-2.16 illustrate the nanofluids temperature profiles across the channel with different parameter variation. Generally, a decrease in the fluid temperature near the channel walls is observed due to

convective heat loss to ambient surrounding. It is noteworthy that the temperature of Cu-water nanofluid is generally higher than that of Al_2O_3-water nanofluid under the same flow condition as shown in Figure 2.10. In Figure 2.11, it is observed that the nanofluid temperature decreases with growing in nanoparticles volume fraction. Similar effect of a decrease in nanofluid temperature is observed in Figure 2.12 with Cu-water as working nanofluid as the Biot number increases. This is expected, since an increase in Biot number indicates a rise in convective cooling due to heat loss to the ambient surrounding from the channel walls. Meanwhile, a combine increase in the suction, Navier slip and viscous dissipation as shown in Figures 2.13-2.15 causes an increase in the nanofluid temperature. This may be attributed to the fact that as Re, λ, Ec increase the internal heat generation within the fluid due velocity gradient increases, leading to a rise in temperature. Figure 2.16 elucidates the temperature profiles with increasing axial distance along the channel. The nanofluid temperature decreases within the channel centreline region and increases near the wall region with increasing axial distance. Moreover, it is interesting to note that at point $\eta = 0.5$ within the channel, the nanofluid temperature is independent of the axial distance.

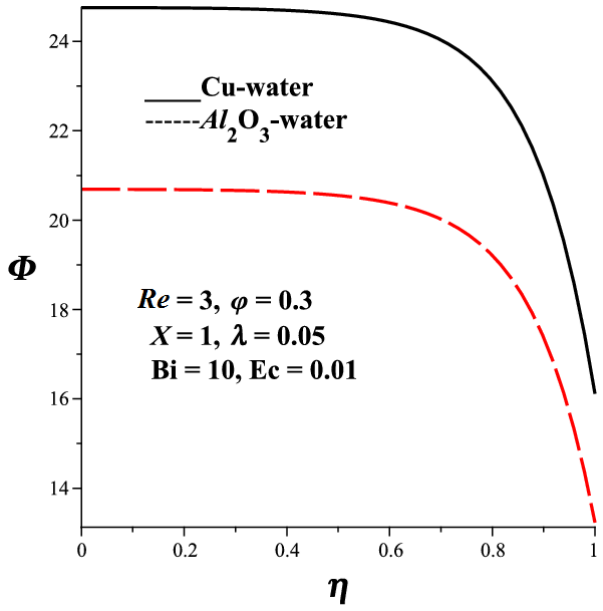

Figure 2.10: Nanofluids temperature profiles

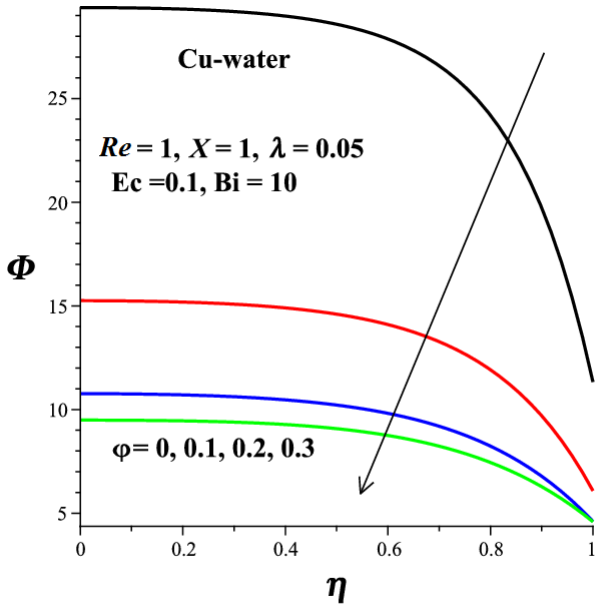

Figure 2.11: Temperature profiles with increasing φ

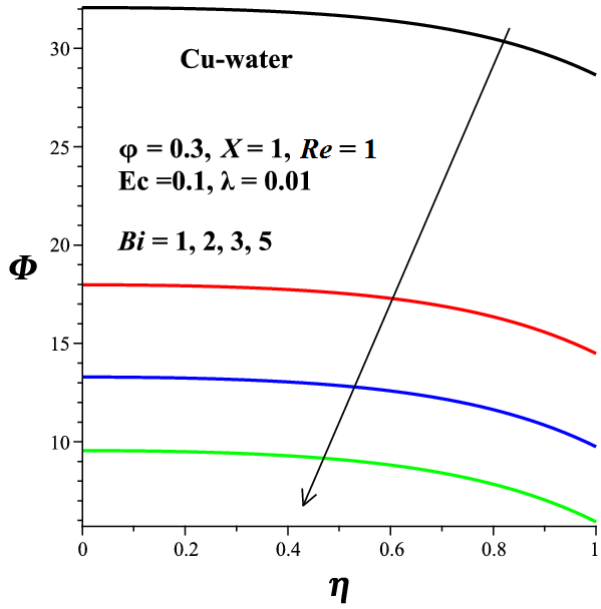

Figure 2.12: Temperature profiles with increasing Bi

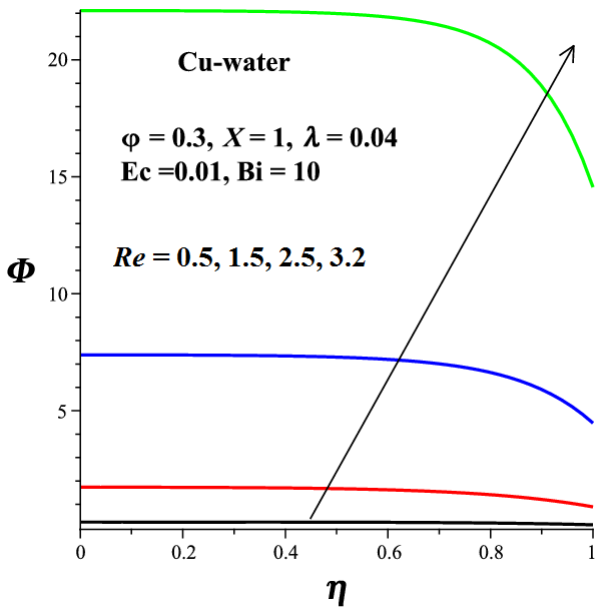

Figure 2.13: Temperature profiles with increasing Re

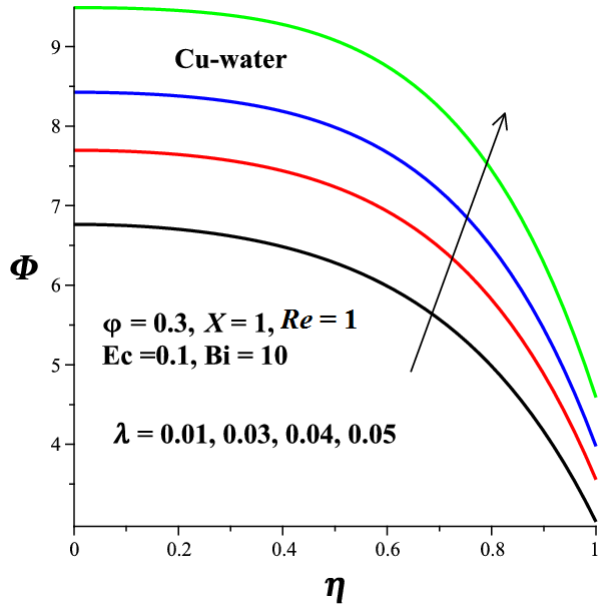

Figure 2.14: Temperature profiles with increasing λ

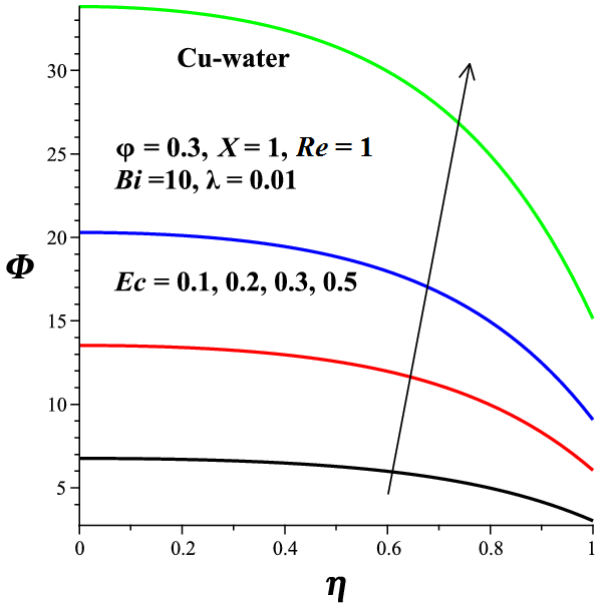

Figure 2.15: Temperature profiles with increasing Ec

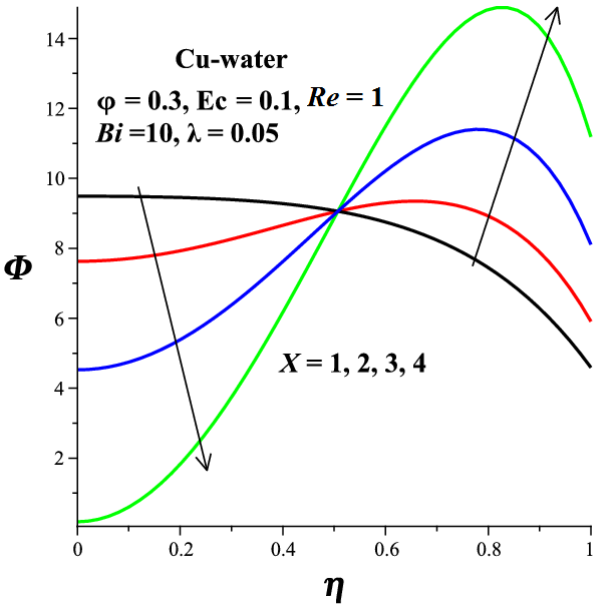

Figure 2.16: Temperature profiles with increasing X

2.5.3 Skin Friction, Pressure Gradient and Nusselt Number

Figures 2.17-2.18 depict the skin friction profiles for both Cu-water and Al_2O_3-water nanofluids at the channel walls. The skin friction generally increases with an increase in nanoparticles volume fraction, however, it is noticed that the skin friction produced by Cu-water is more intense than the one produced

by Al_2O_3-water as shown in Figure 2.17. This is expected since the velocity gradient of Cu-water near the channel walls is higher than thatAl_2O_3-water. In Figure 2.18, we observe that the skin friction generally increases with an increase in Navier slip. Meanwhile, a growing in suction ($Re > 0$) increases the skin friction while a growing in injection ($Re < 0$) decreases the skin friction. The pressure drop along the channel is illustrated in Figures 2.19-2.20. For both Cu-water and Al_2O_3-water nanofluids, the pressure drop increases with increasing nanoparticles volume fraction. Interestingly, the pressure drop produced by Al_2O_3-water is slightly higher than that of Cu-water as shown in Figure 2.19. Figure 2.20 shows a general increase in pressure drop with a rise in Navier slip. A growing in suction ($Re > 0$) decreases the pressure drop while a growing in injection ($Re < 0$) increases the pressure drop along the channel. Figures 2.21-2.23 elucidate the heat transfer rate at the channel walls with different parameter variation. It is observed that the wall heat transfer rate (Nu) decreases with an increase in the nanoparticles volume fraction as shown in Figure 2.21. A slight increase in Al_2O_3-water Nusselt number is noticed as compared to Cu-water Nusselt number. In Figure 2.22, We noted that the increase in the Navier slip parameter results in increase in Nusselt number. This may be due to a rise in the nanofluid temperature gradient at the channel walls. Meanwhile, as the suction increases, the heat flux at the wall increases while a decrease in wall heat is observed with a rise in injection. The strength of the wall heat flux is enhanced with increasing axial distance, viscous dissipation and convective cooling as illustrated in Figure 2.23. This can be attributed to a rise in the temperature gradient due to convective heat exchange with the ambient along the channel walls.

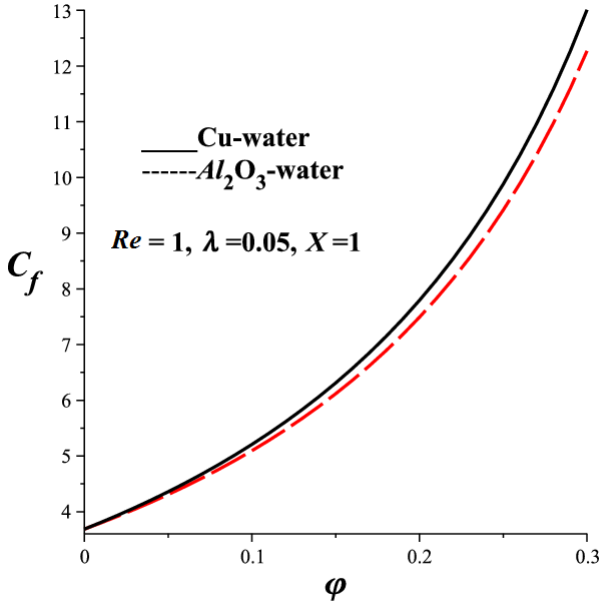

Figure 2.17: Skin friction with increasing φ

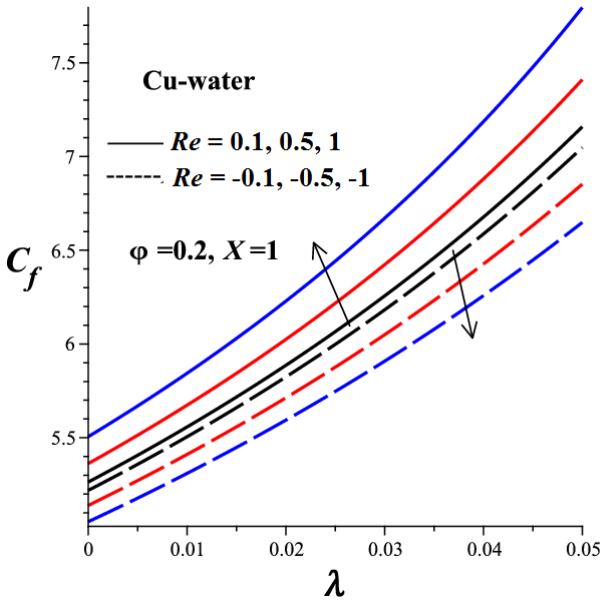

Figure 2.18: Skin friction with increasing Re and λ

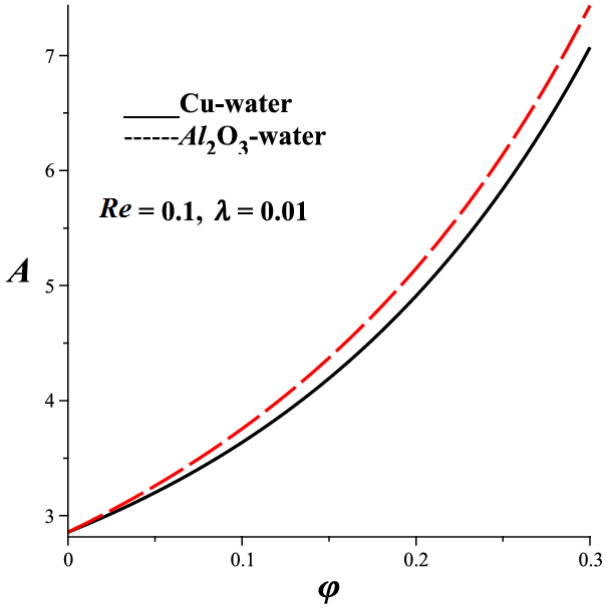

Figure 2.19: Axial pressure gradient with increasing φ

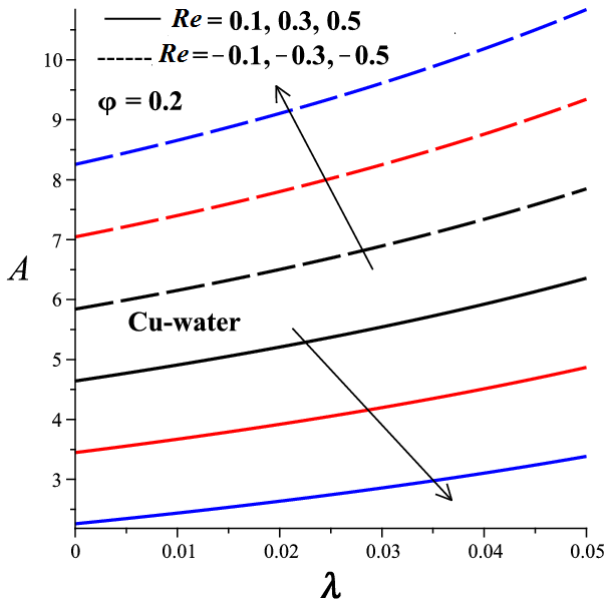

Figure 2.20: Axial pressure gradient with increasing Re and λ.

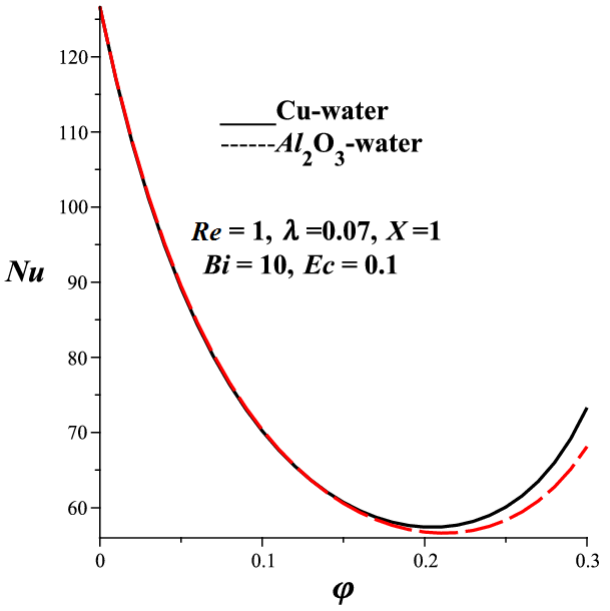

Figure 2.21: Nusselt number with increasing φ

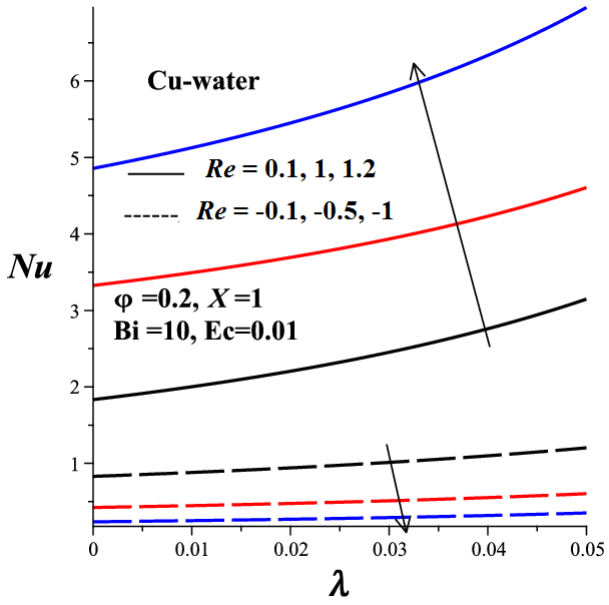

Figure 2.22: Nusselt number with increasing Re and λ.

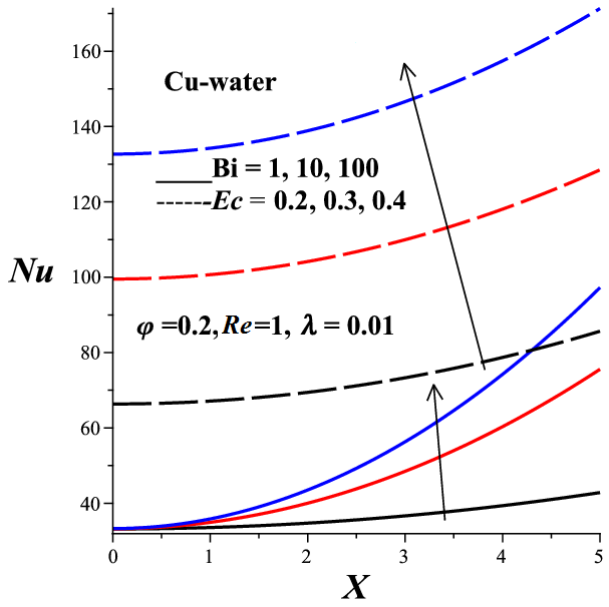

Figure 2.23: Nusselt number with increasing X, Bi and Ec.

2.6 Conclusion

The combined effects of viscous dissipation, Navier slip and convective cooling on Berman flow and heat transfer of water base nanofluids containing Cu and Al_2O_3 as nanoparticles are investigated in this chapter. The nonlinear model problem is tackled both analytically using perturbation series method

and numerically using Runge-Kutta-Fehlberg integration technique coupled with shooting scheme. We summarize below some of the essential features of physical interest from the above analysis.

- Cu-water nanofluid moves faster with enhanced flow reversal at the walls as compared to Al_2O_3 -water nanofluid.
- Nanofluids velocity and flow reversal at the walls increase with suction, λ and φ.
- Cu-water produce higher temperature as compared to Al_2O_3 -water. The nanofluids temperature increases with suction, λ and Ec, but decreases with Bi and φ.
- The skin friction produced by Cu-water is more intense than that of Al_2O_3 -water. The skin friction increases with suction ($Re > 0$), λ and φ but decreases with injection ($Re < 0$).
- The pressure drop produced by Al_2O_3 -water in more than that of Cu-water. The pressure drop is enhanced by injection, λ and φ but decrease by suction.
- The Nusselt number increases with suction, λ, Bi, Ec, X, but decreases with injection and φ. A slight increase in Nu for Al_2O_3 -water is noticed as compared to Cu-water.

CHAPTER THREE

Modelling the Effects of Variable Viscosity in Unsteady Flow of Nanofluids in a Pipe with Permeable Wall and Convective cooling[2]

Summary: In this chapter, we investigated the combined effects of variable viscosity, Brownian motion, thermophoresis and convective cooling on unsteady flow of nanofluids in a cylindrical pipe with permeable wall are investigated. It is assumed that the pipe surface exchange heat with the ambient following the Newton's law of cooling. Using a semi-discretization finite difference method coupled with Runge-Kutta-Fehlberg integration scheme, the nonlinear governing equations of momentum and energy balance, and the equation for nanoparticles concentration are tackled numerically. Useful results for the velocity, temperature, nanoparticles concentration profiles, skin friction and Nusselt number are obtained graphically and discussed quantitatively. The results show that both temperature and velocity profiles enhanced with the increase of viscosity parameter and Eckert number and reduced with the increase of Biot number, the nanoparticles concentration profiles is increasing with thermophoresis parameter and Biot number while decreasing with the increase of Brownian motion parameter.

3.1 Introduction

The classical challenges facing fluid mechanics which have received much attention in several industrial and engineering processes are the problems of heat transfer and fluid flow embedded in geometries with permeable walls. Some examples include; problems dealing with purification and filtration processes, transpiration cooling where the walls of a pipe containing heated fluid are protected from overheating by passing cooler fluid over the exterior surface of the pipe, petroleum technology, isotopes separation of Uranium-235 and Uranium-238 by gaseous diffusion for production of fuel used in nuclear reactor, controlling boundary layer flow over aircraft wings by injection or suction of fluid out of or into the wing, lubrication of porous bearings, ground water hydrology, leakage of water in river beds, methods of reducing rates of heat transfer in combustion chambers exhaust nozzles and porous walled flow reactors see Makinde *et al.* (2014). Several studies have been done to focus this area. Karode (2001) conducted a study on laminar flow in a channel with porous wall. He presented an analytical solution for the pressure drop in fluid flow in a rectangular slit and cylindrical tube for the case of constant wall permeability. Oxarango *et al.* (2004) proposed one-dimensional model to investigate the heat transfer in laminar flow

[2] This chapter is based on the paper:

Sara Khamis, Oluwole Daniel Makinde, Yaw Nkansah-Gyekye (2014). Modelling the effects of variable viscosity in unsteady flow of nanofluids in a pipe with permeable wall and convective cooling. *Applied and Computational Mathematics*, 3:75-84.

of a fluid in a channel with suction/injection w all. An analytic solution describing 2D steady laminar flow over an array of porous pipes for the case of low Reynolds number was presented by Moussy and Snider (2009). Several researchers have conducted the same study on heat transfer problems between two permeable parallel walls under different physical situations (Erdogan and Imrak, 2008; Tsangaris *et al.*, 2007; Theuri and Makinde, 2014; Mutuku-Njane and Makinde, 2014a).

Convectional heat transfer in fluids such as water, mineral oil and ethylene glycol are widely used for heat exchange purposes in the industries and building application. However, conventional fluids remain penalized by their limited thermal properties among which are their low thermal conductivity. An innovative way of improving the heat transfer of these fluids is to suspend small amounts of nanometer sized $(10 - 50nm)$ particles and fibers in the convective fluids. This new kind of fluid has attracted the interest of many researchers due to its thermal enhancement property. Nanofluids have enhanced thermophysical properties such as thermal conductivity, thermal diffusivity, viscosity and convective heat transfer coefficients compared with base fluids (Kaufui and Omar, 2010). Among the important features of nanoparticles suspended in convectional fluids are Brownian motion and thermophoresis (Xuan and Li, 2003). Brownian motion describes the random movement of nanoparticles in the base fluid. This random movement is due to collision of particles into each other. The collision passes on the kinetic energy of the particles to the molecules. Thermophoresis describes the nanoparticles dispersion in the base fluid due to temperature gradient.

Many researches have been conducted to analyze heat and mass transfer in nanofluids flow problems between two permeable walls under different physical situations. Mutuku-Njane and Makinde (2014b) performed a numerical analysis to investigate the combined effects on buoyancy and magnetic on a steady two-dimensional boundary layer flow of an electrically conducting water-based nanofluid containing three different types of nanoparticles: copper, aluminium oxide, and titanium dioxide past a convectively heated porous vertical plate with variable suction. Olanrewaju and Makinde (2013) formulated a problem on the boundary layer stagnation point flow of a nanofluid over a permeable flat surface with Newtonian heating. The combined effects of viscous dissipation and Newtonian heating on boundary-layer flow over a flat plate for three types of water-based nanofluids containing metallic or nonmetallic for a range of nanoparticle volume fractions was investigated by Makinde (2013a). He found that the heat transfer rate at the plate surface increases with increasing nanoparticle volume fraction and Biot number, while it decreases with the Brinkmann number. Recently, heat transfer characteristics of a Berman flow of water based nanofluids containing copper and alumina in a porous channel with Navier slip, viscous dissipation, and convective cooling was reported by Makinde *et al.* (2014). Moreover, many researchers studied the effects of temperature dependent viscosity in a nanofluid flow and heat transfer taking into account thermophoresis and Brownian motion. Makinde (2009) examined the effect of thermal radiation

on inherent irreversibility in the flow of a variable viscosity optically thin fluid through a channel with isothermal walls. Kuppalapalle *et al.* (2013) carried out a numerical study to investigate the effects of the temperature dependent viscosity on the flow and heat transfer of a nanofluid over a flat surface in the presence of viscous dissipation. Furthermore, the effect of variable viscosity on thermal boundary layer over a permeable flat plate with radiation and convective surface boundary condition was reported by Makinde (2012). However, in all studies the effects of variable viscosity in unsteady flow of nanofluids in a pipe with permeable wall and convective cooling have not been investigated.

Therefore, the present study aimed to investigate the combined effects of variable viscosity, Brownian motion, thermophoresis and convective cooling on unsteady flow of nanofluids in a pipe with permeable wall. In the subsequent sections 2 and 3 the details of the model formulation together with the numerical solution techniques employed to tackle the problem are presented. In section 4, pertinent results are displayed graphically and discussed. Finally, conclusions are drawn in section 5.

3.2 Mathematical Model

Consider the unsteady laminar flow of a water base incompressible variable viscosity nanofluids through a cylindrical pipe with permeable wall under the action of a constant axial pressure gradient. It is assumed that $V(>0)$ corresponds to uniform suction velocity at the pipe surface while $V(<0)$ represents fluid injection into the pipe and the pipe surface exchange heat with the ambient surrounding following Newton's law of cooling as depicted in Figure 3.1.

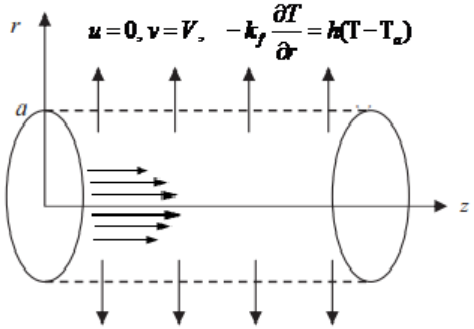

Figure 3.1: Schematic diagram of the problem

Using the Buongiorno nanofluid model (Buongiorno, 2006) with the Brownian motion and thermophoresis effects, the governing equations for continuity, momentum, energy, and nanoparticles concentration are:

$$\frac{\partial u}{\partial z} = 0, \tag{3.1}$$

$$\rho_f\left(\frac{\partial u}{\partial \bar{t}}+V\frac{\partial u}{\partial r}\right)=-\frac{\partial P}{\partial z}+\frac{1}{r}\left(r\mu_f(T)\frac{\partial u}{\partial r}\right), \tag{3.2}$$

$$\frac{\partial T}{\partial \bar{t}}+V\frac{\partial T}{\partial r}=\alpha_f\frac{1}{r}\left(r\frac{\partial T}{\partial r}\right)+\tau\left(D_B\frac{\partial T}{\partial r}\frac{\partial \varphi}{\partial r}+\frac{D_T}{T_0}\left(\frac{\partial T}{\partial r}\right)^2\right)+\frac{\alpha_f\mu_f(T)}{k_f}\left(\frac{\partial u}{\partial r}\right)^2, \tag{3.3}$$

$$\frac{\partial \varphi}{\partial \bar{t}}+V\frac{\partial \varphi}{\partial r}=\frac{D_B}{r}\frac{\partial}{\partial r}\left(r\frac{\partial \varphi}{\partial r}\right)+\left(\frac{\partial D_T}{\partial T_a}\right)\left(\frac{\partial^2 T}{\partial r}\right), \tag{3.4}$$

where D_B and D_T are the Brownian and thermophoretic diffusion coefficients respectively, u is the nanofluid velocity in the z-direction, r is the radial distance, a is the pipe radius, T is the nanofluid temperature, P is the nanofluid pressure, $\bar{t}$ is the time, T_a is the ambient temperature which also corresponds to the nanofluid initial temperature, φ is the concentration of nanoparticles, ρ is the nanofluid density, α_f is the thermal diffusivity of the nanofluid and τ is the ratio of solid particles heat capacitance to that of the nanofluid heat capacitance. The dynamic viscosity of nanofluid is assumed to be temperature dependent which can be expressed in (Theuri and Makinde, 2014; Klemp *et al.*, 1990):

$$\mu_f(T)=\mu_0 e^{-m(T-T_a)}, \tag{3.5}$$

where μ_0 is the nanofluid viscosity at the ambient temperature Ta and m is the variable viscosity parameter.

The initial and boundary conditions are given as follows:

$$u(r,0)=0,\quad T(r,0)=T_a,\quad \varphi(r,0)=\varphi_0, \tag{3.6}$$

$$\frac{\partial u}{\partial r}(0,\bar{t})=\frac{\partial T}{\partial r}(0,\bar{t})=\frac{\partial \varphi}{\partial r}(0,\bar{t})=0, \tag{3.7}$$

$$\begin{aligned} u(a,\bar{t}=0),\quad -k_f\frac{\partial T}{\partial r}(a,\bar{t}=0)&=h(T(a,\bar{t}=0)-T_a),\\ D_B\frac{\partial \varphi}{\partial r}(a,\bar{t}=0)&=-\frac{D_T}{T_a}\frac{\partial T}{\partial r}(a,\bar{t}=0), \end{aligned} \tag{3.8}$$

where h is the heat transfer coefficient, k_f is nanofluid thermal conductivity coefficient and φ_0 is the nanoparticles initial concentration. We introduce the dimensionless variables and parameters as follows:

$$\begin{cases} \theta=\dfrac{T-T_0}{T_a-T_0},\quad W=\dfrac{u}{V},\quad \eta=\dfrac{r}{a},\quad t=\dfrac{\bar{t}\nu_f}{a^2},\quad \nu_f=\dfrac{\mu_0}{\rho_f},\\ Re=\dfrac{Va}{\nu_f},\quad \overline{P}=\dfrac{aP}{\mu_0 V},\quad Nb=\dfrac{\tau D_B\varphi_0}{\alpha_f},\quad G=\dfrac{\partial \overline{P}}{\partial Z},\quad Pr=\dfrac{\mu_0 c_{pf}}{k_f}\\ Z=\dfrac{Z}{a},\quad Ec=\dfrac{V^2}{c_{pf}(T_a-T_0)},\quad H=\dfrac{\varphi}{\varphi_0},\quad N_t=\dfrac{\tau D_T(T_a-T_0)}{T_a\alpha_f},\\ Bi=\dfrac{ha}{k_f},\quad \beta=m(T_a-T_0),\quad Sc=\dfrac{\nu_f}{D_B},\quad \tau=\dfrac{(\rho c_p)_s}{(\rho c_p)_f}. \end{cases} \tag{3.9}$$

The dimensionless governing equations together with the appropriate initial and boundary conditions can be written as:

$$\frac{\partial W}{\partial t} + Re\frac{\partial W}{\partial \eta} = G + e^{-\beta\theta}\left(\frac{\partial^2 W}{\partial \eta^2} + \frac{1}{\eta}\frac{\partial W}{\partial \eta} - \beta\frac{\partial W}{\partial \eta}\frac{\partial \theta}{\partial \eta}\right), \tag{3.10}$$

$$Pr\frac{\partial \theta}{\partial t} + PrRe\frac{\partial \theta}{\partial \eta} = \frac{1}{\eta}\frac{\partial}{\partial \eta}\left(\eta\frac{\partial \theta}{\partial \eta}\right) + \left(Nb\frac{\partial \theta}{\partial \eta}\frac{\partial H}{\partial \eta} + Nt\left(\frac{\partial \theta}{\partial \eta}\right)^2\right) + EcPre^{-\beta\theta}\left(\frac{\partial W}{\partial \eta}\right)^2, \tag{3.11}$$

$$Sc\frac{\partial H}{\partial t} + ScRe\frac{\partial H}{\partial \eta} = \frac{1}{\eta}\frac{\partial}{\partial \eta}\left(\eta\frac{\partial H}{\partial \eta}\right) + \frac{Nb}{Nt}\frac{\partial^2 \theta}{\partial \eta^2}, \tag{3.12}$$

with initial and boundary conditions:

$$W(\eta, 0) = 0, \quad \theta(\eta, 0) = 0, \quad H(\eta, 0) = 1, \tag{3.13}$$

$$\frac{\partial W}{\partial \eta}(0, t) = \frac{\partial \theta}{\partial \eta}(0, t) = \frac{\partial H}{\partial \eta}(0, t) = 0, \tag{3.14}$$

$$W(1, t) = 0, \ \ \frac{\partial \theta}{\partial \eta}(1.t) = -Bi(\theta(1, t) - 1), \ \ \frac{\partial H}{\partial \eta}(1, t) = -\frac{Nt}{Nb}\frac{\partial \theta}{\partial \eta}(1, t), \tag{3.15}$$

where Re is Reynolds number such that $Re > 0$ represents suction, $Re < 0$ represents injection, and $Re = 0$ corresponds to the case of impermeable pipe wall, Nb is the Brownian motion parameter, Nt is the thermophoresis parameter, Bi is the Biot number, β is the variable viscosity parameter, Sc is the Schmidt number, Pr is the Prandtl number, Ec is the Eckert number and G is the pressure gradient parameter. The quantities of practical interest in this study are the skin friction coefficient C_f and the local Nusselt number Nu which are defined as:

$$C_f = \frac{a\tau_w}{\mu_0 V}, \quad Nu = \frac{aq_w}{k_f(T_a - T_0)}, \tag{3.16}$$

where τ_w is the wall shear stress and q_w is the heat flux at the pipe wall given by:

$$\tau_w = \mu_{nf}\left.\frac{\partial u}{\partial r}\right|_{r=a}, \quad q_w = -k_f\left.\frac{\partial T}{\partial z}\right|_{r=a}. \tag{3.17}$$

Substituting equations (3.17) into (3.16) and introducing dimensionless variables we have

$$C_f = e^{-\beta\theta}\left.\frac{\partial W}{\partial \eta}\right|_{\eta=1}, \quad Nu = \left.\frac{\partial \theta}{\partial \eta}\right|_{\eta=1} \quad Sh = \left.\frac{\partial H}{\partial \eta}\right|_{\eta=1} = \frac{Nb}{Nt}Nu. \tag{3.18}$$

3.3 Numerical Procedure

Equations (3.10)-(3.15) constitute a system of nonlinear initial boundary value problem (IBVP) and are solved numerically using a semi-discretization finite difference method known as method of lines (Na, 1979). Spatial interval $0 \leq \eta \leq 1$ is partitioned into N equal parts with grid size $\Delta\eta = 1/N$ and grid points $\eta_i = (i-1)\Delta\eta$, $1 \leq i \leq N+1$. The first and second spatial derivatives in equations (3.10)-(3.12) are approximated with second-order central finite differences. Let $W_i(t)$, $\theta_i(t)$ and $H_i(t)$ be approximation of $W(\eta,t)$, $\theta(\eta,t)$ and $H(\eta,t)$, then the semi-discrete system for the problem becomes:

$$\begin{aligned}\frac{dW_i}{dt} &= G - Re\frac{W_{i+1}-W_{i-1}}{2\Delta\eta} + e^{-\beta\theta_i}\frac{W_{i+1}-2W_i+W_{i-1}}{\Delta\eta^2} \\ &+ e^{-\beta\theta_i}\frac{W_{i+1}-W_{i-1}}{2\eta_i\Delta\eta} - \beta e^{-\beta\theta_i}\frac{(\theta_{i+1}-\theta_{i-1})(W_{i+1}-W_{i-1})}{4\Delta\eta^2},\end{aligned} \tag{3.19}$$

$$\begin{aligned}Pr\frac{d\theta_i}{dt} &= -PrRe\frac{\theta_{i+1}-\theta_{i-1}}{2\Delta\eta} + \frac{\theta_{i+1}-2\theta_i+\theta_{i-1}}{\Delta\eta^2} + \frac{\theta_{i+1}-\theta_{i-1}}{2\eta_i\Delta\eta} \\ &+ Nb\frac{(\theta_{i+1}-\theta_{i-1})(H_{i+1}-H_{i-1})}{4\Delta\eta^2} + Nt\left(\frac{\theta_{i+1}-\theta_{i-1}}{2\Delta\eta}\right)^2 \\ &+ EcPre^{\beta\theta}\left(\frac{W_{i+1}-W_{i-1}}{2\Delta\eta}\right)^2,\end{aligned} \tag{3.20}$$

$$\begin{aligned}Sc\frac{dH_i}{dt} &= -ScRe\frac{H_{i+1}-H_{i-1}}{2\Delta\eta}\frac{H_{i+1}-2H_i+H_{i-1}}{\Delta\eta^2} \\ &+ \frac{H_{i+1}-H_{i-1}}{2\eta_i\Delta\eta} + \frac{Nt}{Nb}\frac{(\theta_{i+1}-2\theta_1+\theta_{i-1})}{\Delta\eta^2},\end{aligned} \tag{3.21}$$

with initial conditions

$$W_i(0) = \theta_i(0) = 0, \quad H_i(0) = 1, \quad 1 \leq i \leq N+1. \tag{3.22}$$

The equations corresponding to the first and last grid points are modified to incorporate the boundary conditions as follows:

$$\begin{aligned}W_2 &= W_1, \quad \theta_2 = \theta_1, \quad H_2 = H_1, \quad W_{N+1} = 0, \\ \theta_{N+1} &= \theta_N(1 - Bi\Delta\eta) + Bi\Delta\eta, \quad H_{N+1} = H_N - Nt\frac{\theta_{N+1}-\theta_N}{Nb}.\end{aligned} \tag{3.23}$$

Equations (3.19)-(3.23) is a system of initial value nonlinear ordinary differential equations and can be solved iteratively using Runge-Kutta-Fehlberg integration technique (Na, 1979) implemented on a computer using MATLAB. From the process of numerical computation, the skin-friction coefficient and the Nusselt number in equation (3.18) are also worked out and their numerical values are presented.

3.4 Results and Discussion

The combined effects of temperature dependent viscosity, Brownian motion, thermophoresis and convective cooling on unsteady flow of nanofluids in a pipe with permeable wall are investigated. The semi-discretization approach is used to solve the governing non-linear partial different equation numerically. The numerical solution for the representative velocity profiles, temperature profiles, nanoparticles concentration profiles, skin friction and Nusselt number have been carried out by assigning some arbitrary chosen specific values to various parameters controlling the flow system. The results are presented in Figures 3.2 - 3.28. The Prandtl number (Pr) is assumed to be 6.2 which is within the range from $6.2 \leq Pr \leq 7.1$ the most encountered fluids in nature and frequently used in engineering and industries (Oztop and Abu-Nada, 2008; Kakac and Pramuanjaroenkij, 2009; Makinde, 2013b). Table 3.1 illustrates the effects of different parameters governing the flow on skin friction and Nusselt number coefficients.

3.4.1 Non-Dimensional Velocity Profiles with Parameter Variation

The effects of parameter variation on velocity profiles are displayed in Figures 3.2-3.9. In Figures 3.2 and 3.3, we observe that the nanofluid velocity is high at the centerline region of the pipe and is decreasing towards the pipe wall. Moreover, the velocity reaches its steady state quickly when the fluid is injected into the pipe ($Re < 0$) compared with suction ($Re > 0$). The velocity at the center of the pipe increases with increasing time and reaches its minimum value towards the pipe surface satisfying the prescribed initial and boundary conditions as demonstrated in Figure 3.4. Figure 3.5 illustrates the variation of nanofluid velocity with variable viscosity parameter. We note that the nanofluid moves faster with increasing variable viscosity parameter in the presence of suction. This is due to the fact that increasing β result in decreasing the viscosity of the nanofluids. Similar trend are observed with growing Eckert number and pressure gradient parameter as illustrated in Figure 3.6 and Figure 3.7, respectively. The opposite behavior is observed with increasing the Biot number as seen in Figure 3.8. Increasing Biot number leads to reduce the nanofluid velocity. This is because an increase in Biot number raises convective cooling due to heat loss to the ambient from the pipe surface and hence reduces the nanofluid velocity. The increases of nanofluid velocity with increasing suction and decreasing with increasing injection is observed from Figure 3.9.

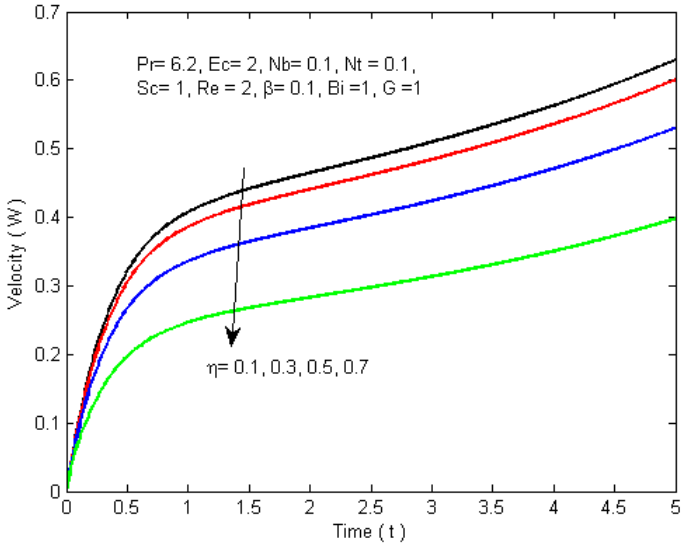

Figure 3.2: Velocity profiles with increasing distance

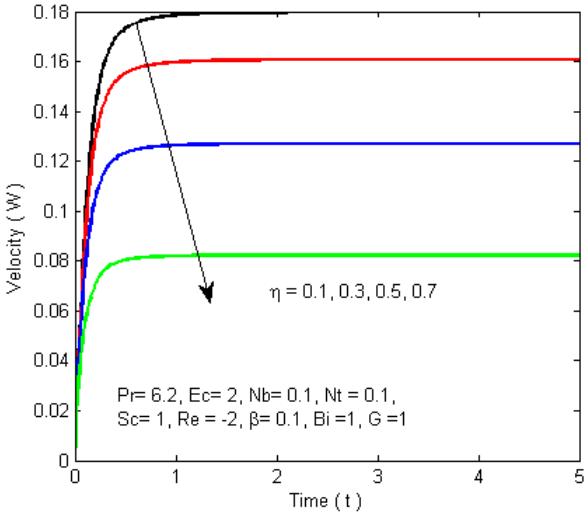

Figure 3.3: Velocity profiles with increasing distance

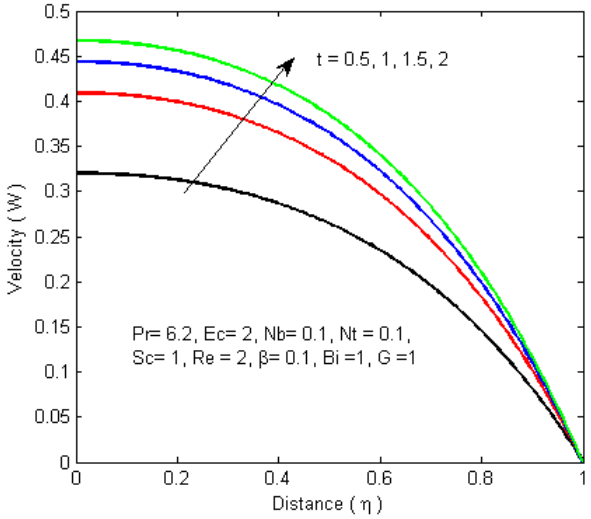

Figure 3.4: Velocity profiles with increasing time

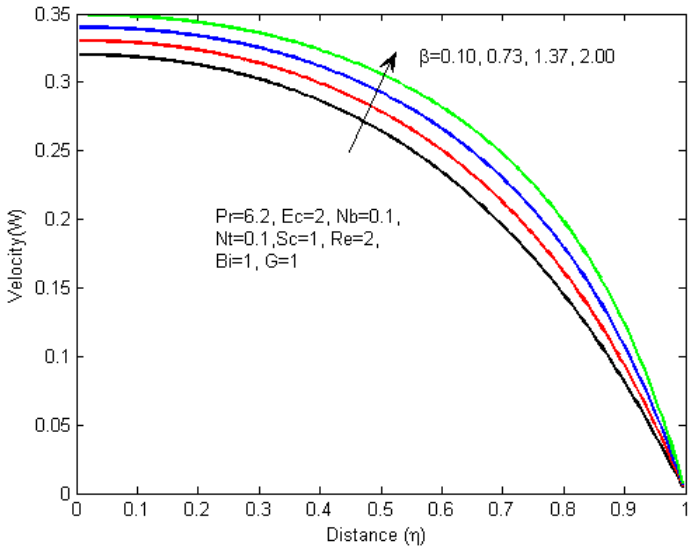

Figure 3.5: Velocity profiles with increasing β

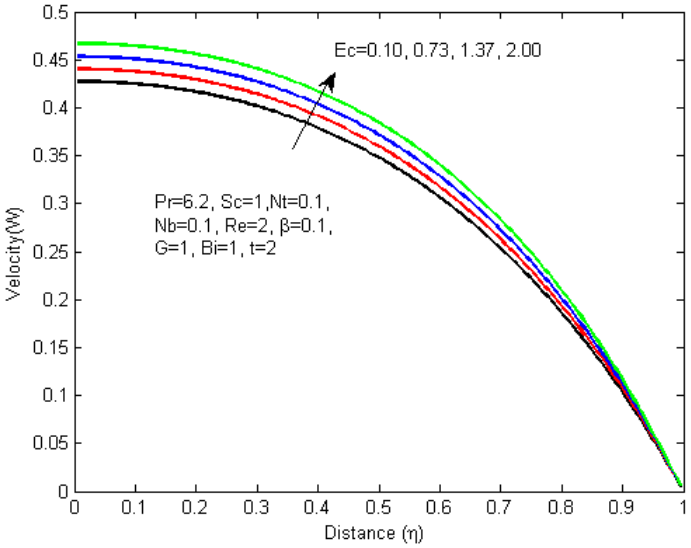

Figure 3.6: Velocity profiles with increasing Ec

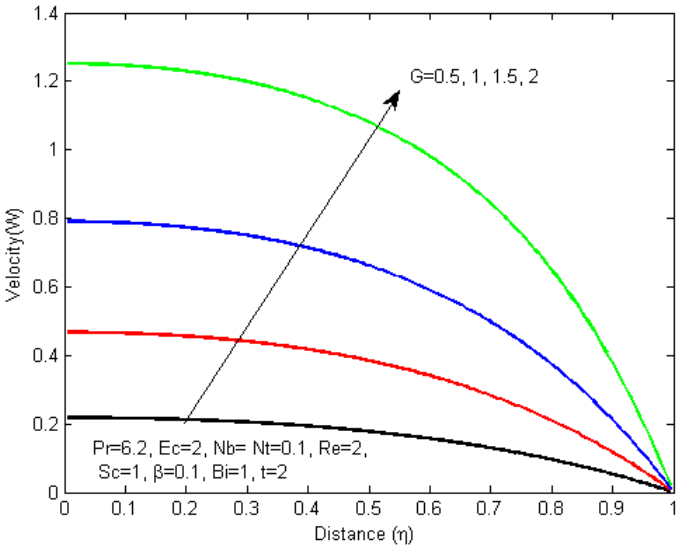

Figure 3.7: Velocity profiles with increasing G

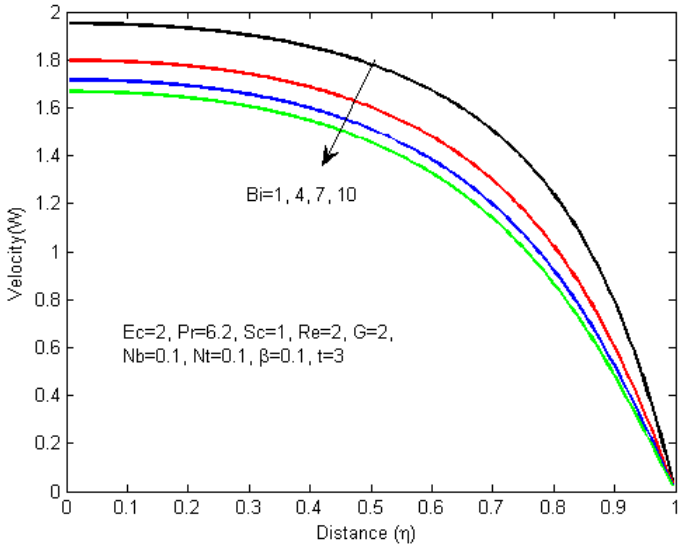

Figure 3.8: Velocity profiles with increasing Bi

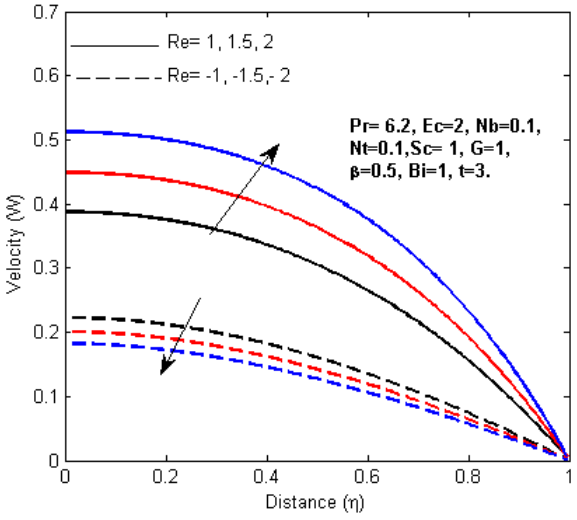

Figure 3.9: Velocity profiles with increasing distance suction and injection Re

3.4.2 Non- Dimensional Temperature Profiles with Parameter Variations

Figures 3.10-3.16 demonstrate the nanofluids temperature profiles across the pipe and the effect of different parameters in the fluid flow system. Generally, due to convective heat loss to ambient surrounding following the Newton's law of cooling, the nanofluid temperature near the pipe wall is shown decreasing. In Figure 3.10 and Figure 3.11, the profiles shows that the nanofluid temperature is higher at the pipe wall. However, the temperature reaches its steady state earlier when the external fluid added in to the pipe fluid (injection) as seen in Figure 3.11. An increase of the nanofluid temperature is observed with

increasing time and Eckert number as shown in Figures 3.12 and 3.13. This may be attributed to the fact that, as Ec increases the internal heat generation within the fluid due velocity gradient increases, leading to a rise in temperature. It is noted that the nanofluid temperature is decreasing at the centre of the pipe before the flow reversal near the pipe wall with increasing variable viscosity parameter as shown in Figure 3.14. The nanofluid temperature is increasing at the centreline region followed by flow reversal towards the pipe wall with increasing Biot as illustrated in Figure 3.15. This can be explained as, increasing Biot number indicates a rise in convective cooling due to heat loss to the ambient surrounding from the pipe surface and hence the temperature at that wall of pipe lead to the overall cooling of the bulk nanofluid. Figure 3.16 elucidates the temperature profiles variation with increasing injection and suction. We also observe that the nanofluid temperature decreases with increasing both suction and injection.

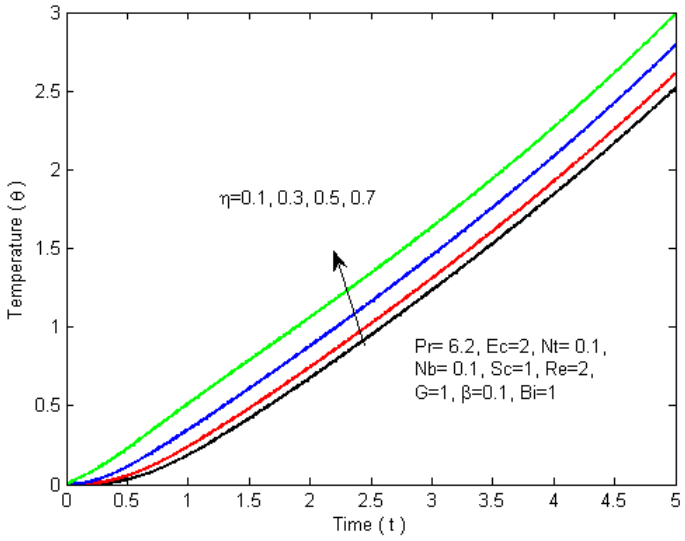

Figure 3.10: Temperature profiles with increasing distance

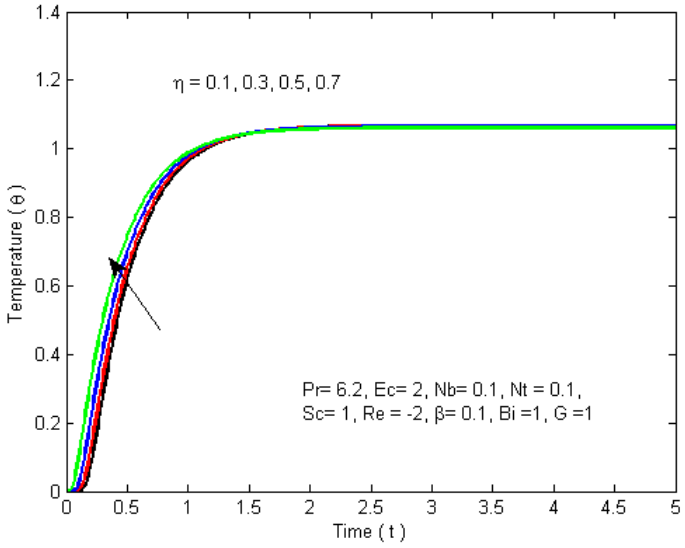

Figure 3.11: Temperature profiles with increasing distance

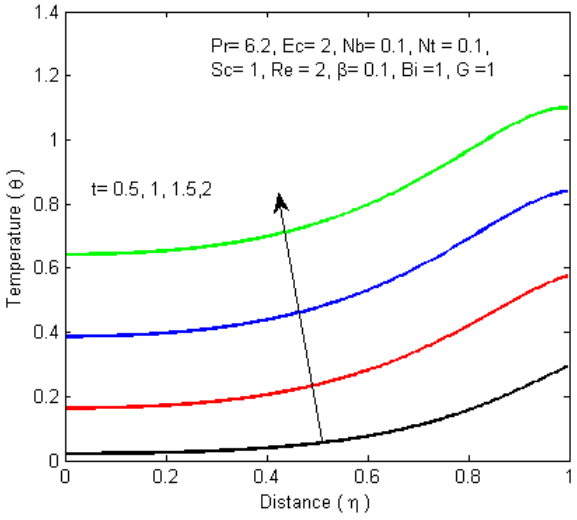

Figure 3.12: Temperature profiles with increasing Time

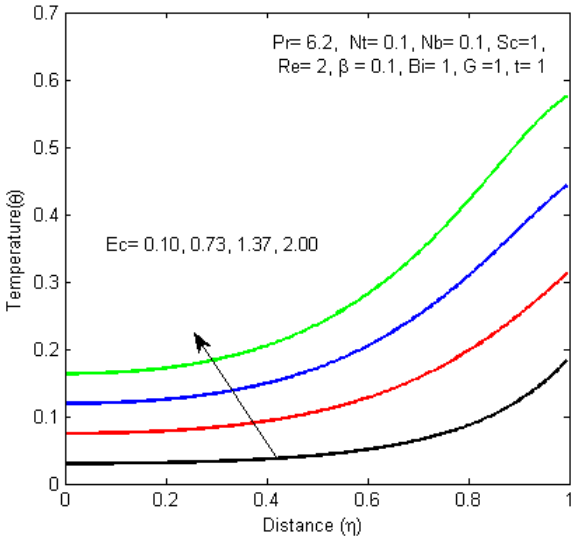

Figure 3.13: Temperature profiles with increasing Ec

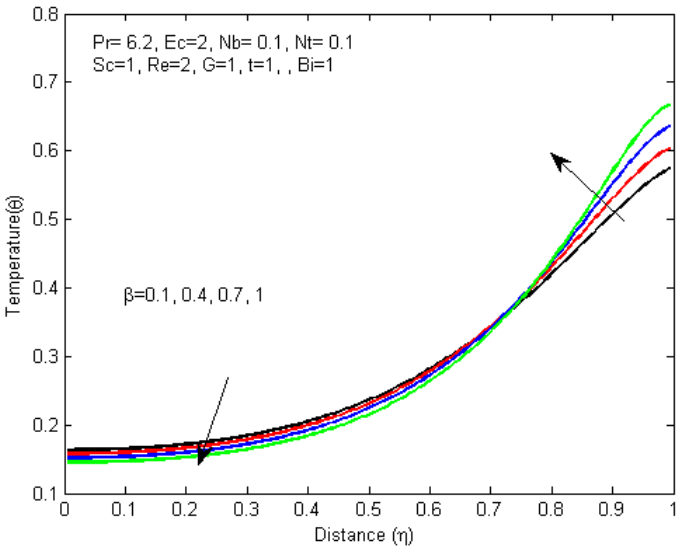

Figure 3.14: Temperature profiles with increasing β

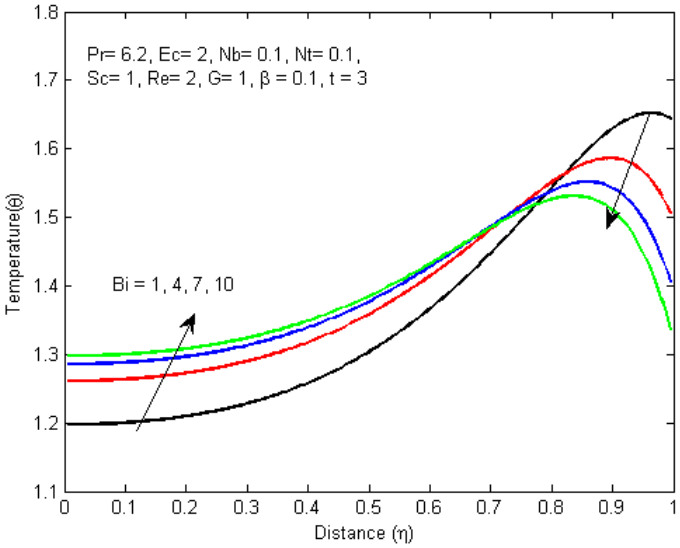

Figure 3.15: Temperature profiles with increasing Bi

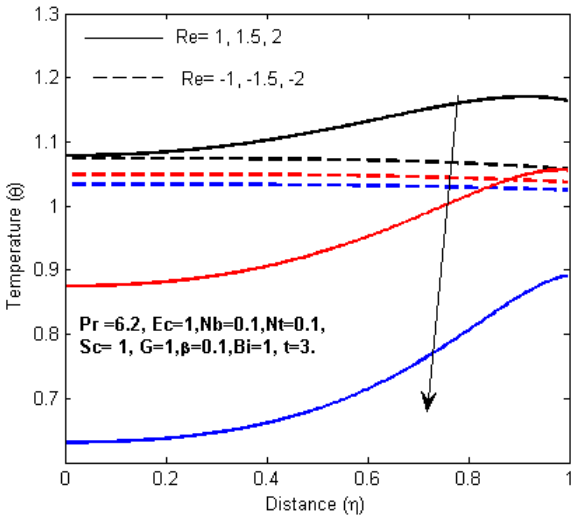

Figure 3.16: Temperature profiles with increasing suction and injection Reynolds number

3.4.3 Non-Dimensional Nanoparticles Volume Concentration Profiles with Parameter Variations

Figures 3.17-3.24 demonstrate the effects of various physical parameters which determine the flow on the nanoparticles concentration profiles. Figure 3.17 shows the effect of increasing distance to nanoparticles concentration. It is noted that at the first time, the nanoparticles volume fraction is high at the pipe wall for a very short time, and then become higher at the center of the pipe as time increases . In Figure 3.18, we note that the nanoparticles volume fraction increases with increasing time. In addition, the nanoparticles concentration at the center of the pipe is higher compared at the pipe surface. The effects of increasing viscosity, viscous dissipation and thermophoresis as shown in Figures 3.19-3.21 causes an increase in the nanoparticles concentration at the centreline region of the pipe and reverse towards the pipe wall. This could be explained as due to variation of kinetic energy of nanoparticles and mixtures of mobile particles in the fluid where the different particle exhibit different responses to the force of a temperature gradient. The opposite results is noted from Figure 3.22, with increasing the motion of particles (Nb), the nanoparticles concentration is decreasing at the centre of the pipe and more concentrated near the pipe wall. In Figure 3.23, the increase of nanoparticles concentration with increasing Biot number is observed. The nanoparticles volume fraction become more concentrated with increasing suction compared with increasing injection as illustrated in Figure 3.24.

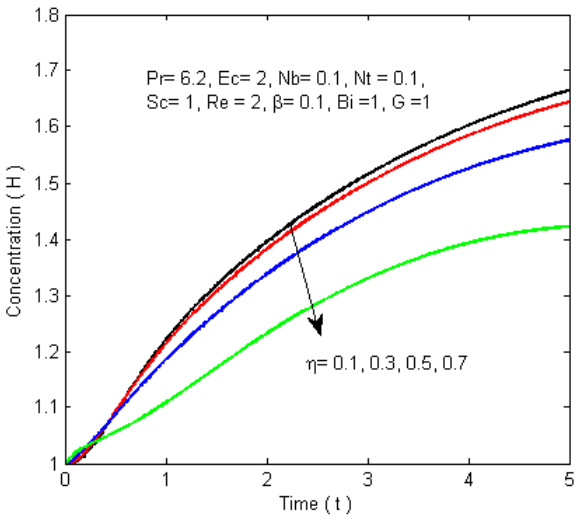

Figure 3.17: Nanoparticles distribution profiles with increasing distance

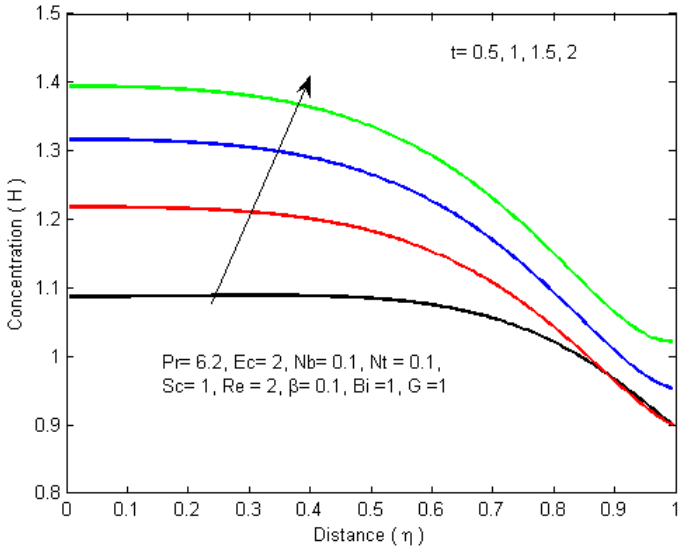

Figure 3.18: Nanoparticles distribution profiles with increasing time

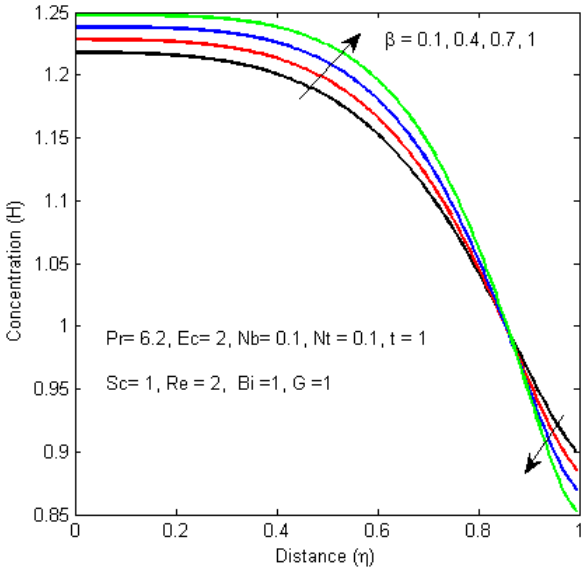

Figure 3.19: Nanoparticles distribution profiles with increasing β

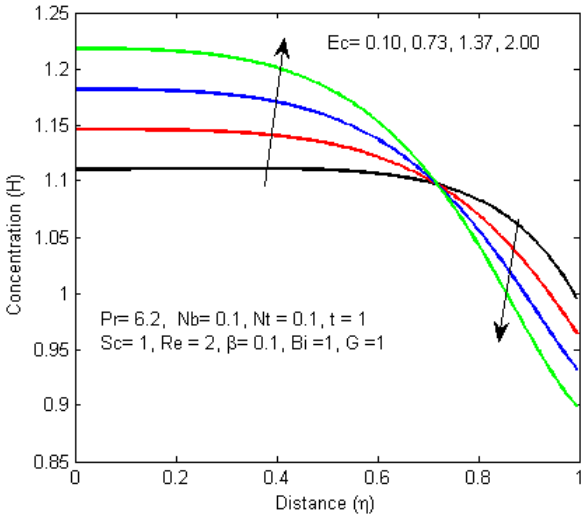

Figure 3.20: Nanoparticles distribution profiles with increasing Ec

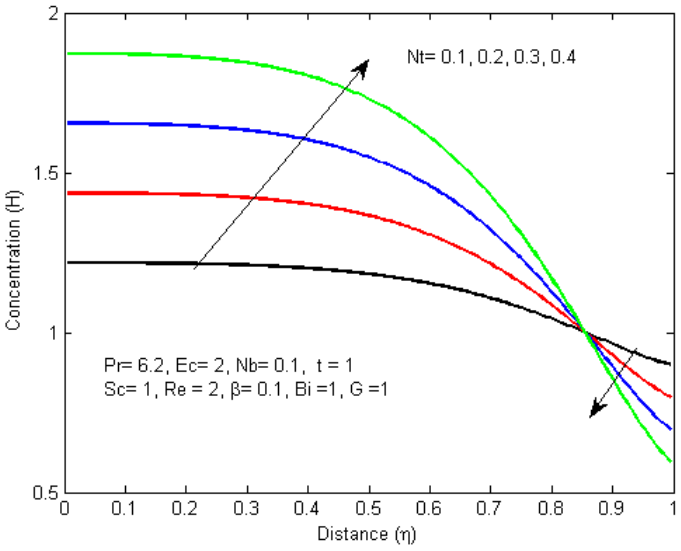

Figure 3.21: Nanoparticles distribution profiles with increasing Nt

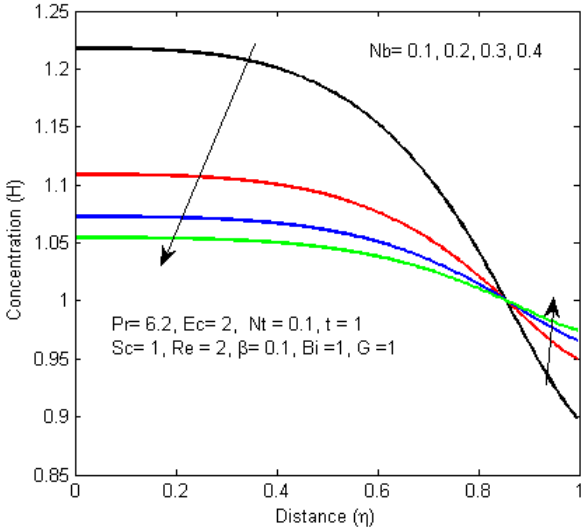

Figure 3.22: Nanoparticles distribution profiles with increasing Nb

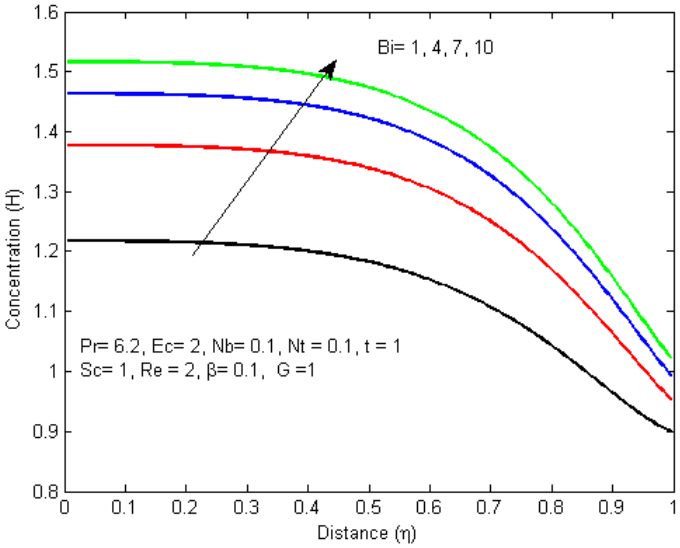

Figure 3.23: Nanoparticles distribution profiles with increasing Bi

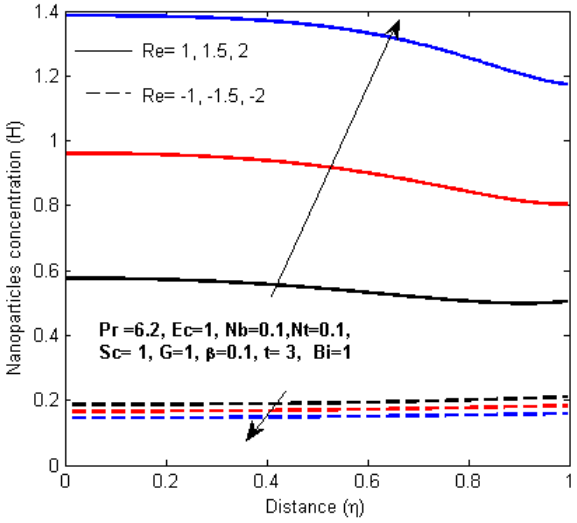

Figure 3.24: Nanoparticles distribution profiles with increasing Re

3.4.4 Skin Friction and Local Nusselt Number with Parameters Variation

Figures 3.25-3.28 together with Table 3.1 demonstrate the variations of skin friction and Nusselt number with different parameters. In general, Biot number, Eckert number, variable viscosity parameter, pressure gradient parameter and Reynolds number have high effects on skin friction and Nusselt number coefficients while Brownian motion and thermophoresis parameters have less effect. Keeping fixed values of parameters, both Nusselt number and skin friction varies with time. We observe that the friction between the pipe surface and nanofluid relative to motion is increasing negatively with increasing, Eckert number, Biot number, and pressure gradient for $t = 3$, as shown in Table 3.1. The opposite observation is seen with Nusselt number. The convective to conductive heat transfer (Nu) at the pipe surface is increasing with Eckert number, Biot number, and pressure gradient. Figures 3.25-3.28 supplement the information obtained from Table 1 for the time interval $[0, 5]$. The friction between the pipe wall and the fluid is decreasing with increasing Ec and β for some range of time and then reverse the behavior as shown in Figure 3.25. Figure 3.26 points out that growth in suction $(R > 0)$ magnifies the skin friction while a growth in injection $(R < 0)$ reduces the skin friction. Figure 3.27 elucidates the rate of heat transfer at the pipe wall with increasing Ec and β. The heat transfer rate (Nu) is high with increasing both Ec and β. The heat transfer rate is increasing with increasing suction and decreasing with increasing injection this is illustrated in Figure 3.28

Table 3.1: computation showing the skin friction and Nusselt number $Pr = 6.2$, $Sc = 1$.

t	Bi		Ec	Nt	Nb	Re	G	C_f	Nu
1	1	0.1	1	0.1	0.1	2	1	-1.0512	-0.6306
3	1	0.1	1	0.1	0.1	2	1	-1.1570	-0.1067
5	1	0.1	1	0.1	0.1	2	1	-1.2245	0.4242
3	5	0.1	1	0.1	0.1	2	1	-1.1742	0.1207
3	10	0.1	1	0.1	0.1	2	1	-1.1816	0.4510
3	1	0.4	1	0.1	0.1	2	1	-1.4389	0.1209
3	1	0.8	1	0.1	0.1	2	1	-2.0621	0.7045
3	1	0.1	2	0.1	0.1	2	1	-1.2184	0.6491
3	1	0.1	3	0.1	0.1	2	1	-1.2902	1.5260
3	1	0.1	1	0.2	0.1	2	1	-1.1570	-0.1058
3	1	0.1	1	0.4	0.1	2	1	-1.1572	-0.1040
3	1	0.1	1	0.1	0.2	2	1	-1.1570	-0.1067
3	1	0.1	1	0.1	0.4	2	1	-1.1570	-0.1067
3	1	0.1	1	0.1	0.1	-2	1	-0.2695	0.0248
3	1	0.1	1	0.1	0.1	0	1	-0.4982	0.1351
3	1	0.1	1	0.1	0.1	2	1.5	-1.8530	0.8558
3	1	0.1	1	0.1	0.1	2	2	-2.7467	2.5565

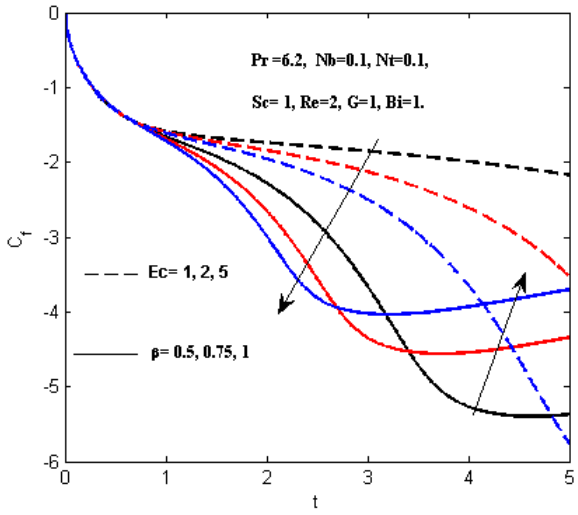

Figure 3.25: Nanoparticles distribution profiles with increasing Re

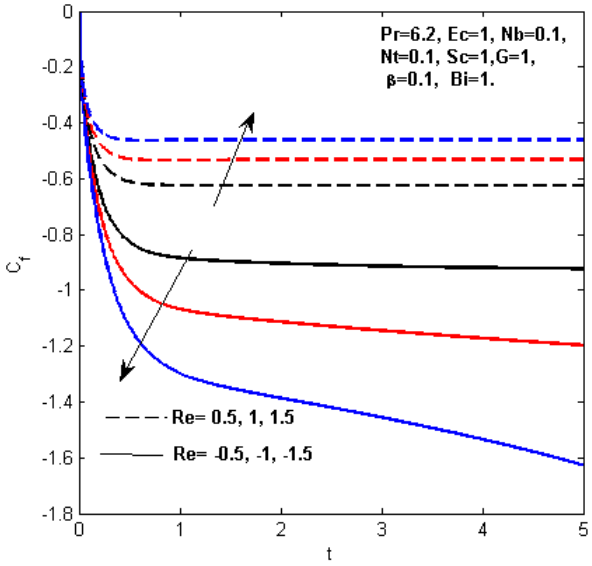

Figure 3.26: Nanoparticles distribution profiles with increasing Re

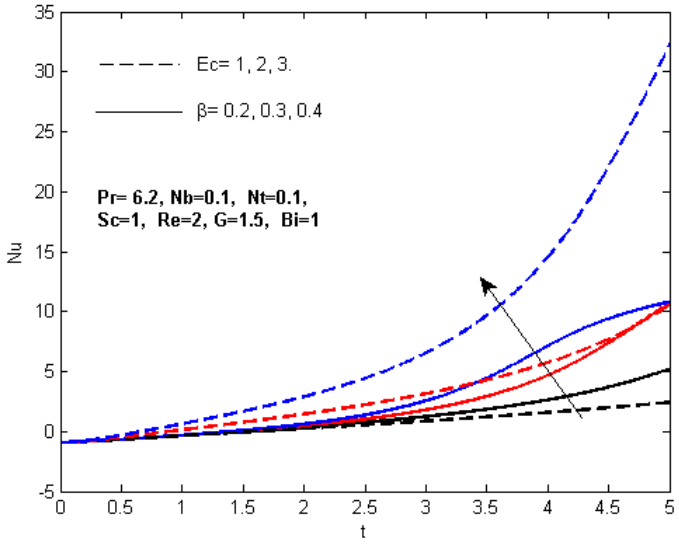

Figure 3.27: Nanoparticles distribution profiles with increasing Re

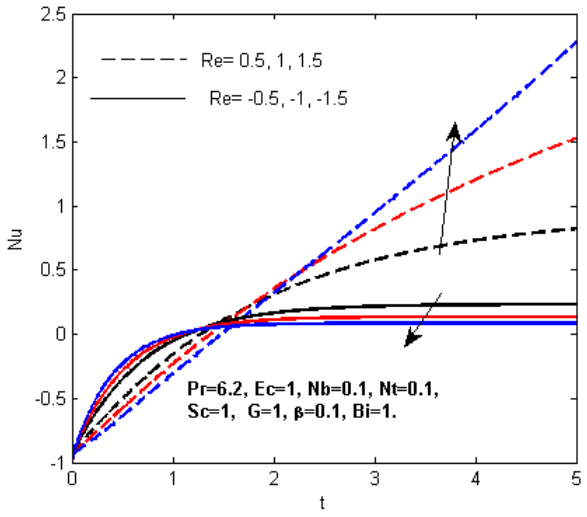

Figure 3.28: Nanoparticles distribution profiles with increasing Re

3.5 Conclusion

In this chapter, the combined effects of temperature dependent viscosity, Brownian motion, thermophoresis and convective cooling on unsteady flow of nanofluids in a pipe with permeable wall are investigated. The coupled nonlinear governing equations were derived, non-dimensionalised and numerically solved using a semi-discretization finite difference method coupled with a Runge-Kutta-Fehlberg integration scheme. Based on the graphical representations, the following main conclusions are drawn:

- The nanofluid velocity and temperature reaches its steady state quickly with injection $(Re < 0)$ compared with suction $(Re > 0)$.
- The nanofluid moves faster with increasing variable viscosity parameter, Eckert number, pressure gradient and suction and reducing with increasing Biot number and injection.
- The nanofluid temperature is increasing near the pipe wall with increasing Eckert number and variable viscosity parameter and reduced due to convective heat loss to ambient following the Newton's law of cooling. The nanofluid temperature decreases with increasing both suction and injection.
- The nanoparticles volume fraction is increasing at the centreline region with increasing Biot number, viscosity parameter, Eckert number, and thermophoresis while decreasing with Brownian motion.
- Skin friction and Nusselt number coefficients are more affected with Biot number, Eckert number, variable viscosity parameter, pressure gradient parameter and Reynolds number while Brownian motion and thermophoresis parameters have less effect.
- Skin friction and Nusselt number are increasing with increasing suction $(Re > 0)$ and decreasing with increasing injection $(Re < 0)$.

CHAPTER FOUR

Modelling the Effects of Variable Viscosity in Unsteady Flow of Nanofluids in a Pipe with Permeable Wall and Convective cooling[3]

Summary: This chapter investigates the combined effects of buoyancy force and variable viscosity on unsteady flow and heat transfer of water base nanofluid containing Copper (Cu) and Alumina (Al_2O_3) as nanoparticles through a cylindrical pipe with permeable wall. The non-linear partial differential equations governing the flow and heat transfer problem are obtained and solved numerically using a semi-discretization finite difference method coupled with Runge-Kutta-Fehlberg integration scheme. The numerical solutions for velocity, temperature, skin friction and Nusselt number have been presented graphically to show the effects of different nanoparticles and parameters embedded in the flow system. Our results show that with suction, Cu-water produces higher skin friction and heat transfer rate than Al_2O_3-water. Both nanofluids velocity and temperature increase with a decrease in viscosity and an increase buoyancy force intensity.

4.1 Introduction

Heat transfer enhancement using nanofluids has become a hot topic in recent years due to their various practical applications in industrial and engineering systems. The thermal conductivity of heat-transfer fluids is fundamental in the development of energy-efficient heat-transfer equipment. However, conventional heat-transfer fluids, such as water, oil and ethylene glycol, are inherently low efficient heat transfer fluids. Fluids containing suspended crystalline solid particles are expected to display significantly enhanced thermal conductivities as crystalline solids have thermal conductivities of 1-3 orders of magnitude larger than those of basic heat transfer fluids. Nanofluids have many applications in the industries since the nanometer size solid materials used have unique chemical and physical properties.The cooling applications of nanofluids include silicon mirror cooling, electronics cooling, vehicle cooling and transformer cooling. Other areas where nanofluids can be employed are in heat exchange electronics systems, micro-electro-mechanical system, auto-mobile engines, welding equipment and cooling of nuclear reactors Choi (1995); Wang *et al.* (1999). Most common techniques used in the production of nanofluids are: the single-step technique in which nanoparticles are evaporated directly into the base fluid and the 2-step technique in which nanoparticles are first prepared by either the inert gas-condensation method or

[3] This chapter is based on the paper:

Sara Khamis, Oluwole Daniel Makinde and Yaw Nkansah-Gyekye (2015). Unsteady flow of Variable Viscosity Cu-water and Al_2O_3-water Nanofluids in a Porous Pipe with Buoyancy force. *International Journal of Numerical Methods for Heat and Fluid Flow*, 25(7).

chemical vapour deposition method and then dispersed into the base fluid (Wang and Mujumdar, 2007). Choi (1995) studied the enhancement of thermal conductivity of fluids using n anoparticles. Thereafter, theoretical, experimental and numerical researches have been done by several authors to demonstrate nanofluids distinctly enhanced heat transfer properties which go up with increasing volumetric fraction of nanoparticles. Wang and Mujumdar (2007) summarizes the researches on flow and heat transfer characteristics of nanofluids in forced and natural convective flows. Kiblinski *et al.* (2002) presented a review to discuss the thermophysical properties of nanofluids and future challenges. Eastman *et al.* (2001) observed that Al203-water and CuO-water with 5% nanoparticles volume fractions increased the thermal conductivity by 29% and 60%, respectively. Oztop and Abu-Nada (2008) performed a numerical inves-tigation on natural convection involving nanofluids in partially heated rectangular enclosures. A detail critical synthesis of thermophysical properties of nanofluids was reported by Khanafer and Vafai (2011). Other authors such as Tham *et al.* (2011); Wen and Ding (2005); Xuan and Li (2003); Wang *et al.* (2013); Makinde (2013b); Kakac and Pramuanjaroenkij (2009); Patrulescu *et al.* (2014) etc., have investigated the nanofluid dynamics and thermophysical characteristics under various physical situations. Meanwhile, buoyancy driven flow and heat transfer in vertical geometries have many significant applica-tions in industrial and engineering systems such as electrical and microelectronic equipments containers, solar-collectors, geothermal engineering, petroleum reservoirs, thermal buildings insulation, etc. Many studies have been published to discuss the importance of buoyancy force on fluid flow and heat transfer under several physical conditions. Eegunjobi and Makinde (2012) investigated the combined effects of buoyancy force and Navier slip on the entropy generation rate in a vertical porous channel with wall suction/injection. They found that increase of Grashof number slightly increases the entropy generation rate at the injection wall. Kuznetsov and Nield (2010) presented a similarity solution of natural convec-tive boundary-layer flow of a nanofluid past a vertical plate. Their results show that the reduced Nusselt number is a decreasing function of each of buoyancy-ratio number Nr, a Brownian motion number Nb and a thermophoresis number Nt. Mutuku-Njane and Makinde (2013) performed a numerical study to investigate the combined effect of buoyancy force and Navier slip on magneto-hydrodynamic flow of a nanofluid over a convectively heated vertical porous plate. The results show that the velocity decreases while local skin friction increases with Grashof number (buoyancy force parameter). Theoretical investi-gation for buoyancy-driven heat transfer in 2D enclosure utilizing nanofluids was published by Khanafer *et al.* (2003). Recently, Nazari *et al.* (2015) studied experimentally the forced convective heat transfer due to flow of Al_2O_3-water nanofluid through a pipe filled with a metal foam. Sheikholeslami *et al.* (2014) presented a study of natural convection heat transfer in a nanofluid filled enclosure with elliptic inner cylinder. Their results reveal that heat transfer rate increases with an increase of nanoparticle volume fraction, Rayleigh numbers and inclination angle. Makinde *et al.* (2014) investigated the heat transfer

characteristics of a Berman flow of water based nanofluids containing copper and alumina in a porous channel with Navier slip, viscous dissipation, and convective cooling. Mansour *et al.* (2014) performed a numerical study investigating natural convection fluid flow and heat transfer inside C-shaped enclosures filled with Cu-water nanofluid using the finite difference met hod. Kandelousi (2014) studied the hydrothermal behavior of nanofluid fluid between two parallel plates to list a fe w. However, the study on transient flow of variable viscosity Cu-water and Al_2O_3-water nanofluids in a porous pipe driven by the buoyancy force effect has not been reported yet in the literature. Therefore, the objective of the present work is to study the combined effect of buoyancy force and variable viscosity parameters on an unsteady nanofluids flow past a vertical porous pipe. The numerical solution of dimensionless velocity profiles, temperature profiles, skin friction and Nusselt number profiles for wide range of parameters under axisymmetric conditions are presented graphically and discussed quantitatively.

4.2 Mathematical Model

Consider an unsteady laminar flow of incompressible water base nanofluids containing two types of nanoparticles, i.e., Copper (Cu) and Alumina (Al_2O_3) with variable viscosity and buoyancy force in a cylindrical pipe with permeable wall under the action of a constant axial pressure gradient and uniform suction/injection. We assume that $V > 0$ corresponds to uniform suction velocity at the pipe surface while $V < 0$ represent fluid injection into the pipe. We also assumed that both the base fluid (i.e., water) and the nanoparticles are in thermal equilibrium and no slip occurs between them. A cylindrical coordinate system (r, z) is considered where, z-axis is taken along centre of the pipe and r-axis is normal to the pipe surface as seen in Figure 4.1 below.

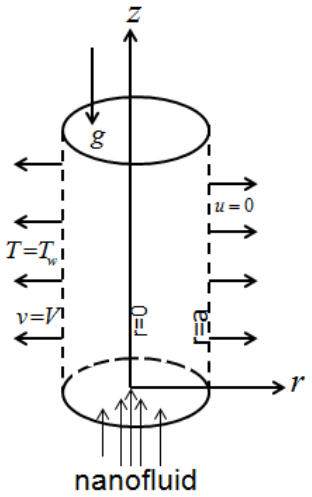

Figure 4.1: Physical geometry and coordinate system

Under Bousinessq approximation for density variation due to temperature with the Buongiorno nanofluid model (Buongiorno, 2006). The governing equations for the continuity, momentum, and energy describing the flow are as follows:

$$\frac{\partial u}{\partial z} = 0, \tag{4.1}$$

$$\rho_{nf}\left(\frac{\partial u}{\partial \bar{t}} + V\frac{\partial u}{\partial r}\right) = -\frac{\partial \bar{P}}{\partial z} + \frac{1}{r}\left(r\mu_f(T)\frac{\partial u}{\partial r}\right) + \rho_{nf}\gamma_{nf}(T - T_0), \tag{4.2}$$

$$(\rho c_p)nf\left(\frac{\partial T}{\partial \bar{t}} + V\frac{\partial T}{\partial r}\right) = k_{nf}\frac{1}{r}\left(r\frac{\partial T}{\partial r}\right) + \mu_{nf}(T)\left(\frac{\partial u}{\partial r}\right)^2, \tag{4.3}$$

with initial and boundary conditions:

$$u(r,0) = 0, \quad T(r,0) = T_0, \tag{4.4}$$

$$\frac{\partial u}{\partial r}(0,\bar{t}) = \frac{\partial T}{\partial r}(0,\bar{t}) = 0, \tag{4.5}$$

$$u(a,\bar{t}=0), \quad T(a,\bar{t}) = T_w. \tag{4.6}$$

The dynamic viscosity of the nanofluid is assumed to be temperature dependent expressed as (Ahmad *et al.*, 2011; Sahin, 1999; Klemp *et al.*, 1990)

$$\mu_{nf}(T) = \mu_0 e^{-m(T-T_0)}, \tag{4.7}$$

where u is the nanofluid axial velocity, P is the pressure, T is the bulk nanofluid temperature, T_0 is the nanofluid initial temperature, T_w is the pipe surface temperature, g is the gravitational acceleration, μ_0 is the initial dynamics viscosity, m is the variable viscosity parameter, $\mu_{nf}, \gamma_{nf}, k_{nf}, \rho_{nf}, \alpha_{nf}, (\rho c_p)_{nf}$ is the effective dynamic viscosity, volumetric expansion coefficient, thermal conductivity, density, thermal diffusivity and heat capacitance of the nanofluid respectively which are defined as (Mutuku-Njane and Makinde, 2013):

$$\left.\begin{aligned} &\mu_{nf} = \frac{\mu_f}{(1-\varphi)^{2.5}}, \quad \rho_{nf} = (1-\varphi)\rho_f + \varphi\rho_s, \quad \alpha_{nf} = \frac{k_{nf}}{(\rho c_p)_{nf}}, \\ &\gamma_{nf} = (1-\phi)\gamma_f + \varphi\gamma_s, \quad \frac{k_{nf}}{k_f} = \frac{k_s + 2k_f - 2\varphi(k_f - k_s)}{k_s + 2k_f + \varphi(k_f - k_s)}, \\ &(\rho c_p)_{nf} = (1-\varphi)(\rho c_p)_f + \varphi(\rho c_p)_s. \end{aligned}\right\} \tag{4.8}$$

In equation (4.8), φ is the nanoparticles solid volume fraction, ρ_f is the reference density of the fluid fraction, ρ_s is the reference density of the solid fraction, γ_f is the volumetric expansion of the fluid, γ_s is the volumetric expansion of solid fraction, μ_f is the viscosity of the fluid fraction, k_f is the thermal conductivity of the fluid fraction, c_p is the specific heat at constant pressure and k_s is the

thermal conductivity of the solid volume fraction. We introduce the following dimensionless variables and parameters:

$$\left.\begin{aligned}
&\theta = \frac{T - T_0}{T_w - T_0}, \quad W = \frac{u}{V}, \quad \eta = \frac{r}{a}, \quad t = \frac{\bar{t}\nu_f}{a^2}, \quad \nu_f = \frac{\mu_0}{\rho_f}, \quad Re = \frac{Va}{\nu_f} \\
&\tau = \frac{(\rho c_p)_s}{\rho c_p)_f}, \quad \overline{P} = \frac{aP}{\mu_0 V}, \quad Gr = \frac{g(\rho\gamma)_f (T_w - T_0)a^2}{V\mu_0}, \quad A = \frac{\partial \overline{P}}{\partial Z}, \\
&Z = \frac{z}{a}, \quad Ec = \frac{V^2}{c_{pf}(T_a - T_0)}, \quad \beta = m(T_w - T_0), \quad Pr = \frac{\mu_0 c_{pf}}{k_f}, \\
&b_1 = \frac{\rho_f}{\rho_{nf}}, \quad b_2 = 1 - \varphi + \varphi\gamma_s/\gamma_f, \quad b_3 = \frac{k_s + 2k_f - 2\varphi(k_f - k_s)}{k_s + 2k_f + \varphi(k_f - k_s)}.
\end{aligned}\right\} \tag{4.9}$$

The dimensionless momentum and energy equations together with its initial and boundary conditions can be written as;

$$\frac{\partial W}{\partial t} + Re\frac{\partial W}{\partial \eta} = b_1 A + \frac{b_1 e^{-\beta\theta}}{(1-\varphi)^{2.5}}\left(\frac{\partial^2 W}{\partial \eta^2} + \frac{1}{\eta}\frac{\partial W}{\partial \eta} - \beta\frac{\partial W}{\partial \eta}\frac{\partial \theta}{\partial \eta}\right) + b_2 Gr\theta, \tag{4.10}$$

$$Pr\frac{\partial \theta}{\partial t} + PrRe\frac{\partial \theta}{\partial \eta} = \frac{b_3}{1 - \varphi + \varphi\tau}\left(\frac{1}{\eta}\frac{\partial \theta}{\partial \eta} + \frac{\partial^2 \theta}{\partial \eta^2}\right) + \frac{PrEc}{(1-\varphi)^{2.5}(1-\varphi\tau)} e^{-\beta\theta}\left(\frac{\partial W}{\partial \eta}\right)^2, \tag{4.11}$$

with initial and boundary conditions:

$$W(\eta, 0) = 0, \quad \theta(\eta, 0) = 0, \tag{4.12}$$

$$\frac{\partial W}{\partial \eta}(0, t) = \frac{\partial \theta}{\partial \eta}(0, t) = 0, \tag{4.13}$$

$$W(1, t) = 0, \quad \theta(1, t) = 1, \tag{4.14}$$

where $Re(> 0)$ is suction / injection (< 0) Reynolds number, β is the variable viscosity parameter, Pr is the Prandtl number, Gr is the Grashof number, Ec is the Eckert number, A is the pressure gradient parameter and b_1, b_2 and b_3 can be determined from the thermophysical properties of the base fluid and the nanoparticles. The wall shear stress (skin friction coefficient) C_f and the heat transfer rate at the pipe wall (Nusselt number) Nu are the important physical parameters for this type of study which are defined as:

$$C_f = \frac{a\tau_w}{\mu_0 V}, \quad Nu = \frac{aq_w}{k_f(T_W - T_0)}, \tag{4.15}$$

where τ_w is the wall shear stress and q_w is the heat flux at the pipe wall given by:

$$\tau_w = -\mu_{nf} \left.\frac{\partial u}{\partial r}\right|_{r=a}, \quad q_w = -k_n f \left.\frac{\partial T}{\partial r}\right|_{r=a}. \tag{4.16}$$

Substituting equations (4.16) into (4.15) and introducing dimensionless variables, we obtain

$$C_f = -\frac{e^{-\beta\theta}}{(1-\varphi)^{2.5}} \left.\frac{\partial W}{\partial \eta}\right|_{\eta=1}, \quad Nu = -b_3 \left.\frac{\partial \theta}{\partial \eta}\right|_{\eta=1}. \tag{4.17}$$

4.3 Numerical Procedure

Equations (4.10)-(4.14) is a system of nonlinear Initial Boundary Value Problem (IBVP). The system is solved numerically using a semi-discretization finite difference method known as the method of lines (Na, 1979). Spatial interval is partitioned into N equal parts with mesh size and mesh grid points . The first and second spatial derivatives in equation (4.10) and equation (4.11) are approximated with second-order central finite differences. Let $W_i(t)$ and $\theta_i(t)$ be approximation of $W(\eta_i, t)$ and $\theta(\eta_i, t)$, then the semi-discrete system for the problem becomes:

$$\begin{aligned} \frac{dW_i}{dt} &= b_1 A - Re\frac{W_{i+1} - W_{i-1}}{2\Delta\eta} \\ &+ \frac{b_1 e^{-\beta\theta_i}}{(1-\varphi)^{2.5}} \left(\frac{W_{i+1} - 2W_i + W_{i-1}}{\Delta\eta^2} + \frac{W_{i+1} - W_{i-1}}{2\eta_i \Delta\eta}\right) \\ &- \frac{b_1 e^{-\beta\theta_i}}{(1-\varphi)^{2.5}} \left(\beta\frac{(\theta_{i+1} - \theta_{i-1})(W_{i+1} - W_{i-1})}{4\Delta\eta^2}\right) + b_2 Gr\theta_i, \end{aligned} \tag{4.18}$$

$$\begin{aligned} Pr\frac{d\theta_i}{dt} &= \frac{b_3}{(1-\varphi+\varphi)} \left(\frac{\theta_{i+1} - 2\theta_i + \theta_{i-1}}{\Delta\eta^2} + \frac{\theta_{i+1} - \theta_{i-1}}{2\eta_i \Delta\eta}\right) \\ &+ \frac{EcPre^{\beta\theta}}{(1-\varphi)^{2.5}(1-\varphi+\varphi\tau)} \left(\frac{W_{i+1} - W_{i-1}}{2\Delta\eta}\right)^2 \\ &- PrRe\frac{\theta_{i+1} - \theta_{i-1}}{2\Delta\eta}, \end{aligned} \tag{4.19}$$

with initial conditions:

$$W_i(0) = 0, \quad \theta_i(0) = 0, \quad 1 \le i \le N+1. \tag{4.20}$$

The equations corresponding to the first and last grid points are modified to incorporate the boundary conditions as follows:

$$W_1 = W_0, \quad \theta_1 = \theta_0, \quad W_{N+1} = 0, \quad \theta_{N+1} = 1. \tag{4.21}$$

Equations (4.18)-(4.21) is a system of initial value nonlinear ODEs and can be solved iteratively using Runge-Kutta-Fehlberg integration technique (Na, 1979) implemented on a computer using MATLAB. The Runge-Kutta-Fehlberg (RKF) method is used to guarantee the accuracy in the solution of

Table 4.1: Thermophysical properties of the fluid phase (water) and nanoparticles (Kuznetsov and Nield, 2010)

	$\rho(kg/m^3)$	$C_p(J/kgK)$	$k(W/mK)$	$\gamma(1/K)$
Pure water	997.1	4179	0.613	21×10^{-5}
Copper(Cu)	8933	385	401	1.67×10^{-5}
Aluminium	3970	765	40	0.85×10^{-5}

equations (4.18)-(4.21). RKF algorithm decides if the appropriate step size is being used. At each step, two different approximations for the solution are computed and compared. If the two answers are in close agreement, the approximation is accepted. If the two answers do not agree to a specified accuracy, the step size is reduced. If the answers agree to more significant digits than required, the step size is increased. From the process of numerical computation, the skin-friction coefficient and the Nusselt number in equation (4.17) are also highlighted and their numerical values are presented. The thermophysical values for water and nanoparticles used in a considered problem are shown in Table 4.1.

4.4 Results and Discussion

In the present study, the effects of Buoyancy force and temperature dependent viscosity on unsteady nanofluid flow past a vertical porous pipe are investigated using two types of nanoparticles with water as base fluid. The nanoparticles used are copper (Cu) and alumina (Al_2O_3). The effects of various thermophysical parameters on temperature and velocity profiles of nanofluid flow are analysed. The local skin friction and Nusselt number are also highlighted. The default values of the thermophysical parameters are specified as: $\varphi = 0.3$, $A = 1$, $Gr = 0.1$, $Re = 1$, $Pr = 6.2$, $Ec = 1$, $\Delta\eta = 0.005$, $\Delta t = 0.01$ and $\beta = 0.5$. All profiles therefore correspond to these values unless otherwise indicated. Moreover, the steady-state solution is assumed to have been reached, when the absolute difference between the values of velocity, as well as temperature at two consecutive time are very small. Cu-water nanofluid delayed to reach its steady state than Al_2O_3-water, but we have noticed that for ($t > 17$) both temperature and velocity reaches their steady state for both nanofluids.

4.4.1 Transient and steady flow analysis

Figures 4.2-4.7 displays the transient solutions of velocity and temperature from the time where the nanofluids begin to flow until a steady state is reached. Both velocity and temperature time evolutions demonstrate the transient increase in fluid quantities as shown in Figure 4.2 and Figure 4.3. Figure 4.3 in

particular show the development of the temperature fields from the initial state in which the temperature at the wall is higher than the bulk temperature. Figure 4.4 and Figure 4.5 demonstrate the general overview for the velocity and temperature for all nanofluid. It is noticed that the nanofluid temperature and velocity for Cu-water are higher than that of Al_2O_3-water. However the Al_2O_3-water nanofluids temperature and velocity reaches its steady state earlier than Cu-water nanofluid. Figure 4.6 and Figure 4.7 compare the numerical solutions obtained using semi-discretization technique for unsteady flow ($t = 20$) with steady state numerical method known as shooting method. No significant differences were observed.

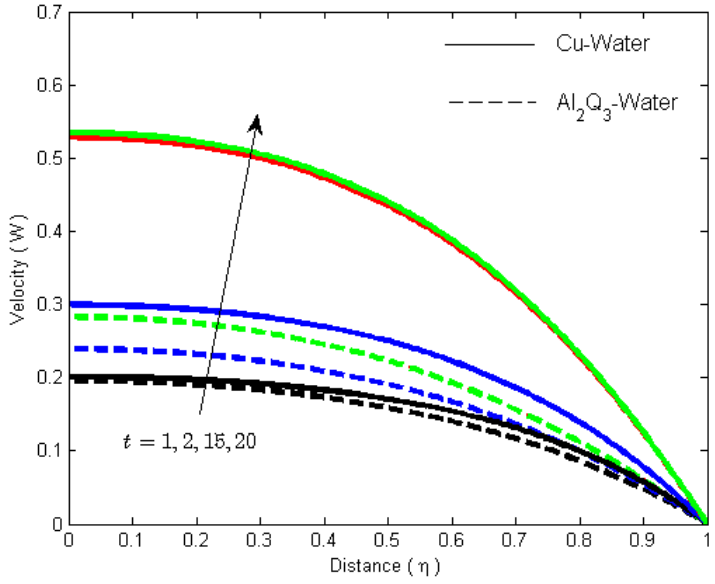

Figure 4.2: Transient and steady state velocity profiles

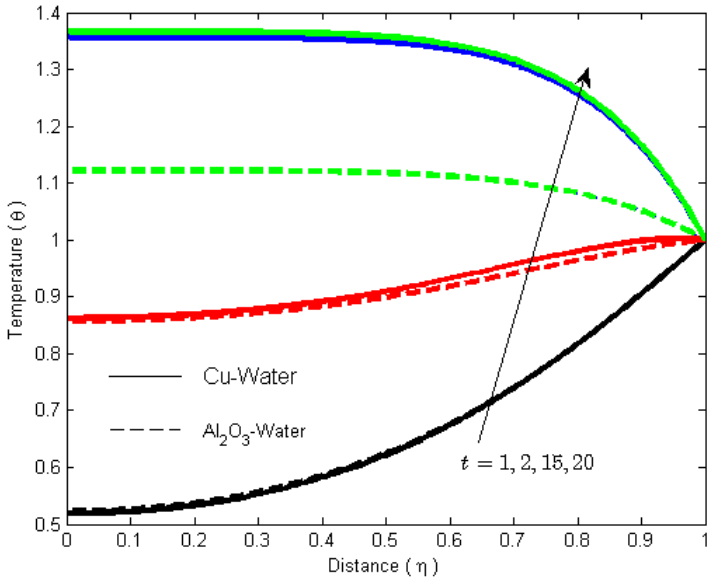

Figure 4.3: Transient and steady state temperature profiles

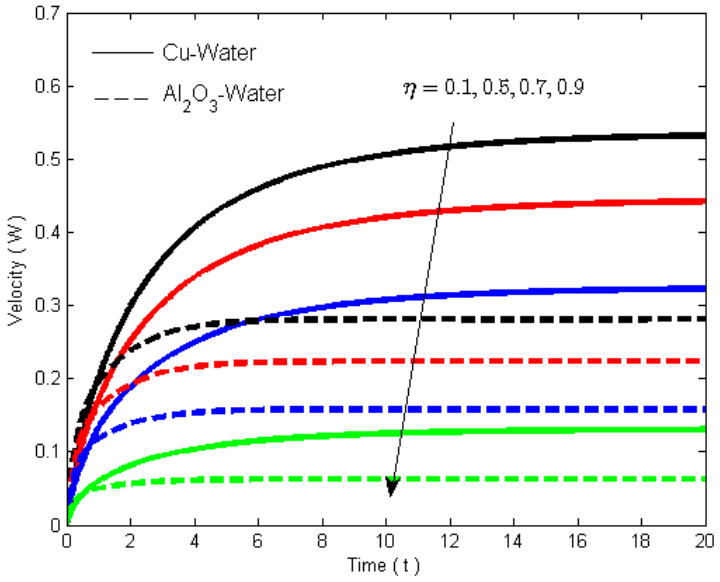

Figure 4.4: Nanofluids velocity profiles with increasing distance

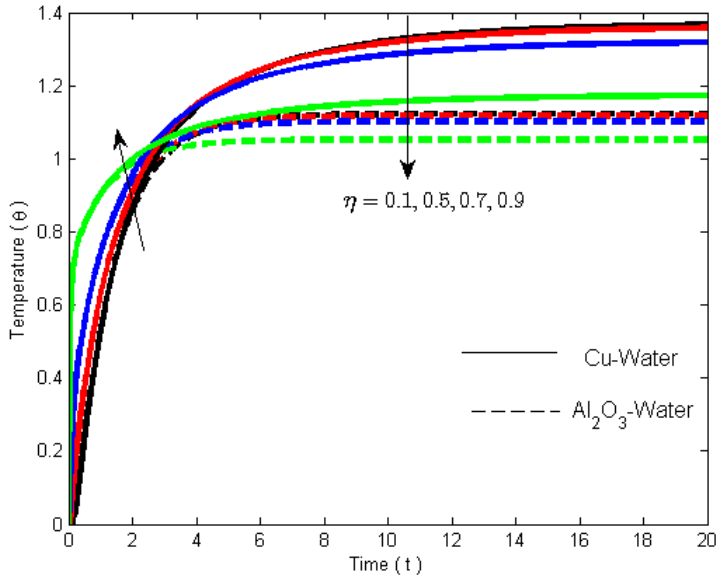

Figure 4.5: Nanofluids temperature profiles with increasing distance

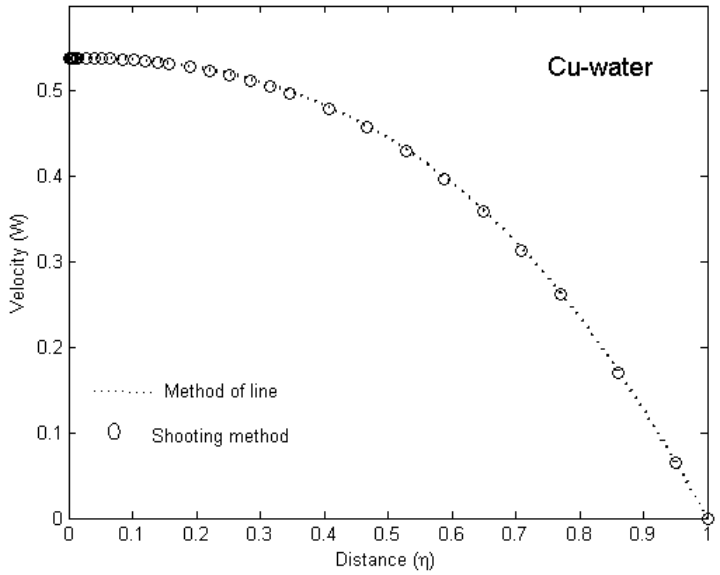

Figure 4.6: Nanofluid velocity solution from shooting method and method of lines

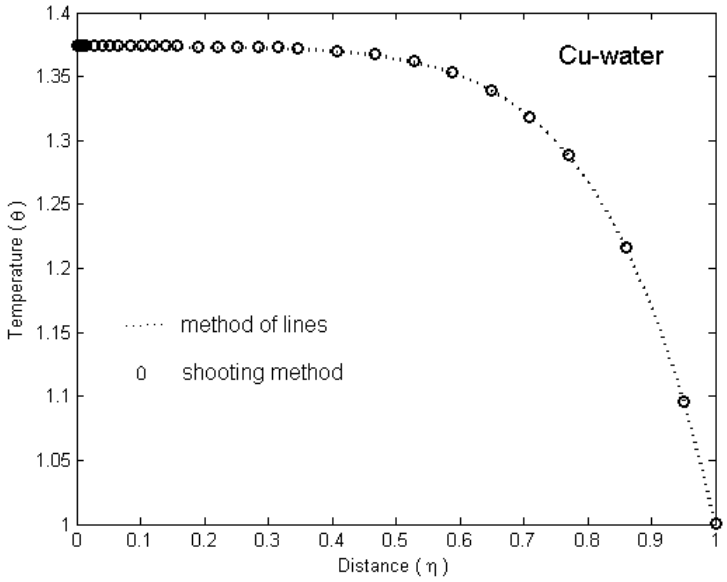

Figure 4.7: Nanofluid Temperature solution from shooting method and method of lines

4.4.2 Dimensionless velocity profile with parameters variations

Figures 4.8-4.12 demonstrate the effects of various thermophysical parameters on the nanofluids velocity profiles. Generally, the nanofluid velocity is lower at the pipe surface due to no-slip condition and increases to the free stream value at the center of the pipe satisfying the flow field conditions. The nanofluid velocity is observed to slow down when more nanoparticles are added in to the base as illustrated in Figure 4.8. This is expected since both the density and the dynamic viscosity of the nanofluid increase with increasing nanoparticles volume fraction leading to decrease in the velocity. An increase of viscosity parameter means a decrease in fluid viscosity and hence reduces the flow resistance which results in increasing the nanofluid velocity within the pipe as illustrated in Figure 4.9. The same trend is observed with increasing pressure gradient and Grashof number as seen in Figures 4.10-4.11, an increase of Grashof number has the tendency to increase the thermal and mass buoyancy which leads to the increasing of nanofluid velocity. Meanwhile, it is important to note that ($Re > 0$) corresponds to uniform suction at the pipe wall while ($Re < 0$) represents uniform injection. Figure 4.12, the profiles shows that the nanofluid velocity increases with an increase in wall suction and decreases with an increase in fluid injection at the pipe wall. The increase in nanofluid velocity due to uniform suction or decrease due to injection may be attributed to the combined effects of pressure gradient and thermal buoyancy.

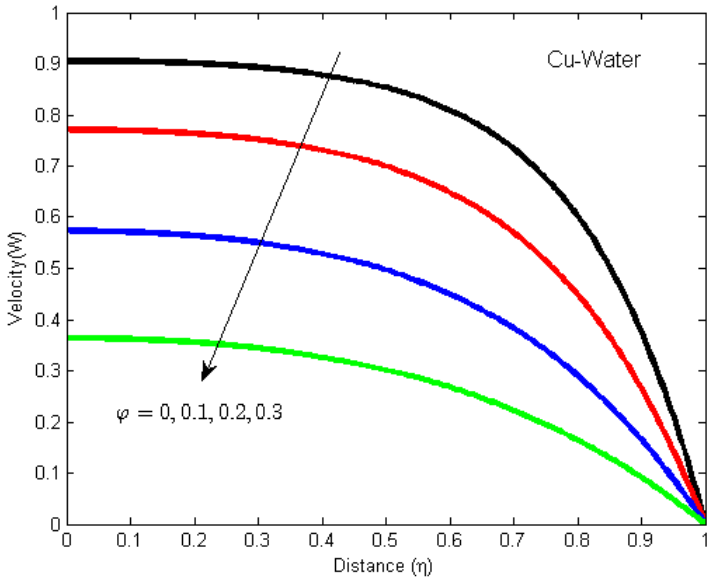

Figure 4.8: Nanofluids velocity profiles with increasing φ

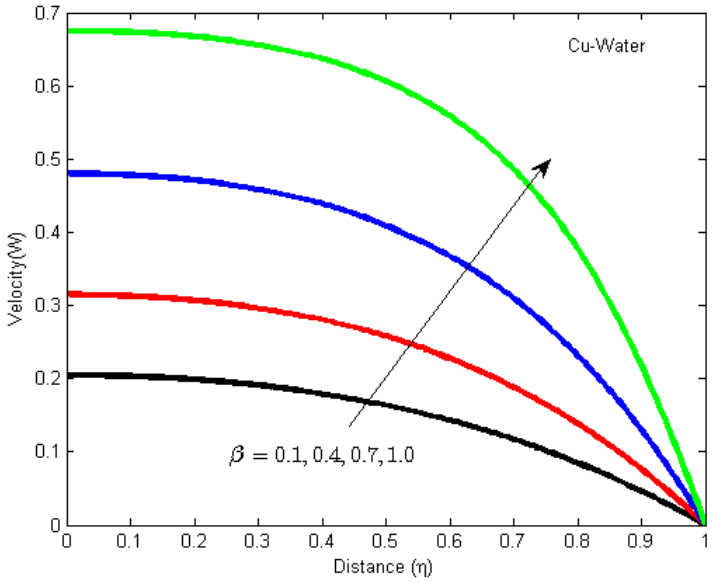

Figure 4.9: Nanofluids velocity profiles with increasing β

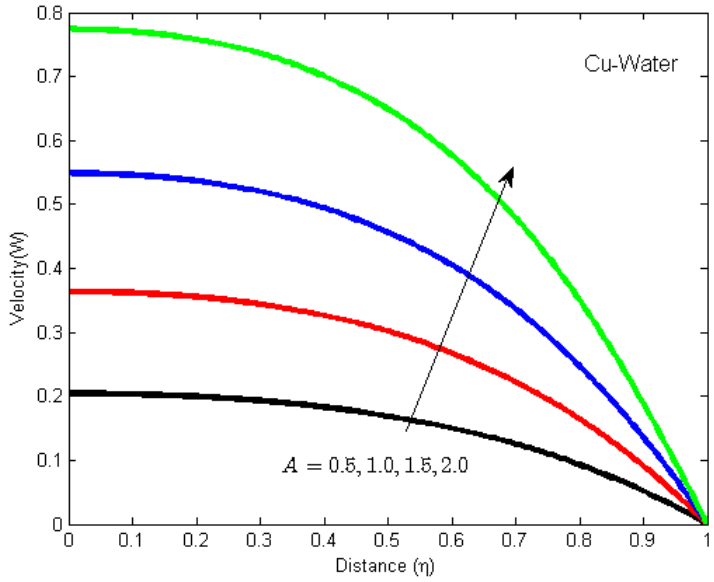

Figure 4.10: Nanofluids velocity profiles with increasing A

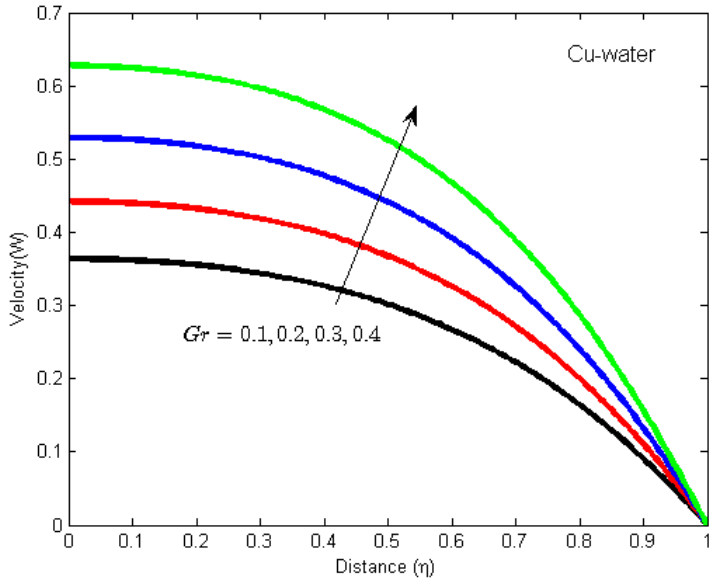

Figure 4.11: Nanofluids velocity profiles with increasing Gr

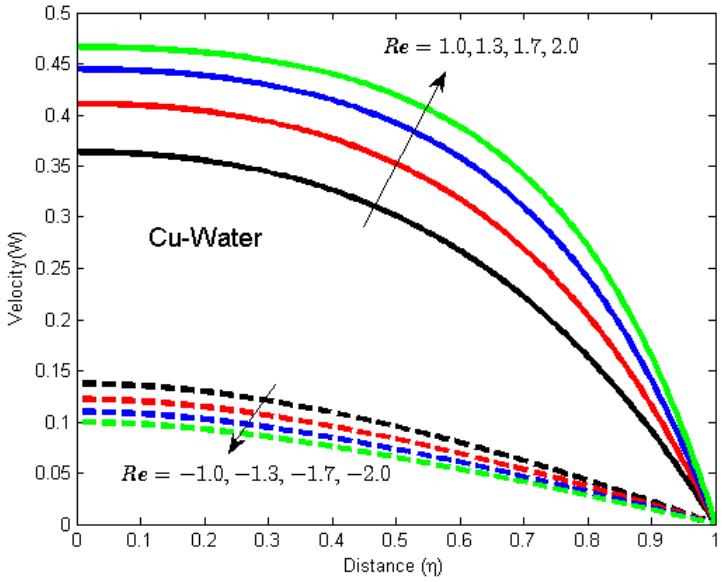

Figure 4.12: Nanofluids velocity profiles with increasing Re

4.4.3 Dimensionless temperature profile with parameters variations

The effects of variation in the thermophysical parameters on the nanofluid temperatures profiles are illustrated in Figures 4.13-4.17. An increase in the nanoparticles volume fraction causes a decrease in the nanofluid temperature as illustrated in Figure 4.13 . This may be due to a decrease in the velocity gradient as φ. increases, consequently, the overall bulk temperature decreases. Meanwhile, a sharp rise in the temperature near the pipe wall is observed with a decrease in the nanoparticles volume fraction and this rise in temperature near the pipe wall attained its peak value when pure water is considered i.e., at $\varphi = 0$. The temperature increase near the pipe wall may be attributed to the combined effects of fluid suction and increasing velocity gradient as the nanoparticles volume fraction decreases. In Figure 4.14, the growing of temperature is observed with increasing Eckert number; this is expected since the terms linked to the Eckert number act as strong heat source in energy equation. Similar trend has been noticed with increasing Grashof number, viscosity parameter and suction Reynolds number. Nanofluid temperature increases with increasing Grashof number, viscosity parameter and suction Reynolds (i.e., the axisymmetric suction strength) as demonstrated in Figures 4.15-4.17.

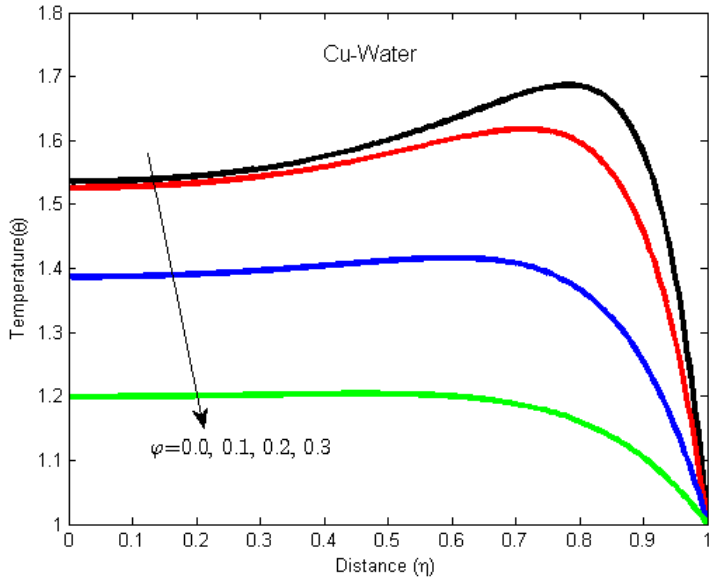

Figure 4.13: Nanofluid temperature profiles with increasing φ

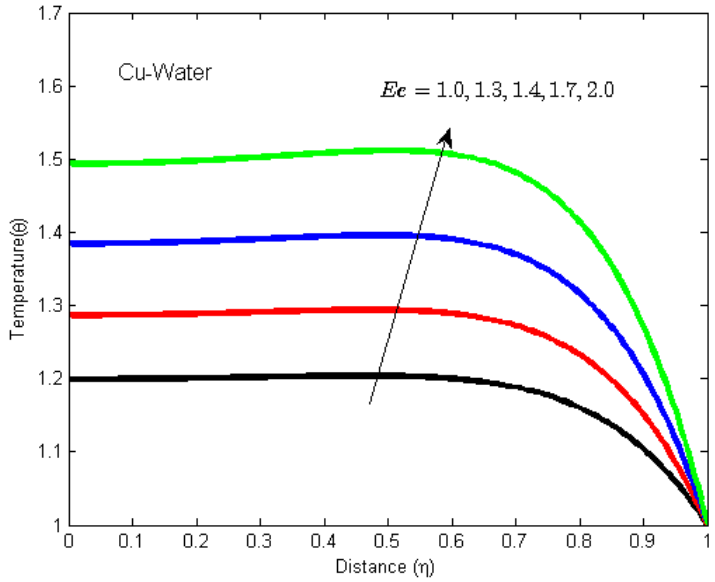

Figure 4.14: Nanofluid temperature profiles with increasing Ec

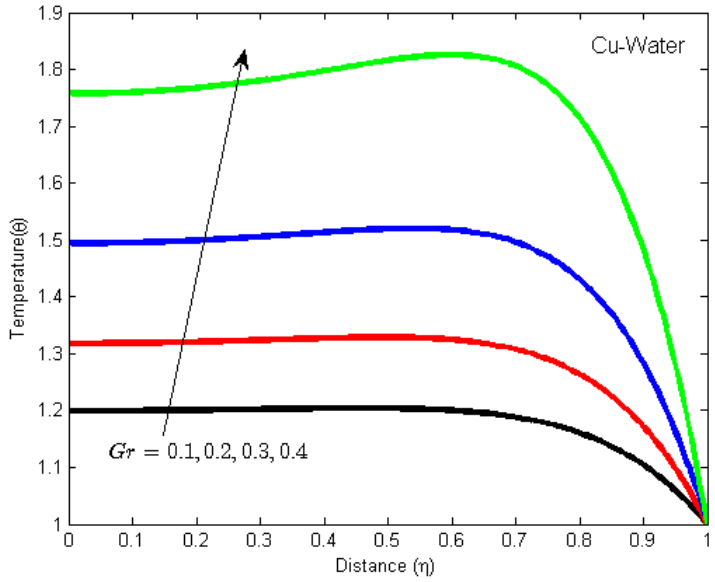

Figure 4.15: Nanofluid temperature profiles with increasing Gr

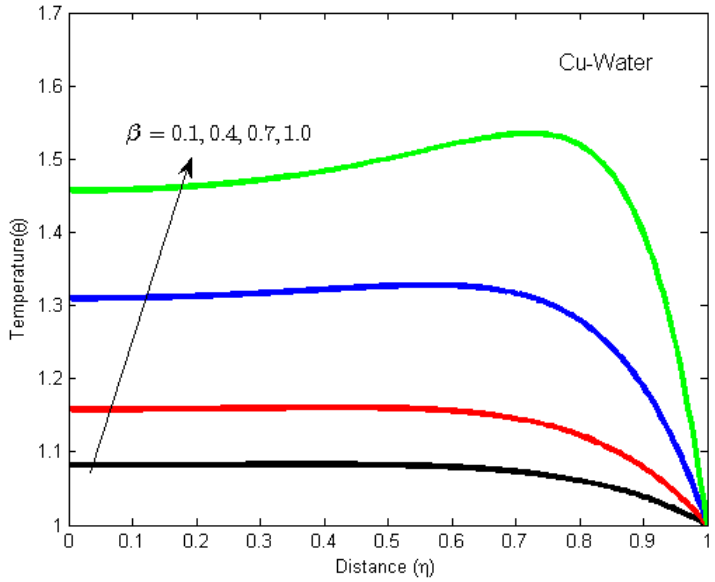

Figure 4.16: Nanofluid temperature profiles with increasing β

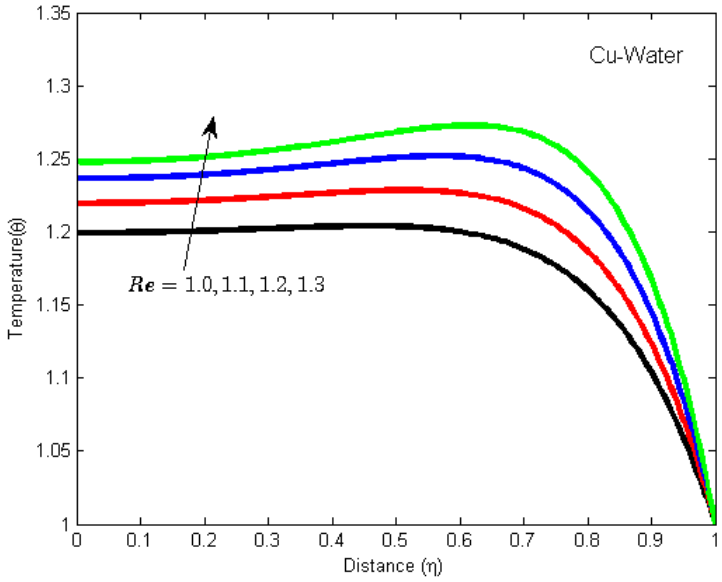

Figure 4.17: Nanofluid temperature profiles with increasing suction Re

4.4.4 Wall shear stress and heat transfer rate

Figures 4.18-4.22 illustrate the effects of various pertinent parameters for the skin friction coefficient and the local Nusselt number at the pipe surface.The wall shear stress against time is plotted in Figure 4.18 which compares the skin friction coefficients profiles for Cu-water and Al_2O_3-water nanofluids. Both skin friction produced by Cu-water and Al_2O_3-water nanofluid increase with increasing time and the Cu-water nanofluid demonstrated the highest shear stress than Al_2O_3-water. The wall shear stress at the pipe wall ($\eta = 1$) dependence on nanoparticles volume fraction φ is illustrated in Figure 4.19 and Figure 4.20, for varying Re, Gr and β. The results shows that, the shear stress is increasing with increasing suction Re, Gr and β and decreasing with increasing nanoparticles concentration and injection Re. Figure 4.21 illustrate the heat transfer rate for both nanofluids. The heat transfer rate produced by Cu-water nanofluid is higher than that of Al_2O_3-water nanofluid. In Figure 4.22, the heat transfer profiles are plotted against φ with various parameters variation. There is an increase in the rate of heat transfer with increasing each of the parameter Gr, β and Ec and decreased with increasing parameter φ.

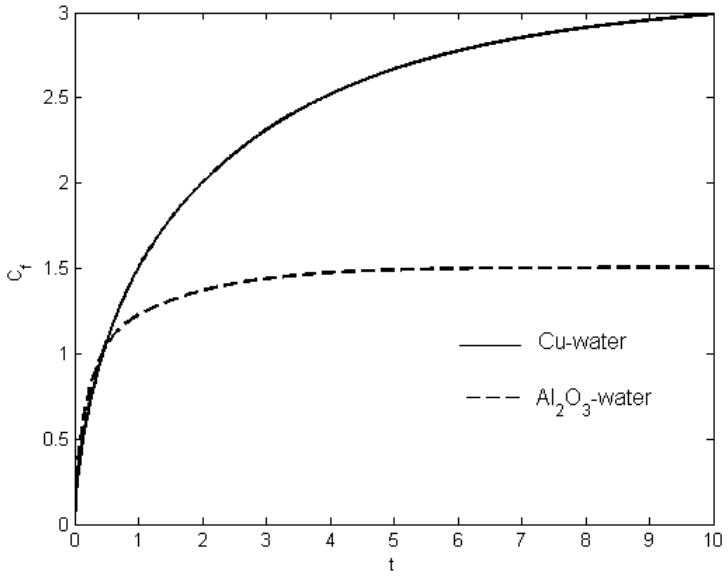

Figure 4.18: Skin friction profiles for both nanofluids

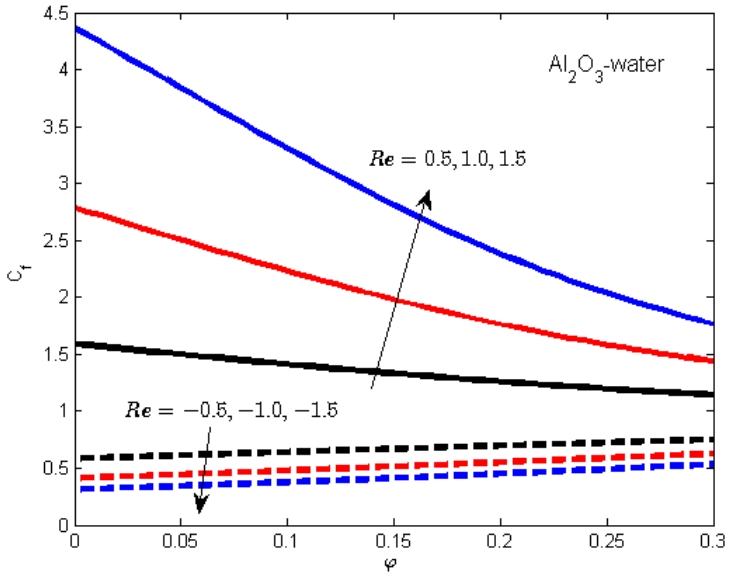

Figure 4.19: Skin friction profiles with increasing φ and Re

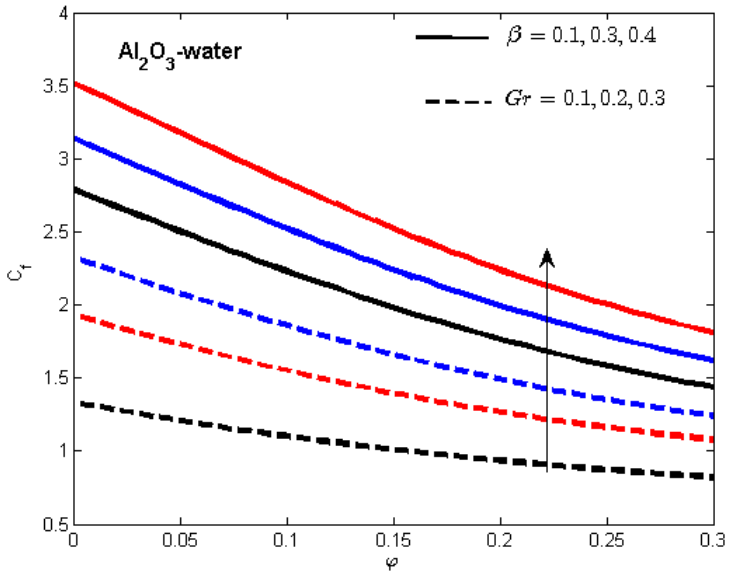

Figure 4.20: Skin friction profiles with increasing φ, Gr and β

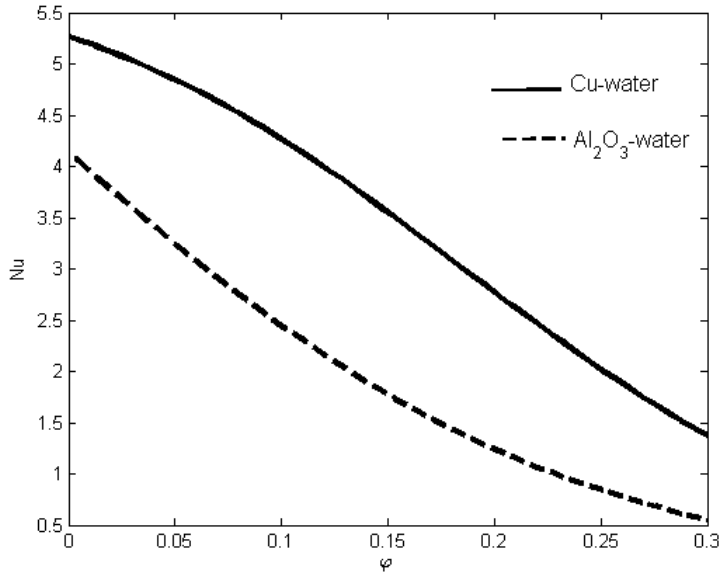

Figure 4.21: Nusselt number profiles with increasing φ for both nanofluids

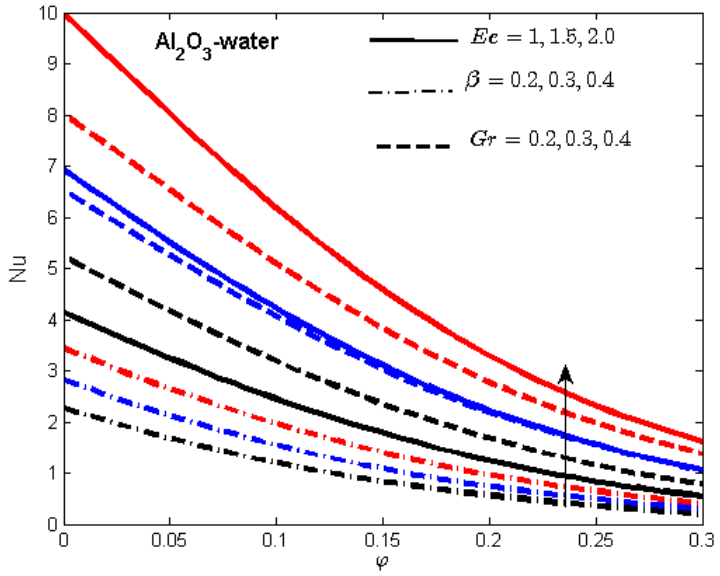

Figure 4.22: Nusselt number profiles with increasing φ, β. Ec and Gr

4.5 Conclusion

In the present chapter, we studied the laminar unsteady flow of variable viscosity past a vertical porous pipe of water-based nanofluids containing copper and alumina. The governing nonlinear PDEs are solved numerically using a semi-discretization finite difference method together with Runge-Kutta-Fehlberg integration scheme. The main results are summarised as follows:

- The Cu-water nanofluid tends to flow faster than Al_2O_3-water nanofluid.
- The nanofluid velocity increases with increasing β, A, Gr and suction Re and decreases with increasing φ and injection Re.
- The nanofluid temperature of Cu-water is higher than that of Al_2O_3-water.
- The nanofluid temperature profile increases with Ec, Gr, β and suction Re and decreases with φ.
- The temperature and velocity for Al_2O_3-water nanofluid reaches steady state earlier than Cu - water nanofluid.
- The Cu-water nanofluid produces higher wall shear stress than Al_2O_3-water nanofluid and increases with increasing Gr, β and suction Re while decreases with increasing φ and injection Re.
- The Cu-water nanofluid produces more heat transfer rate than Al_2O_3-water nanofluid. The heat transfer rate increases with increasing β, Ec, and Gr and decreases with increasing φ.

CHAPTER FIVE

Buoyancy-Driven Heat Transfer of Water-Based Nanofluid in a Permeable Cylindrical Pipe with Navier Slip Through Saturated Porous Medium[4]

Summary: The combined effect of buoyancy-driven force, variable viscosity and Navier slip on heat transfer of unsteady water-based nanofluid flow containing copper and alumina nanoparticles in a permeable cylindrical pipe through saturated porous medium is investigated numerically. The Darcy-Brinkman-Forchheimer model was adopted to describe the flow. The non-linear PDEs governing the problem were obtained and solved numerically using a semi-discretization finite difference method together with Runge-Kutta-Fehlberg integration scheme. The numerical solutions for velocity, temperature, skin friction and Nusselt number have been presented graphically and discussed quantitatively. The results reveal that both nanofluid temperature and velocity are enhanced with increasing nanoparticles volume fraction and Grashof number and reduced with the increasing viscosity, Navier slip parameter, porous media resistance parameter and porous media shape factor parameter.

5.1 Introduction

A nanofluid is a colloidal suspension of nano-sized particles and fibres which are below 100 nm in a base fluid. Common fluids such as water, ethanol or engine oils are typically used as base fluids. The variety of nanoparticles which are used in preparation of nanofluids includes: metallic oxides such as Al_2O_3, CuO, TiO_2; metal carbides such as SiC, TiC; nitride ceramics such as AlN and SiN; metals such as Al, Cu, Ag, Au and Fe; non-metals such as graphite and carbon-nanotubes etc. Since the term nanofluid coined by Choi (1995), the understanding of the so-called anomalous increase in thermal conductivity of nanofluids has generated considerable research interest. Buongiorno (2006) developed a two-component four-equation non-homogeneous equilibrium model for mass, momentum, and heat transport in nanofluid to study convective transport in nanofluids. Buongiorno reported that the absolute nanoparticle velocity can be viewed as the sum of the base fluid velocity and a relative slip velocity. Seven slip mechanisms including inertia, Brownian diffusion, thermophoresis, diffusiophoresis, Magnus effect, fluid drainage, and gravity settling are proposed.

Research related to convective flow and heat transfer using porous medium technique has gained great interest in recent decades due to the fact that this structure encountered in many engineering applications

[4] This chapter is based on published paper:

Sara Khamis, Oluwole Daniel Makinde & Yaw Nkansah-Gyekye (2015). Buoyancy-Driven Heat Transfer of Water-Based Nanofluid in a Permeable Cylindrical Pipe with Navier Slip Through Saturated Porous Medium. *Journal of Porous Media*, 18 (12): 11691180.

such as design of canisters for nuclear waste disposal, nuclear reactors, thermal insulation, geothermal systems, cooling of electronic circuits, ceramic processing, filtration processes, oil recovery drying processes, heat exchangers as well as building constructions (Ahmad and Pop, 2010; Vafai and Tien, 1982). The analysis of convective transport in a porous medium with the inclusion of non-Darcian effects has also been a matter of study in recent years. The inertia effect is expected to be important at a higher flow rate and it can be accounted through the addition of a velocity squared term in the momentum equation, which is known as the Forchheimers extension of Darcys law. Bansod (2003) performed a comprehensive study on combined heat mass transfer by natural convection along the horizontal surface in a fluid saturated porous medium. The Von-Karmann integral method was used together with similarity method for the solution to the problem. It was shown that with increasing of buoyancy ratio, both the heat and mass transfer rates increase while the Lewis number is found to have more effect on the concentration field than it does on the flow and temperature fields. Furthermore, a considerable number of studies on convective heat and fluid flow of porous media saturated by a nanofluid have been done analytically and numerically (Kuznetov and Nield, 2009, 2010a,b). Rana *et al.* (2014) reported the thermosolutal instability problem in a horizontal layer of an elastic-viscous nanofluid in porous medium. They used Walters fluid model to describe the rheological behavior of the nanofluid and for the porous medium. Makinde and Eegunjobi (2013) use the first and second law of thermodynamics to analyze numerically the inherent irreversibility in a steady flow of a couple stress fluid through a vertical channel filled with porous media. Analysis of nanofluid heat transfer in parallel plate vertical channel partially filled with porous medi-um using Brinkman-Forchheimer extended Darcy model is reported by Hajipour and Dehkordi (2012). They used different viscous dissipation models to account for viscous heating. They reported that the presence of nanoparticles in the base fluid enhances the heat-transfer process significantly. Gorla and Chamkha (2011) analyze the natural convection past an isothermal horizontal plate in a porous medium saturated by a nanofluid; their results show that as the buoyancy ratio and thermophoresis parameters are increased, the friction factor increases whereas the heat transfer and mass transfer rate decreases. Targui and Kahalerras (2014) presented a numerical simulation of nanofluids flow in a double pipe heat exchanger provided with porous baffles. They observed that the addition of nanoparticles enhances the rate of heat transfer in comparison to conventional fluids.
From literature survey, to the best of our knowledge, we have found that no study has been reported on heat transfer flow of nanofluid with Navier slip and variable viscosity in a cylindrical pipe with permeable wall. Thus, the purpose of this study is to numerically investigate the effect of buoyancy force, variable viscosity and Navier slip past a permeable cylindrical pipe embedded in a porous medium filled with nanofluid. The model formulation equations in dimensional and non-dimensional form are established in section two. The numerical computation is done using semi-discretization technique to transform the

PDEs in to a set of ODEs which are then solved numerically using Runge-Kutta-Fehlberg integration scheme; this is explained in section three. Numerical solutions for the velocity, temperature, skin friction and Nusselt number are presented and discussed in section four with various parameters variation governing the flow. Finally, the conclusions are drawn in section five.

5.2 Problem Formulation

Consider unsteady, axisymmetric incompressible flow of water-based nanofluids containing two types of nanoparticles namely; copper and alumina through a cylindrical pipe with permeable of length $L >> r$ and radius r embedded in saturated porous media. The pipe surface is subjected to Navier slip condition. The geometry of the problem and coordinate system are shown in Figure 5.1. The mathematical equations describing the physical model are based upon the following assumptions:

i The fluid is laminar, Newtonian and fully developed.

ii The thermophyiscal parameters for the fluid flow are constant except, for the density in the buoyancy force which is approximated using Boussinesq model.

iii The fluid phase and nanoparticles are in thermal equilibrium state.

iv The porous media is homogeneous and in local thermal equilibrium with the fluid.

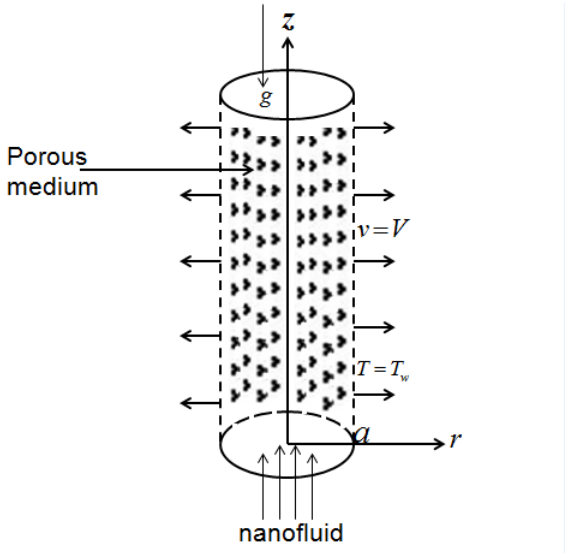

Figure 5.1: Schematic diagram of the physical system

Under the above mentioned assumptions and based on Brinkman-Forchheimer model the one dimensional governing equations in a dimensional form are as follows, see for example (Eegunjobi and

Makinde, 2012; Ozkol *et al.*, 2007; Makinde *et al.*, 2011; Stokes, 1984)

Continuity equation:

$$\frac{\partial u}{\partial z} = 0, \tag{5.1}$$

Momentum equation:

$$\rho_{nf}\left(\frac{\partial u}{\partial \bar{t}} + V\frac{\partial u}{\partial r}\right) = -\frac{\partial \bar{P}}{\partial z} + \frac{1}{r}\left(r\mu_f(T)\frac{\partial u}{\partial r}\right) + \rho_{nf}\gamma_{nf}(T - T_0) - \frac{\mu_{nf}(T)u}{K} - \frac{Fu^2}{\sqrt{K}}, \tag{5.2}$$

Energy equation:

$$(\rho c_p)nf\left(\frac{\partial T}{\partial \bar{t}} + V\frac{\partial T}{\partial r}\right) = k_{nf}\frac{1}{r}\left(r\frac{\partial T}{\partial r}\right) + \mu_{nf}(T)\left(\frac{\partial u}{\partial r}\right)^2 + \frac{\mu_{nf}(T)}{K}u^2 + \frac{F}{\sqrt{K}}u^3, \tag{5.3}$$

with initial and boundary conditions:

$$u(r,0) = 0, \quad T(r,0) = T_0, \tag{5.4}$$

$$\frac{\partial u}{\partial r}(0,\bar{t}) = \frac{\partial T}{\partial r}(0,\bar{t}) = 0 \quad \bar{t} > 0, \tag{5.5}$$

$$\xi u(a,\bar{t}) = \mu_{nf}\frac{\partial u}{\partial r}, \quad T(a,\bar{t}) = T_w \quad \bar{t} > 0. \tag{5.6}$$

where: u is the nanofluid axial velocity, P is the pressure, T is the nanofluid temperature, T_o is the nanofluid initial temperature, T_w is the pipe wall temperature, g is the gravitational acceleration, K is the porous media permeability, F is the empirical constant in the second order (porous inertia) resistance such that $F = 0$ corresponds to the Darcy law, ξ is the Navier slip coefficient. Moreover, μ_{nf} is the nanofluid dynamic viscosity, k_{nf} is the nanofluid thermal conductivity ρ_{nf} is the nanofluid density, γ_{nf} is the nanofluid volumetric expansion coefficient and $(\rho c_p)_{nf}$ is the heat capacitance of the nanofluid as given in reference (Anbuchezhian *et al.*, 2012) which are defined as:

$$\left.\begin{aligned} &\mu_{nf} = \frac{\mu_f}{(1-\varphi)^{2.5}}, \quad \rho_{nf} = (1-\varphi)\rho_f + \varphi\rho_s, \quad \alpha_{nf} = \frac{k_{nf}}{(\rho c_p)_{nf}}, \\ &\gamma_{nf} = (1-\phi)\gamma_f + \varphi\gamma_s, \quad \frac{k_{nf}}{k_f} = \frac{k_s + 2k_f - 2\varphi(k_f - k_s)}{k_s + 2k_f + \varphi(k_f - k_s)}, \\ &(\rho c_p)_{nf} = (1-\varphi)(\rho c_p)_f + \varphi(\rho c_p)_s. \end{aligned}\right\} \tag{5.7}$$

In equation (5.7), φ is the nanoparticles solid volume fraction such that $\varphi = 0$ refer to the base fluid (water), ρ_f is the reference density of the fluid fraction, ρ_s is the reference density of the solid fraction, γ_f is the volumetric expansion of the fluid, γ_s is the volumetric expansion of solid fraction, μ_f is the viscosity of the fluid fraction, k_f is the thermal conductivity of the fluid fraction, c_p is the specific heat at constant pressure and k_s is the thermal conductivity of the solid volume fraction.

The viscosity of the nanofluid is assumed to be temperature dependent and can expressed as (Abu-Nada and Chamkha, 2010; Namburu *et al.*, 2007):

$$\mu_f(T) = \mu_0 e^{-m(T-T_0)}, \tag{5.8}$$

where, μ_0 is the initial dynamics viscosity and m is the viscosity variation parameter.

The mathematical analysis of the problem is simplified by introducing the following dimensionless quantities:

$$\left.\begin{aligned}
&\theta = \frac{T-T_0}{T_w-T_0}, \quad W = \frac{u}{V}, \quad \eta = \frac{r}{a}, \quad t = \frac{\bar{t}\nu_f}{a^2}, \quad \nu_f = \frac{\mu_0}{\rho_f}, \quad Re = \frac{Va}{\nu_f} \\
&\tau = \frac{(\rho c_p)_s}{(\rho c_p)_f}, \quad \overline{P} = \frac{aP}{\mu_0 V}, \quad Gr = \frac{g(\rho\gamma)_f(T_w-T_0)a^2}{V\mu_0}, \quad A = \frac{\partial \overline{P}}{\partial Z}, \\
&Z = \frac{z}{a}, \quad Ec = \frac{V^2}{c_{pf}(T_a-T_0)}, \quad \beta = m(T_w-T_0), \quad Pr = \frac{\mu_0 c_{pf}}{k_f}, \\
&S = \tfrac{a^2}{K}, \quad Da = \tfrac{1}{S}, \quad M = \tfrac{Fa}{\rho_f\sqrt{K}}.
\end{aligned}\right\} \tag{5.9}$$

The dimensionless momentum and energy equations together with their initial and boundary conditions can be written as:

$$\begin{aligned}
\frac{\partial W}{\partial t} + Re\frac{\partial W}{\partial \eta} &= a_1 A + \frac{a_1 e^{-\beta\theta}}{(1-\varphi)^{2.5}}\left(\frac{\partial^2 W}{\partial \eta^2} + \frac{1}{\eta}\frac{\partial W}{\partial \eta} - \beta\frac{\partial W}{\partial \eta}\frac{\partial \theta}{\partial \eta}\right) \\
&+ a_2 Gr\theta - \frac{Sa_1 e^{-\beta\theta}}{(1-\varphi)^{2.5}} - Ma_1 ReW^2,
\end{aligned} \tag{5.10}$$

$$\begin{aligned}
Pr\frac{\partial \theta}{\partial t} + PrRe\frac{\partial \theta}{\partial \eta} &= \frac{a_3}{1-\varphi+\varphi\tau}\left(\frac{1}{\eta}\frac{\partial \theta}{\partial \eta} + \frac{\partial^2 \theta}{\partial \eta^2}\right) \\
&+ \frac{PrEc}{(1-\varphi)^{2.5}(1-\varphi\tau)} e^{-\beta\theta}\left(\frac{\partial W}{\partial \eta}\right)^2 \\
&+ \frac{PrEc}{(1-\varphi)^{2.5}(1-\varphi\tau)}\left(Se^{-\beta\theta}W^2 + MRe(1-\varphi)^{2.5}W^3\right),
\end{aligned} \tag{5.11}$$

with initial and boundary conditions:

$$\left.\begin{aligned}
&W(\eta,0) = 0, \quad \theta(\eta,0) = 0, \\
&\frac{\partial W}{\partial \eta}(0,t) = \frac{\partial \theta}{\partial \eta}(0,t) = 0, \quad t > 0, \\
&W(1,t) = \frac{\lambda e^{-\beta\theta}}{(1-\varphi)^{2.5}}\frac{\partial W}{\partial \eta}(1,t), \quad \theta(1,t) = 1, \quad t > 0.
\end{aligned}\right\} \tag{5.12}$$

where: $Re(>0)$ is suction / injection (<0) Reynolds number, β is the variable viscosity parameter, λ is the Navier slip parameter such that $\lambda = 0$ corresponds to no slip condition and $\lambda \to \infty$ describes full lubrication, Pr is the Prandtl number, Gr is the Grashof number, Ec is the Eckert number, S is the porous media shape factor parameter, M is the second order porous media resistance parameter, A is the

pressure gradient parameter and τ is the ratio of nanoparticles heat capacity. The constants a_1, a_2 and a_3 can be determined from the thermophysical properties of the base fluid and the nanoparticles which are described as:

$$\left.\begin{aligned} a_1 &= \frac{\rho_f}{\rho_{nf}} = \frac{1}{1-\varphi+\varphi\rho_s/\rho_f}, \\ a_2 &= 1-\varphi+\varphi\gamma_s/\gamma_f, \\ a_3 &= \frac{(k_s+2k_f)-2\varphi(k_f-k_s)}{(k_s+2k_f)+\varphi(k_f-k_s)}. \end{aligned}\right\} \tag{5.13}$$

The wall shear stress (skin friction coefficient) C_f and the heat transfer rate (Nusselt number) Nu are the important physical quantities of interest in this type of study which are defined as:

$$C_f = \frac{a\tau_w}{\mu_0 V}, \quad Nu = \frac{aq_w}{k_f(T_W - T_0)}, \tag{5.14}$$

where τ_w is the wall shear stress and q_w is the heat flux at the pipe wall given by:

$$\tau_w = \mu_{nf}\left.\frac{\partial u}{\partial r}\right|_{r=a}, \quad q_w = -k_n f\left.\frac{\partial T}{\partial r}\right|_{r=a}. \tag{5.15}$$

Substituting equations (5.15) into (5.14) and introducing dimensionless variables we obtain:

$$\left.\begin{aligned} C_f &= \frac{e^{-\beta\theta}}{(1-\varphi)^{2.5}}\frac{\partial W}{\partial \eta}, \\ Nu &= -a_3\frac{\partial \theta}{\partial \eta}, \end{aligned}\right\} \eta = 1. \tag{5.16}$$

5.3 Numerical Procedure

In this section, the numerical procedure employed to tackle the system of nonlinear IBVP given in equations (5.10)-(5.13) is presented. The semi-discretization finite difference method known as method of lines (Na, 1979; Morton and Mayers, 2005) is used to solve the system numerically. The discretization is based on a linear Cartesian mesh and uniform grid on which finite differences are taken. The spatial interval $0 \leq \eta \leq \eta_{max}$ is partitioned into N equal parts with mesh size $\Delta\eta = 1/N$ and mesh grid points $\eta_i = (i-1)\Delta\eta, \;\; 1 \leq i \leq N+1$. The first and second spatial derivatives in equation (5.10) and equation (5.12) are approximated with second-order central finite differences. Let $Wi(t)$ and $\theta_i(t)$ be approximation of $W(\eta_i, t)$ and $\theta(\eta_i, t)$, then the semi-discrete system for the problem becomes:

$$\begin{aligned} \frac{dW_i}{dt} &= a_1 A + \frac{a_1 e^{-\beta\theta_i}}{(1-\varphi)^{2.5}}\left(\frac{W_{i+1}-2W_i+W_{i-1}}{\Delta\eta^2} + \frac{W_{i+1}-W_{i-1}}{2\eta_i\Delta\eta}\right) \\ &- \frac{a_1 e^{-\beta\theta_i}}{(1-\varphi)^{2.5}}\left(\beta\frac{(\theta_{i+1}-\theta_{i-1})(W_{i+1}-W_{i-1})}{(2\Delta\eta)^2}\right) \\ &+ a_2 Gr\theta_i - Re\frac{(W_{i+1}-W_{i-1})}{2\Delta\eta} - \frac{Sa_1 e^{\beta\theta_i}}{(1-\varphi)^{2.5}}W_i - MRea_1 W_i^2, \end{aligned} \tag{5.17}$$

$$
\begin{aligned}
Pr\frac{d\theta_i}{dt} &= \frac{a_3}{(1-\varphi+\varphi)}\left(\frac{\theta_{i+1}-2\theta_i+\theta_{i-1}}{\Delta\eta^2}+\frac{\theta_{i+1}-\theta_{i-1}}{2\eta_i\Delta\eta}\right) \\
&+ \frac{PrEc}{(1-\varphi)^{2.5}(1-\varphi+\varphi\tau)}e^{-\beta\theta_i}\left(\frac{W_{i+1}-W_{i-1}}{2\Delta\eta}\right)^2 \\
&+ \frac{PrEc}{(1-\varphi)^{2.5}(1-\varphi+\varphi\tau)}\left(Se^{-\beta\theta_i}W_I^2+MRe(1-\varphi)^{2.5}W^3\right) \\
&- PrRe\frac{\theta_{i+1}-\theta_{i-1}}{2\Delta\eta},
\end{aligned} \tag{5.18}
$$

with initial conditions:

$$
W_i(0)=0, \quad \theta_i(0)=0, \quad 1\le i\le N+1. \tag{5.19}
$$

The equations corresponding to the first and last grid points are modified to incorporate the boundary conditions as follows:

$$
\left.
\begin{aligned}
&W_1=W_0, \quad \theta_1=\theta_0, \\
&W_{i+1}=\frac{\lambda e^{\beta\theta_{N+1}}}{\lambda e^{-\beta\theta_{N+1}}-\Delta\eta(1-\varphi)^{2.5}}W_N, \quad \theta_{N+1}=1.
\end{aligned}
\right\} \tag{5.20}
$$

Equations (5.18)-(5.20) is a set of initial value nonlinear ordinary differential equations that can be solved iteratively using Runge-Kutta -Fehlberg integration technique (Morton and Mayers, 2005) implemented on computer using MATLAB. From the process of numerical computation, the skin-friction coefficient and the Nusselt number in equation (5.16) are also highlighted and their numerical values are presented. The thermophysical values for water and nanoparticles used are shown in Table 5.1.

Table 5.1: Thermophysical properties of the water and nanoparticles (Oztop and Abu-Nada, 2008)

Materials	ρ(kg/m^3)	c_p(J/kgK)	k(W/mK)	$\gamma(1/K)$
Pure water (H_2O)	997.1	4179.0	6.13$\times10^{-1}$	21×10^{-5}
Alumina (Al_2O_3)	3970.0	765.0	4$\times10^{1}$	0.85×10^{-5}
Copper (Cu)	8933.0	385.0	4.01$\times10^{2}$	1.67×10^{-5}

5.4 Results and Discussion

In this section, the effects of some of the emerging flow controlling parameters on the dimensionless velocity, temperature, skin friction factor and heat transfer rate are investigated and presented graphically. The numerical results for the representative velocity field are displayed in Figures 5.2-5.8, Figures 5.9-5.15 for temperature field and Figures 5.16-5.21 for skin friction and heat transfer rate respectively.

Moreover the numerical values for skin friction and the Nusselt number are computed for various values of the parameters Gr, β,Re, λ, Ec, A, S and M and their results are presented in Table 5.2. In our analysis where no nanoparticles are compared, the Al_2O_3-water nanofluid was used for both profiles. The detailed discussions for the graphical representation solution are reported in subsequent sections.

5.4.1 Velocity Profile with Parameters Variation

Figures 5.2-5.8 illustrate the variation effects of the various parameters on transient velocity profiles. Figure 5.2 gives an insight of evolution of velocity profiles from the time where the nanofluid begins to flow until steady state is reached for both nanofluids. As expected the nanofluid velocity increases with increasing time until steady state is achieved. The nanofluid velocity for Cu-water is higher than that of Al_2O_3-water before it reverses the order near the pipe wall. Interestingly, the results shows that the nanofluid velocity is higher at the pipe wall than at the centreline region of the pipe; this is due to the Navier slip boundary condition applied at the pipe wall. The response of nanoparticles volume fraction (φ) with reference to Al_2O_3-water nanofluid on velocity profiles are seen in Figure 5.3. The transient velocity is enhanced with the increase of φ; however this behaviour changes near the pipe wall. The opposite response is observed with growing viscosity parameter (β), the increases of β caused the nanofluid velocity to decelerate at the centreline region and causes flow reversal near the pipe wall as described in Figure 5.4. The transient velocity profiles increases with increasing Grashof number (Gr) as demonstrated in Figure 5.5. An increase in Gr means increases the buoyancy force and subsequently the fluid velocity in the flow direction. In Figure 5.6, the transient nanofluid velocity decreases with the increase of Navier slip parameter λ; this trend continue until $\lambda \to \infty$(i.e. full lubrication). Then velocity at the center becomes the same as that at the pipe wall as expected. Also the velocity at the wall becomes zero when the no slip condition is considered. Figure 5.7 and Figure 5.8 show the effects of porous media resistance parameter (M) and porous media shape factor parameter (S). It is noticed that as M and S are increasing the transient nanofluid velocity decreases. This is because the presence of porous medium increases the flow resistances which result in reducing the bulk nanofluid velocity within the pipe.

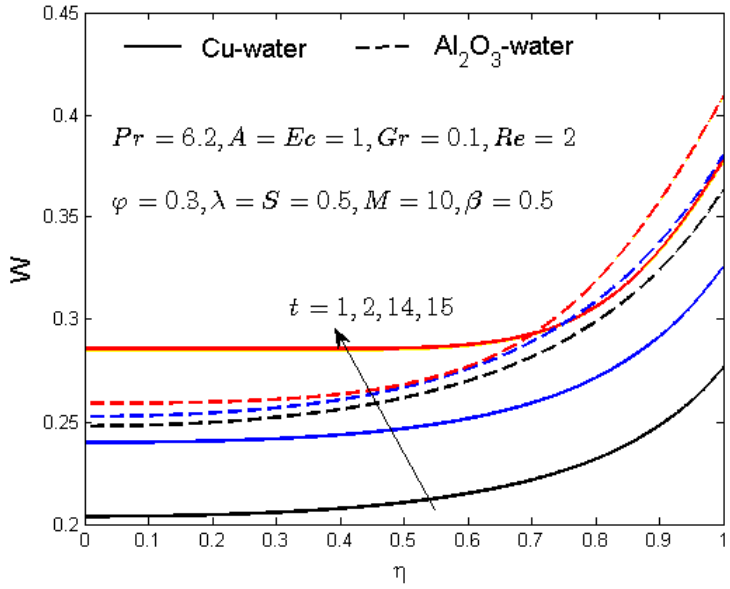

Figure 5.2: Transient and steady state non-dimensional velocity evolutions for Cu-water and Al_2O_3-water nanofluids

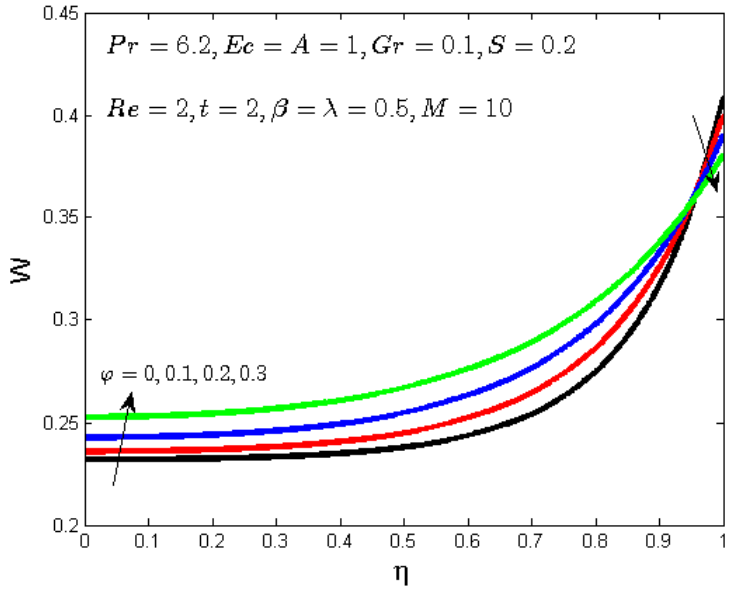

Figure 5.3: Non-dimensional velocity evolutions with increasing nanoparticles volume fraction φ

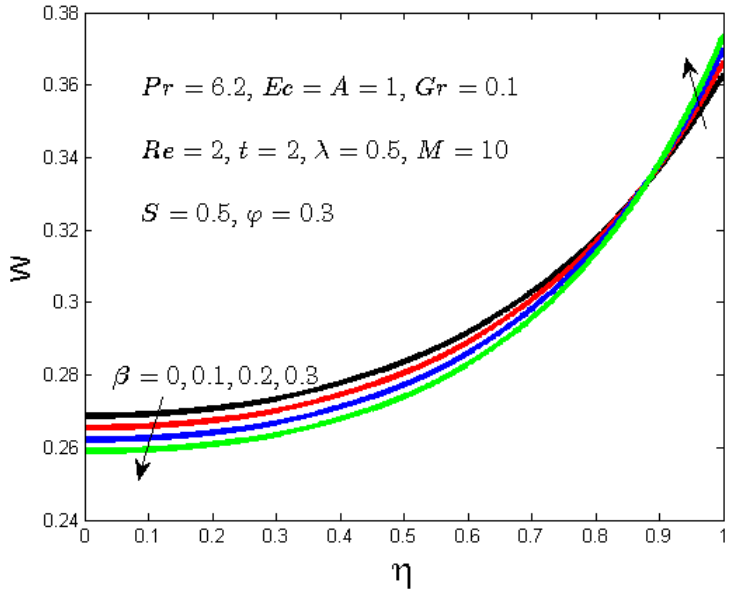

Figure 5.4: Non-dimensional velocity evolutions with increasing β

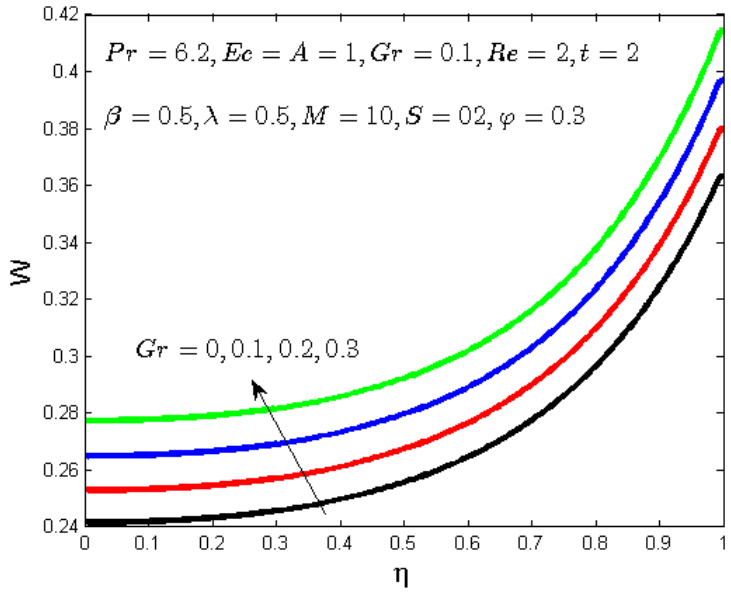

Figure 5.5: Non-dimensional velocity evolutions with increasing Gr

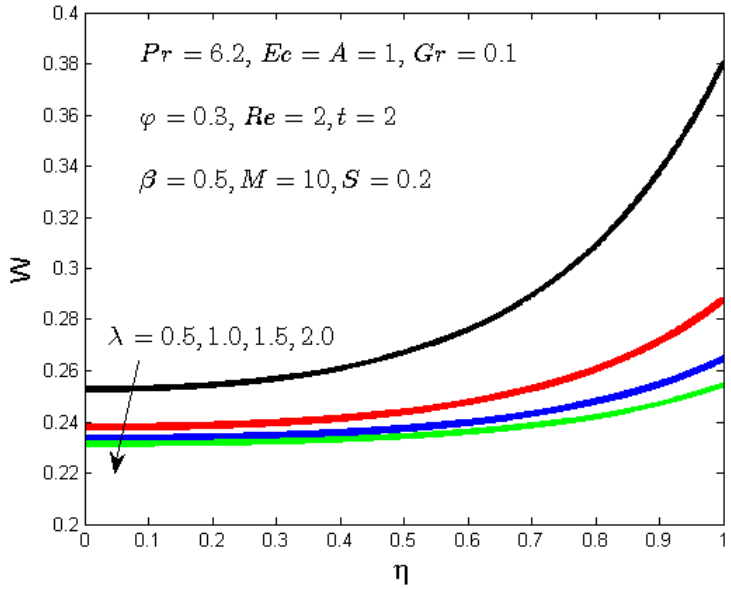

Figure 5.6: Non-dimensional velocity evolutions with increasing λ

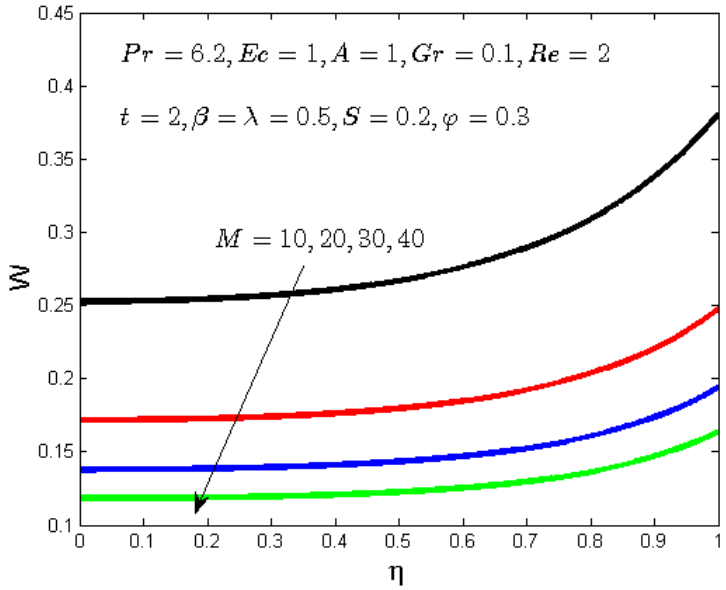

Figure 5.7: Non-dimensional velocity evolutions with increasing M

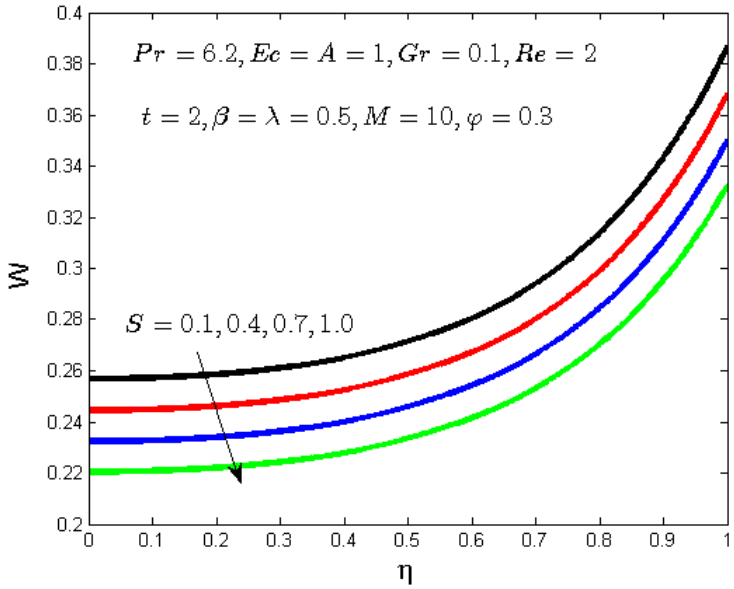

Figure 5.8: Non-dimensional velocity evolutions with increasing S

5.4.2 Temperature Profiles with Parameters Variation

The responses of the variation of parameters on temperature profiles are reported graphically in Figures 5.9 - 5.15. In Figure 5.9, the non-dimensional temperature is plotted against radius for different time value i.e., for $t = 1,\ 2,\ 14,\ 15$. The profiles shows that, by increasing time the temperature increases until a steady state is achieved. In addition, the temperature at the centerline region of the pipe becomes higher as time increased and then reduced gradually to the prescribed value at the pipe wall (i.e.,$\theta = 1$ at $\eta = 1$). Figure 5.10 and Figure 5.11 show the increase of temperature by increasing of nanoparticles volume fraction (φ) and Grashof number (Gr) respectively. Expectedly, increasing of φ enhances the nanofluid temperature inside the pipe; this is due to the fact that nanoparticles have high thermal conductivity compared to pure water. Increasing Gr means increasing buoyancy force which enhances both the flow velocity and temperature as highlighted in the previous section. Meanwhile, Figures 5.12-5.15 show the variation of nanofluid temperature profiles with increasing each of the parameter β, λ, M and S. The profiles shows that the nanofluid temperature reduced by increasing each of these parameters when Al_2O_3-water nanofluid is used.

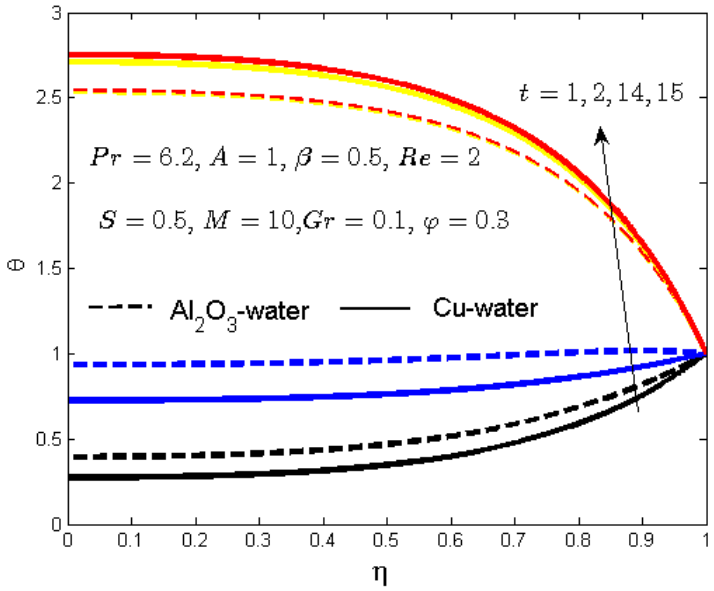

Figure 5.9: Transient and steady state non-dimensional temperature evolutions for Cu-water and Al_2O_3-water nanofluids

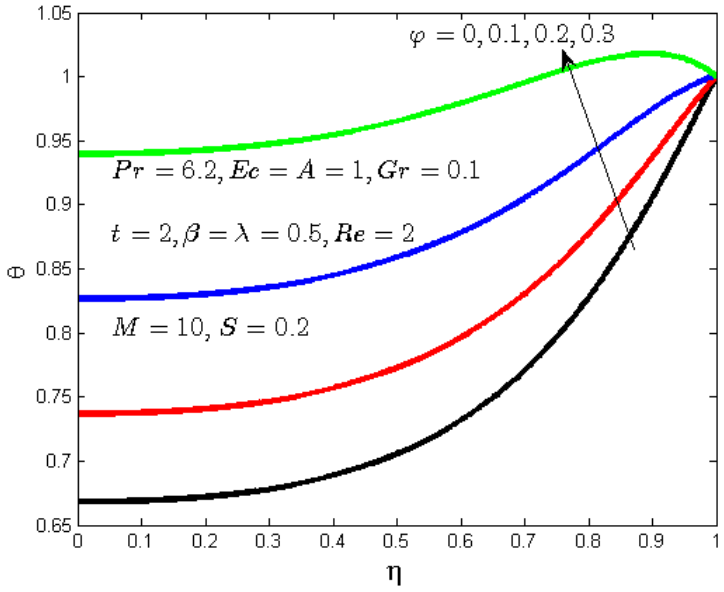

Figure 5.10: Non-dimensional temperature evolutions with increasing φ

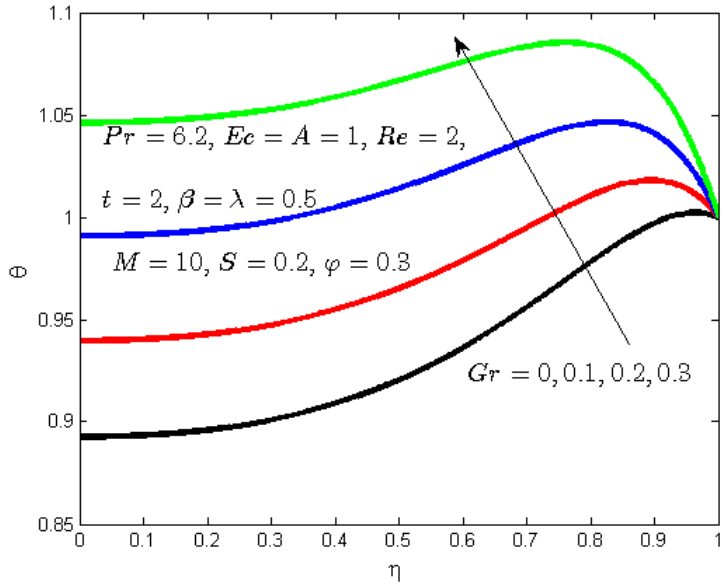

Figure 5.11: Non-dimensional temperature evolutions with increasing Gr

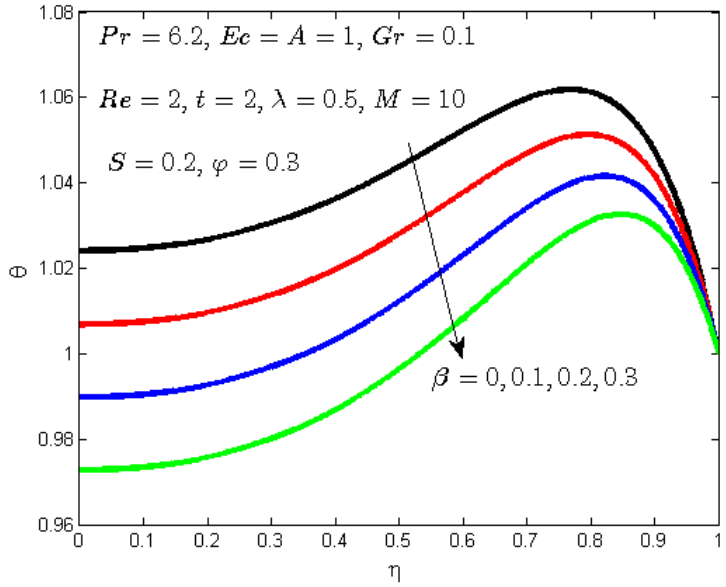

Figure 5.12: Non-dimensional temperature evolutions with increasing β

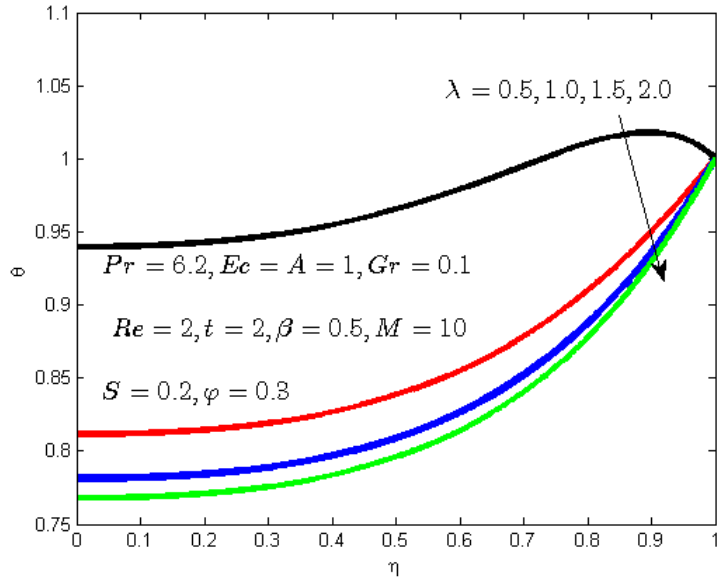

Figure 5.13: Non- dimensional temperature evolution with increasing λ

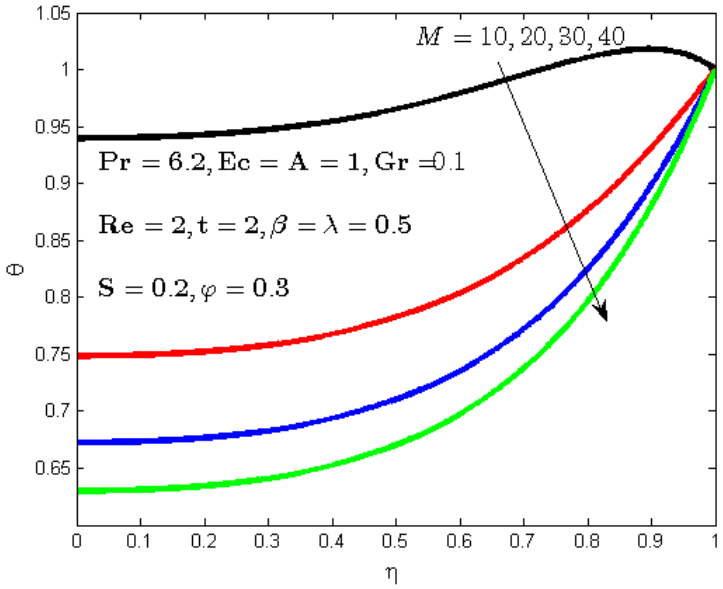

Figure 5.14: Non-dimensional velocity evolutions with increasing M

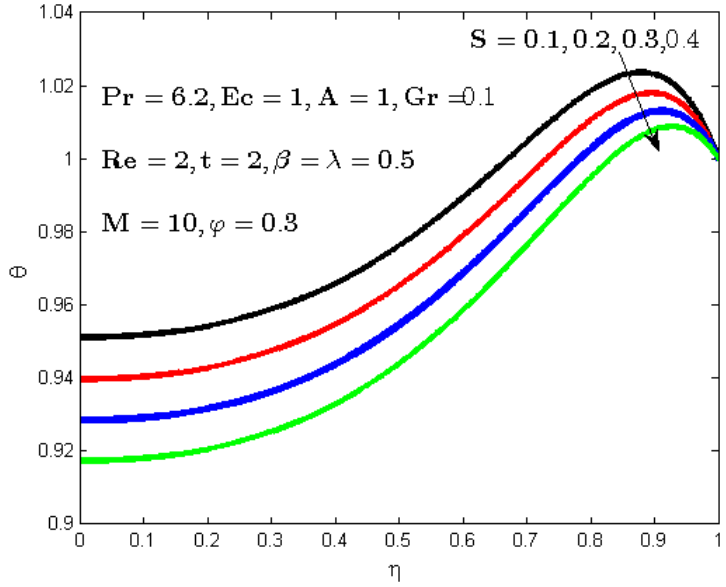

Figure 5.15: Non-dimensional temperature evolution with increasing S

5.4.3 Skin Friction and Nusselt Number with Parameters variation

The effects of various parameters on skin friction and Nusselt number are discussed in this section. Table 5.2 shows the numerical computation for skin friction and Nusselt number for some selected parameters values by fixing time and nanoparticle volume fraction. The results from the table shows that, the skin friction is increasing with the increase of Gr, β, Ec and A while decreasing with the increase of λ, Re, M and S. The results illustrates that the effect of increasing Gr, Ec and A is to increase the heat transfer rate, whereas increasing β, λ, Re, M and S is to reduce the heat transfer rate at the pipe wall. Moreover, the effect of embedded parameters values on skin friction is highlighted in Figures 5.16-5.18. Figure 5.16, compares the skin friction of Cu-water and Al_2O_3-water nanofluids. The profiles shows that the skin friction is higher with Cu-water than that of Al_2O_3-water nanofluids. The results also show that the skin friction is reduced by increasing φ and enhanced by increasing β as seen in Figure 5.17. Figure 5.18 shows that with increasing M and S the wall shear stress are reduced. The influence of embedded parameters on Nusselt number is displayed in Figures 5.19 - 5.21. Figure 5.19 demonstrates the skin friction for both Cu-water and Al_2O_3-water nanofluid. Interestingly, the profiles shows that the heat transfer rate of Al_2O_3-water is higher compared to Cu-water. Moreover, the response of increasing φ is to enhance the wall heat transfer rate while increasing β is to reduce the wall heat transfer rate as illustrated in Figure 5.20. The profiles shows that the wall transfer rate is reduced by increasing S and M as seen Figure 5.21.

Table 5.2: Computation showing the C_f and Nu for various values of embedded parameters for $t = 2,\ \varphi = 0.3$

Gr	β	Re	λ	Ec	A	S	M	C_f	Nu
0.1	0.5	2	0.5	1	1	0.5	10	0.0159	0.4837
0.2	0.5	2	0.5	1	1	0.5	10	0.0171	1.1073
0.3	0.5	2	0.5	1	1	0.5	10	0.0185	1.7902
0.1	0.1	2	0.5	1	1	0.5	10	0.0081	0.8543
0.1	0.4	2	0.5	1	1	0.5	10	0.0134	0.5837
0.1	0.9	2	0.5	1	1	0.5	10	0.0317	0.0626
0.1	0.5	1.5	0.5	1	1	0.5	10	0.0187	4.1548
0.1	0.5	2	0.5	1	1	0.7	10	0.0102	-0.7796
0.1	0.5	2	0.5	1	1	0.9	10	0.0075	-1.2840
0.1	0.5	2	0.5	1.5	1	0.5	10	0.0168	3.5800
0.1	0.5	2	0.5	2	1	0.5	10	0.0178	6.7031
0.1	0.5	2	0.5	1	1.5	0.5	10	0.0214	4.5196
0.1	0.5	2	0.5	1	2.0	0.5	10	0.0270	9.0739
0.1	0.5	2	0.5	1	1	0.6	10	0.0155	0.3436
0.1	0.5	2	0.5	1	1	1.0	10	0.0142	-0.1907
0.1	0.5	2	0.5	1	1	0.6	12	0.0146	-0.2388
0.1	0.5	2	0.5	1	1	0.6	15	0.0132	-0.9936

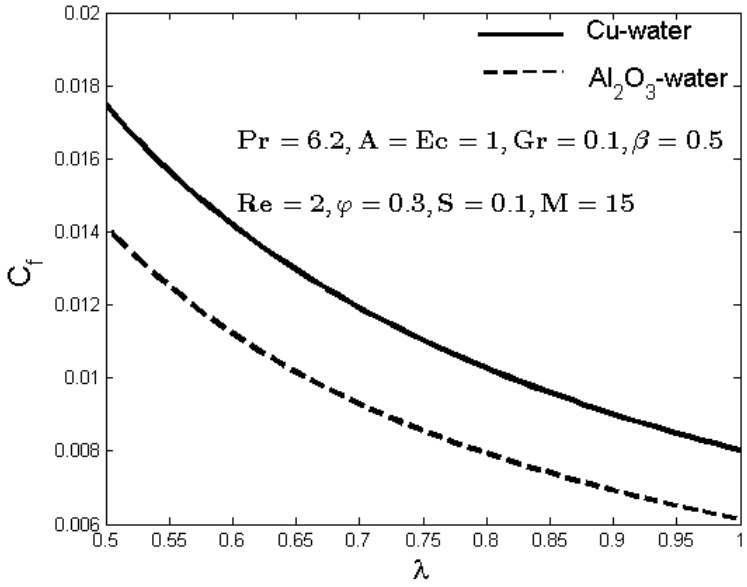

Figure 5.16: Skin friction profiles for Cu-water and Al_2O_3-water nanofluids

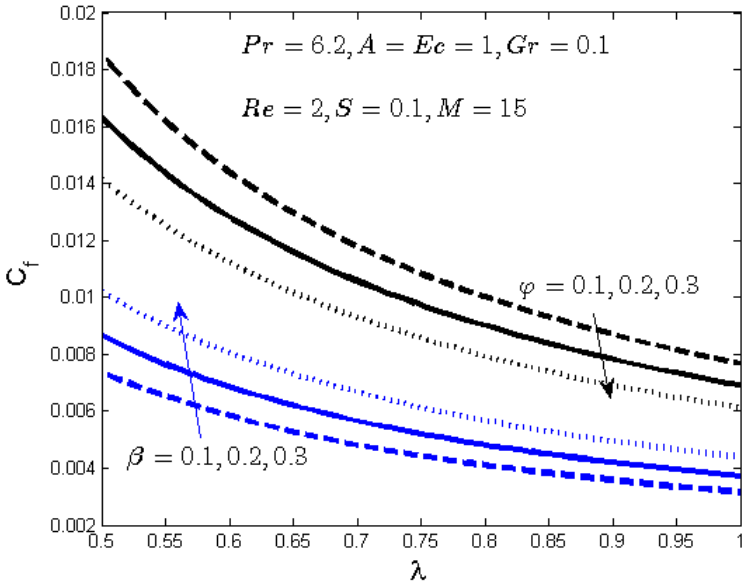

Figure 5.17: Skin fiction profiles with increasing φ,β and λ

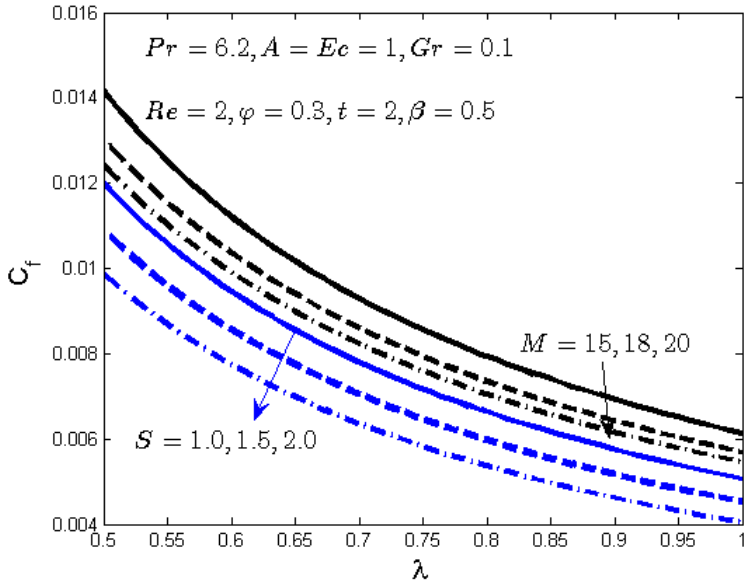

Figure 5.18: Skin fiction profiles with increasing M, S and λ

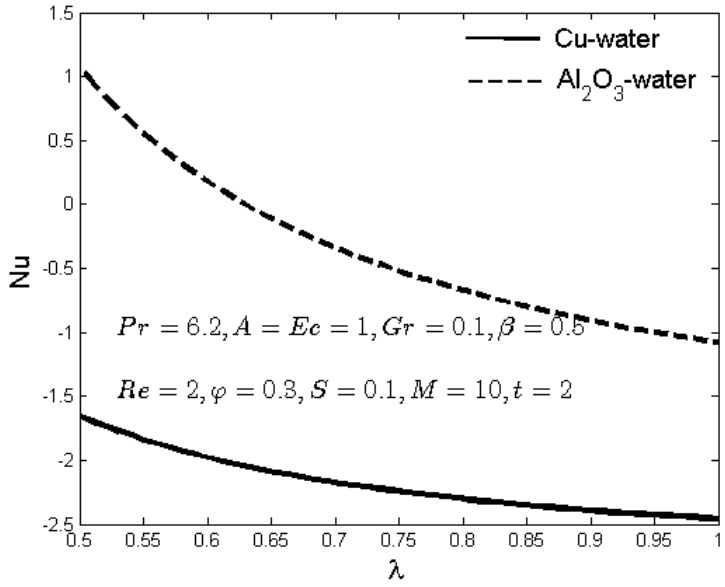

Figure 5.19: Nusselt number profiles for Cu-water and Al_2O_3-water nanofluids

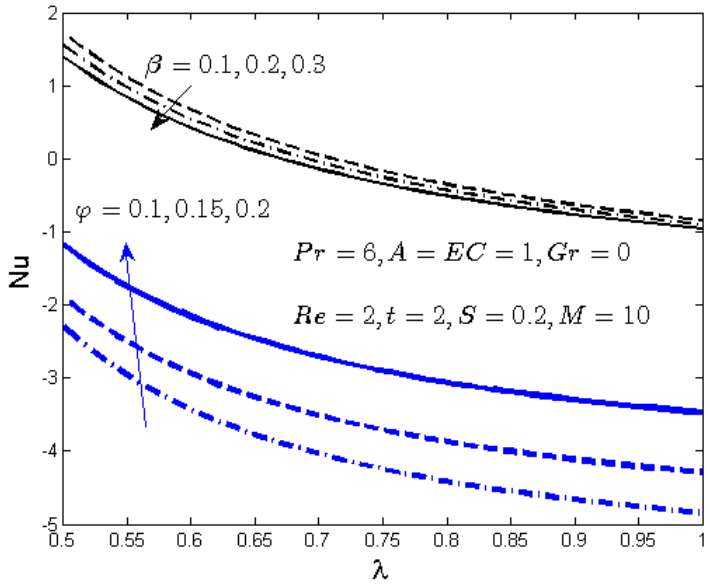

Figure 5.20: Nusselt number profiles with increasing φ, β, and λ

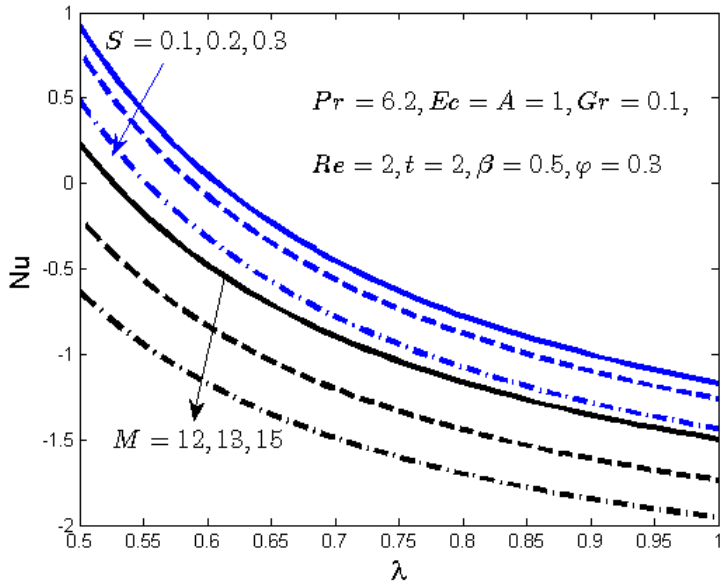

Figure 5.21: Nusselt number profiles with increasing M, S and λ

5.5 Conclusion

In this chapter, we investigated numerically the combined effect of buoyancy-driven force, temperature dependent viscosity and Navier slip on heat transfer for unsteady copper-water and alumina-water nanofluids in a permeable cylindrical pipe filled with saturated porous medium. The nonlinear governing PDEs are transformed into a set of initial value ODEs using semi-discretization finite difference method.

The resultant ODEs were solved numerically using Runge-Kutta-Fehlberg integration scheme implemented on a computer using MATLAB. The nanofluid velocity, temperature, skin friction and Nusselt number profiles were discussed for various parameters values governing the flow. The results reveal, among other conclusions, that:

- Both velocity and temperature profiles increases with increasing time until the steady state is achieved. The Al_2O_3-water nanofluid reaches its steady state earlier as compared to Cu-water.
- Both velocity and temperature profiles increases with the increasing of nanoparticles volume fraction and Grashof number while decreases with the increasing of variable viscosity parameter, Navier slip parameter, porous media resistance parameter and porous media shape factor parameter.
- The skin friction at the pipe wall is reduced with increasing nanoparticles volume fraction, Navier slip parameter, porous media resistance parameter and porous media shape factor parameter and enhanced with the increasing of variable viscosity parameter.
- Nusselt number is increased with increasing nanoparticles volume fraction and decreased with increasing variable viscosity parameter, porous media resistance parameter and porous media shape factor parameter.

CHAPTER SIX

6.1 General Discussion

In this study, we considered the analysis of steady and unsteady axisymmetric laminar nanofluid flow of incompressible fluids with some variable parameters through a channel and cylindrical pipes with permeable boundary walls. The nanoparticles used in our analysis were copper (Cu) and alumina (Al_2O_3). The governing PDE for mass, momentum and energy were obtained. The nonlinear partial differential equations were then dimensionalized and transformed into ODE by using the method of lines for the case of unsteady formulated models and Berman similarity transformation for the case of steady nanofluid formulated model. The resulting dimensionless nonlinear ordinary differential equations were then solved numerically using the well-known fourth order Runge-Kutta-Fehlberg method with shooting technique and analytically using regular perturbation method. The numerical results for the velocity, temperature, skin-friction coefficient, and Nusselt number profiles and the effect of pertinent parameters are studied and plotted graphically and in tabular form. We compared our numerical and analytical results and also our present results with one existing in literature for the flow of conventional fluid in a symmetrical porous wall channel.

In chapter 2, we investigated the heat transfer characteristics of a Berman flow of water based nanofluids in a porous channel with Navier slip, viscous dissipation and convective cooling. We assume that the exchange of heat with the ambient surrounding takes place at the channel walls following the Newton's law of cooling. The governing non-linear partial differential equations were transformed to non-linear ordinary differential equations using Berman similarity transformation. We solved the resultant nonlinear problem using both analytical and numerical techniques. The numerical results show a good agreement with the exact solution and consistent with prior published result.

In chapter 3, the combined effects of variable viscosity, Brownian motion, thermophoresis and convective cooling on unsteady flow of nanofluids in a pipe with permeable wall were investigated. The non-linear PDE were non-dimensionalized and transformed into a set of non-linear ODE by using semi-discretization technique. The non-dimensional governing equations of momentum and energy balance, and the equation for nanoparticles concentration were then solved numerically. The numerical solution for the representative velocity profiles, temperature profiles, nanoparticles concentration profiles, skin friction and Nusselt number have been carried out by assigning some arbitrary values to various parameters controlling the flow system and presented graphically. The effects of different parameters governing the flow on skin friction and Nusselt number coefficients were tested. The results revealed that velocity is increasing with a decrease of viscosity and increasing of suction Reynolds number while decreasing with an increase of convective cooling and injection Reynolds number. Furthermore, the temperature

is decreasing with an increase of convective cooling and decreasing with a decrease of viscosity before flow reversal at the pipe surface. Also the nanoparticles concentration is increasing with an increase of thermophoresis and decreasing with an increase of Brownian motion before flow reversal at the pipe surface.

In chapter 4, we investigated the effects of buoyancy force and temperature dependent viscosity on unsteady nanofluid flow past a vertical porous pipe. We developed the governing equations for continuity, momentum, and energy by using Bousinessq approximation for density variation due to temperature with the Buongiorno nanofluid model. The set of non-linear partial differential equations were then transformed into non-linear ordinary differential equations using semi-discretization approach. The numerical solutions for the temperature, velocity, skin friction and Nusselt number were obtained and presented graphically. The effects of various thermophysical parameters on temperature and velocity profiles as well as skin friction and Nusselt number were analysed. Our results reveals that both nanofluids velocity and temperature increase with a decrease in viscosity and an increase in buoyancy force intensity.

In chapter 5, the combined effect of buoyancy-driven force, variable viscosity and Navier slip on heat transfer of unsteady water-based nanofluid flow in a permeable cylinder through saturated porous medium were investigated numerically. The Darcy- Brinkman-Forchheimer model was adopted to formulate the equations of the flow. The non-linear PDE governing the flow were obtained, non-dimensionalized and transformed into ODE and then solved numerically. The numerical solutions for velocity, temperature, skin friction and Nusselt number have been presented graphically and discussed quantitatively. The results reveal that both nanofluid temperature and velocity are enhanced with increasing Grashof number and Darcy number but reduced with the increasing of viscosity, Navier slip parameter and porous media resistance parameter.

6.2 Conclusion

Different mathematical models of nanofluids flow and heat transfer through a cylindrical pipe and channel with porous wall are formulated and analyzed under various physical situation. In general, the study considers axisymmetric, Newtonian and laminar nanofluids flow models of incompressible fluid with variable parameters. The nonlinear models are tackled both analytically and numerically using different approaches as explained in the earlier chapters and the results are presented graphically and in tabular form. The effects of pertinent parameters have been tested. We validate our results by comparing with the existing one in the literature and also by solving the problem using different approaches. One of the main findings we have observed is that the nanoparticles volume fraction enhances the heat transfer as presented in many other studies obtained from the literature, and this conclude that the nanofluids is

an advanced fluid in cooling or heating system compared with the normal fluids like water. Thus, the models and analysis presented in this dissertation will aid the research community in understanding the mechanism of heat transfer in nanofluids. Moreover, it was observed from the analysis that, using the same base fluid and the same types of nanoparticles some results differ from one model to another depending on the geometry orientation and boundary conditions. However, some of the essential features of physical interest are summarized below:

- Both Cu-water and Al_2O_3 -water nanofluids profiles varies with time before it reaches their steady state, Al_2O_3 -water reaches its steady state earlier than Cu-water.

- Cu-water nanofluid moves faster as compared to Al_2O_3 -water nanofluids. The nanofluid velocity is increased with nanoparticles volume concentration when slip condition is used and the situation reverse when no slip condition is used at the boundaries. Also the profiles illustrate that the velocity is increasing with suction, Grashof number and Darcy number while decreasing with the increase of viscosity, injection and porous media resistance parameter.

- Cu-water nanofluid produced higher temperature as compared to Al_2O_3 -water. The nanofluids temperature increases with suction, viscous dissipation, buoyancy force and Darcy number. Furthermore, nanofluid temperature increases with slip parameter and nanoparticles volume concentration however this behaviour changes depending on the boundary conditions and geometry orientation, for example when convective cooling is applied in the boundary the temperature reduced otherwise it raised. Moreover, the nanofluid temperature is decreased with increasing convective cooling, injection viscosity and porous media resistance parameter.

- The pressure drop produced by Al_2O_3 -water in more than that of Cu-water. The pressure drop is enhanced by injection, Navier slip parameter and nanoparticles volume fraction but decrease by suction.

- The skin friction produced by Cu-water is more intense than that of Al_2O_3 -water. The skin friction increases with suction, Grashof number, Darcy number. In addition, the skin friction is also increases with Navier slip parameter and nanoparticles volume fraction for the case of channel flow with convective cooling in the boundary while the skin friction decreases for the same parameter for the case of vertical pipe with no convective cooling at the boundary. Moreover the skin friction decreases with increasing injection, viscosity, porous media resistance parameter and nanoparticles volume fraction.

- The Nusselt number of Al_2O_3-water is higher for some cases compared to Cu-water. The Nusselt number increases with suction, Biot number, Eckert number and Navier slip while decreases with

injection, viscosity, porous media resistance parameter and nanoparticles volume fraction.

6.3 Recommendations

The findings of this research are useful for industrial purposes specifically in heat transfer systems design. Thus, a practical applicability of the findings will improve the existing design in cooling system by making use of nanofluids.

Getting the knowledge from other field related to this study for the purpose of practical use of the models will integrate strongly theoretically and experimentally.

Suggestions for Future Work

This study can be extended in different number of ways for instance:

- One can consider the interaction of nanoparticles for turbulent flow.
- The same geometry of pipe flow could also be considered for the non-Newtonian fluids.
- Extensions to the three dimensional porous walled channel and two dimensional pipe or annular flows with porous or accelerating walls could also be considered.
- Different fluids or fluid-like materials could also be considered by amending the constitutive equation relating the stresses and shear-rates within the fluid elements.
- Similar problems as presented here, can be considered by simply changing the wall boundary conditions.

REFERENCES

Abu-Nada, E. and Chamkha, A. J. (2010). Effect of nanofluid variable properties on natural convection in enclosures filled with a CuO-EG-Water nanofluid. *International Journal of Thermal Science*, **49**(12):2339–2352.

Ahmad, S. and Pop, I. (2010). Mixed convection boundary layer flow from a vertical flat plate embedded in a porous medium filled with nanofluids. *International Communication of Heat Mass Tranfer*, **37**(8):987–991.

Ahmad, S., Rohni, A. M., and Pop, I. (2011). Blasius and sakiadis problems in nanofluids. *Acta Mechanica*, **218**(3-4):195–204.

Alexandre, C. and Jerrold, E. M. (1992). *A Mathematical Introduction to Fluid Mechanics*. Springer-Verlag Publishing Company, Inc.

Anbuchezhian, N., Srinivasan, K., Chandrasekaran, K., and Kanasamy, R. (2012). Thermoporesis and Brownian motion effects on boundary layer flow of nanofluid in presence of thermal stratification due to solar energy. *Applied Mathematics and Mechanics*, **33**(6):765–780.

Bansod, V. J. (2003). The Darcy model for boundary layer flows in a horizontal porous medium induced by combined buoyancy forces. *Journal of Porous Media*, **6**(4):273–281.

Batchelor, G. K. (1977). The effect of Brownian motion on the bulk stress in the suspension of spherical particles. *Journal of Fluid Mechanical*, **83**(01):97–117.

Berman, A. S. (1953). Laminar flow in channels with porous wall. *Journal of Applied Physics*, **24**(9):1232–1235.

Blazeki, J. (2005). *Computational Fluid Dynamics: Principle and Application*. Elsevier Ltd, Oxford, UK, second edition.

Brinkman, H. C. (1952). The viscosity of concentrated suspensions and solution. *Journal of Chemical Physics*, **20**(4):571–581.

Buongiorno, J. (2006). Convective transport in nanofluids. *Journal of Heat transfer*, **128**(3):240–250.

Choi, S. U. S. (1995). Enhancing thermal conductivity of fluids with nanoparticles. In Singer, D. and Wang, H., editors, *Development and Applications of Non-Newtonian Flows*, volume **66**, pages 99–106. American Society of Mechanical Engineers, New York.

Das, S. K., Putra, N., and Roetzel, W. (2003a). Pool boiling characteristics of nanofluids. *International Journal of Heat and Mass Transfer*, **46**(5):851–862.

Das, S. K., Putra, N., Thiesen, P., and Roetzel, W. (2003b). Temperature dependence of thermal conductivity enhancement for nanofluids. *Transactions of the ASME. Journal of Heat Transfer*, **125**(4):567–574.

Deswita, L., Ishak, A., and Nazar, R. (2010). Powerlaw fluid flow on a moving wall with suction and injection effects. *Australian Journal of Basic and Applied Sciences*, **4**(8):2250–2256.

Eastman, J. A., Choi, S. U. S., Li, S., Yu, W., and Thompson, L. J. (2001). Anomalously increased effective thermal conductivity of ethylene glycol-based nanofluids containing copper nanoparticles. *Applied Physics Letter*, **78**(6):718–720.

Eastman, J. A., Phillpot, S. R., Choi, S. U. S., and Keblinski, P. (2004). Thermal transport in nanofluids. *Annual Review of Materials Research*, **34**(1):219–246.

Eegunjobi, A. S. and Makinde, O. D. (2012). Combined effect of buoyancy force and Navier slip on entropy generation in a vertical porous channel. *Entropy*, **14**(6):1028–1044.

Einstein, A. (1906). A new determination of the molecular dimensions. *Annalen Der Physik*, **19**(2):289–306.

Erdogan, M. E. and Imrak, C. E. (2008). On the flow in a uniformly porous pipe. *International Journal of Non-Linear Mechanics*, **43**(4):292–301.

Gorla, R. and Chamkha, A. (2011). Natural convection boundary layer flow over a horizontal plate embedded in a porous medium saturated with nanofluid. *Journal of Modern Physics*, **2**(2):62–71.

Hadamard, J. (1902). *Sur les problmes aux drives partielles et leur signification physique*. Princeton University Bulletin.

Hajipour, M. and Dehkordi, M. (2012). Analysis of nanofluid heat transfer in parallel-plate vertical channels partially filled with porous media. *International Journal of Thermal Science*, **55**:103–113.

Ho, C. J., Liu, W. K., S, C. Y., and Lin, C. C. (2010). Natural convection heat transfer of alumina-water nanofluid in vertical square enclosures: an experimental study. *International Journal of Thermal Sciences*, **49**(8):1345–1353.

Huang, P. and Breuer, K. S. (2007). Direct measurement of slip length in electrolyte solutions. *Physics of Fluids*, **19**(2):028104.

Hwang, K. S., Lee, J. H., and Jang, S. P. (2007). Buoyancy-driven heat transfer of water-based Al_2O_3 nanofluids in a rectangular cavity. *International Journal of Heat and Mass Transfer*, **50**(19):4003–4010.

Ishak, A. (2009). Mixed convection boundary layer flow over a horizontal plate with thermal radiation. *International Journal of Heat and Mass Transfer*, **46**(2):147–151.

John, H. Y. (2008). *A Heat Transfer Text Book*. Phlogiston Press, Cambridge Massachusetts, third edition.

Kakac, S. and Pramuanjaroenkij, A. (2009). Review of convective heat transfer enhancement with nanofluids. *International Journal of Heat and Mass Transfer*, **52**(13):3187–3196.

Kamyar, A., Saidur, R., and Hasanuzzaman, M. (2012). Application of computational fluid dynamics for nanofluids. *International Journal of Heat and Mass Transfer*, **55**(15):4104–4115.

Kandelousi, M. S. (2014). KKL correlation for simulation of nanofluid flow and heat transfer in a permeable channel. *Physics Letters A*, **378**(45):3331–3339.

Karode, S. K. (2001). Laminar flow in channels with porous walls, revisited. *Journal of Membrane Science*, **191**(1-2):237–241.

Kaufui, V. W. and Omar, D. L. (2010). Applications of nanofluids: current and future. *Advances in Mechanical Engineering*, **2**:11pages.

Khanafer, K. and Vafai, K. (2011). A critical synthesis of thermophysical characteristics of nanofluids. *International Journal of Heat and Mass Transfer*, **54**(19-20):4410–4428.

Khanafer, K., Vafai, K., and Lightstone, M. (2003). Buoyancy-driven heat transfer enhancement in a two-dimensional enclosure utilizing nanofluids. *International Journal of Heat and Mass Transfer*, **46**(19):3639–3653.

Kiblinski, P., Phillpot, S. R., Choi, S. U. S., and Eastman, J. A. (2002). Mechanism of heat flow is suspensions of nano-sized particles (nanofluids). *International Journal of Heat and Mass Transfer*, **45**(4):855–863.

Klemp, K., Herwig, H., and Selmann, M. (1990). Entrance flow in channel with temperature dependent viscosity including viscous dissipation effects. *Proceedings of the Third International Congress Fluid Mechanics*, **3**:1257–1266.

Kumar, R., Ibrahim, A., and Veena, S. (2013). A numerical study of free convection heat and mass transfer in a Rivlin-Ericksen viscoelastic flow past an impulsively started vertical plate with variable temperature and concentration. *International Journal of Heat and Fluid Flow*, **44**:258–264.

Kuppalapalle, V., Kerehalli, P. V., and Chiu-on, N. (2013). The effect of variable viscosity on the flow and heat transfer of a viscous ag-water and cu-water nanofluids. *Journal of Hydrodynamics*, **25**(1):8pages.

Kuznetov, A. V. and Nield, D. A. (2009). Thermal instability in a porous medium layer saturated by a nanofluid. *International Journal of Heat and Mass Transfer*, **52**(25-26):5796–5801.

Kuznetov, A. V. and Nield, D. A. (2010a). The onset of convection in a layer of cellular porous material: effect of temperature-dependent conductivity arising from radiative transfer. *Journal of Heat Transfer*, **132**(7):4–12.

Kuznetov, A. V. and Nield, D. A. (2010b). The onset of double-diffusive nanofluid convective in a layer of a saturated porous medium. *Transport in Porous Media*, **85**(3):941–951.

Kuznetsov, V. D. and Nield, A. (2010). Natural convective boundary layer flow of nanofluid past a vertical plate. *International Journal of Thermal Science*, **49**(2):243–247.

Makinde, O. D. (1999). Extending the utility of perturbation series in problems of laminar flow in a porous pipe and a diverging channel. *Journal of Australian Mathematical Society*, **41**(01):118–128.

Makinde, O. D. (2009). Hermite-Pade approach to thermal radiation effect on inherent irreversibility in a variable viscosity channel flow. *Computers and Mathematics with Applications*, **58**(11):2330–2338.

Makinde, O. D. (2012). Effects of variable viscosity on thermal boundary layer over a permeable flat plate with radiation and convective surface boundary condition. *Journal of Mechanical Science and Technology*, **26**(5):1615–1622.

Makinde, O. D. (2013a). Computational modelling of nanofluids flow over a convectively heated unsteady stretching sheet. *Current Nanoscience*, **9**(5):673–678.

Makinde, O. D. (2013b). Effects of viscous dissipation and Newtonian heating on boundary layer flow of nanofluids over a flat plate. *International Journal of Numerical Methods for Heat and Fluid flow*, **23**(8):1291–1303.

Makinde, O. D., Chinyoka, T., and Rundora, L. (2011). Unsteady flow of a reactive variable viscosity non-Newtonian fluid through a porous saturated medium with asymmetric convective boundary conditions. *Computational Mathematics and Application*, **62**(9):3343–3352.

Makinde, O. D. and Eegunjobi, A. S. (2013). Entropy generation in a couple stress fluid flow throgh vertical channel filled with saturated porous media. *Entropy*, **15**(11):4589–4606.

Makinde, O. D., Khamis, S. A., Tshehla, M. S., and Franks, O. (2014). Analysis of heat transfer in Berman flow of nanofluids with Navier slip, viscous dissipation, and convective cooling. *Advances in Mathematical Physics*, **2014**:13pages.

Mansour, M. A., Bakeir, M. A., and Chamkha, A. (2014). Natural convection inside a C-shaped nanofluid-filled enclosure with localized heat sources. *International Journal of Numerical Methods for Heat and Fluid Flow*, **24**(8):1954–1978.

Martin, M. J. and Boyd, D. I. (2006). Momentum and heat transfer in a laminar boundary layer with slip flow. *Journal of Thermophysics and Heat Transfer*, **20**(4):710–719.

Maxwell, J. C. (1881). *Treatise on Electricity and Magnetism*. Clarendon, Oxford, UK, 2rd edition.

Maxwell, J. C. (1904). *Electricity and magnetism*. Clarendon, Oxford, 3rd edition.

Morton, K. W. and Mayers, D. F. (2005). *Numerical Solution of Partial Differential Equations: An Introduction*. Cambridge University Press.

Motsumi, T. and Makinde, O. D. (2012). Effects of thermal radiation and viscous dissipation on boundary layer flow of nanofluids over a permeable moving flat plate. *Physica Scripta*, **86**(4):8pages.

Moussy, Y. and Snider, A. D. (2009). Laminar flow over pipes with injection and suction through the porous wall at low Reynolds numbers. *Journal of Membrane Science*, **327**(1):104–107.

Mutuku-Njane, W. N. and Makinde, O. D. (2013). Combined effect of buoyancy force and navier slip on MHD flow of a nanofluid over a convectively heated vertical porous plate. *The Scientific World Journal*, **49**:8pages.

Mutuku-Njane, W. N. and Makinde, O. D. (2014a). Hydromagnetic bioconvection of nanofluid over a permeable vertical plate due to gyrotactic microorganisms. *Computer and Fluids*, **95**:88–97.

Mutuku-Njane, W. N. and Makinde, O. D. (2014b). MHD nanofluid flow over a permeable vertical plate with convective heating. *Journal of Computational and Theoretical Nanoscience*, **11**(3):667–675.

Na, T. Y. (1979). *Computational Methods in Engineering Boundary Value Problems*. Academic Press, New York.

Namburu, P. K., Misra, D., and Das, D. K. (2007). Viscosity of copper oxide nanoparticles dispersed in ethylene glycol and water mixture. *Experimental Thermamal and Fluid Science*, **32**(2):397–402.

Navier, C. L. M. H. (1823). Memoire sur les lois du mouvement des fluides. *Memoires de l'Academie Royale des Sciences de l'Institutde France*, **6**:389–440.

Nazari, M., Ashouri, M., Kayhani, M. H., and Tamayol, A. (2015). Experimental study of convective heat transfer of a nanofluid through a pipe filled with metal foam. *International Journal of Thermal Science*, **88**:33–39.

Olanrewaju, A. M. and Makinde, O. D. (2013). On boundary layer stagnation point flow of a nanofluid over a permeable flat surface with Newtonian heating. *Chemical Engineering Communications*, **200**(6):836–852.

Oxarango, L., Schmitz, P., and Quintard, M. (2004). Laminar flow in channels with wall suction or injection: a new model to study multi-channel filtration systems. *Chemical Engineering Science*, **59**(5):1039–1051.

Ozkol, I., Komurgoz, G., and Arikoglu, A. (2007). Entropy generation in the laminar natural convection from a constant temperature vertical plate in an infinite fluid. *Journal of Power Energy*, **221**(5):609–616.

Oztop, H. F. and Abu-Nada, E. (2008). Numerical study of natural convection in partially heated rectangular enclosures filled with nanofluids. *International Journal of Heat and Fluid Flow*, **29**(5):1326–1336.

Pak, B. C. and Cho, Y. I. (1998). Hydrodynamic and heat transfer study of dispersed fluids with submicron metallic oxide particles. *Experimental Heat Transfer*, **11**(2):151–170.

Patrulescu, F. O., Grosan, T., and Pop, I. (2014). Mixed convection boundary layer flow from a vertical truncated cone in a nanofluid. *International Journal of Numerical Methods for Heat and Fluid Flow*, **24**(5):1175–1190.

Paul, A. D. and Gorazo, M. (2007). *Fluid Dynamics with a Computational Perspective*. Cambridge University Press, New York.

Pawel, K., Ravi, P., and Jacob, E. (2008). Thermal conductance of nanofluids: is the controversy over? *Journal of Nanoparticle*, **10**(7):1089–1097.

Pederson, R. J. and Kinney, R. B. (1971). Entrance-region heat transfer for laminar flow in porous tubes. *International Journal of Heat and Mass Transfer*, **14**(1):159–161.

Raithby, G. D. (1971). Laminar heat transfer in the thermal entrance region of circular tubes and two-dimensional rectangular ducts with wall suction and injection. *International Journal of Heat and Mass Transfer*, **14**(2):224–243.

Raju, K. S. N. (2011). *Fluid Mechanics, Heat Transfer, and Mass Transfer*. John Wiley &Sons, Inc.,Hoboken, New Jersey.

Rana, G. C., Thakur, R. C., and Kango, S. K. (2014). On the onset of thermosolutal insatability in a layer of an elastico-viscous nanofluid in porous media. *FME Transactions*, **42**(1):1–9.

Sahin, A. Z. (1999). Effect of variable viscosity on the entropy generation and pumping power in a laminar fluid flow through a duct subjected to constant heat flux. *Heat and Mass Transfer*, **35**(6):499–506.

Sellars, J. R. (1955). Laminar flow in channels with porous walls at high suction Reynolds numbers. *Journal of Applied Physics*, **26**(4):489–490.

Senthilkumar, R., Vaidyanathan, S., and Sivaraman, B. (2012). Effect of inclination angle in heat pipe performance using copper nanofluid. *Procedia Engineering*, **38**:3715–3721.

Sheikholeslami, M., Ellahi, R., Hassan, M., and Soleimani, S. (2014). A study of natural convection heat transfer in a nanofluid filled enclosure with elliptic inner cylinder. *International Journal of Numerical Methods for Heat and Fluid Flow*, **24**(8):1906–1927.

Singh, P., Tomer, N. S., Kumar, S., and Sinha, D. (2010). MHD oblique stagnation-point flow towards a stretching sheet with heat transfer. *International Journal of Applied Mathematics and Mechanics*, **6**(13):94–111.

Sorour, M. M., Hassab, M. A., and Estafanous, S. (1987). Developing laminar flow in a semiporous two-dimensional channel with nonuniform transpiration. *International Journal of Heat and Fluid Flow*, **8**(1):44–54.

Stokes, V. K. (1984). *Theories of Fluids with Microstructure: An Introduction*. Springer: New York.

Targui, N. and Kahalerras, H. (2014). Analysis of a double pipe heat exchanger performance by use of porous baffles and nanofluids. *International Journal of Mechanical, Aerospace, Industrial, Mechatronic and Manufacturing Engineerig*, **8**(9):1581–1586.

Terrill, R. M. (1982). An exact solution for flow in a porous pipe. *Journal of Applied Mathematical Physics*, **33**(4):547–552.

Terrill, R. M. (1983). Laminar flow in a porous tube. *Journal of Fluids Engineering*, **105**(3):303–307.

Tham, L., Nazar, R., and Pop, I. (2011). Mixed convection boundary layer flow from a horizontal circular cylinder in a nanofluid. *International Journal of Numerical Methods for Heat and Fluid Flow*, **22**(5):576–606.

Theuri, D. and Makinde, O. D. (2014). Thermodynamic analysis of variable viscosity MHD unsteady generalized Couette flow with permeable walls. *Applied and Computational Mathematics*, **3**:1–8.

Tsangaris, S., Kondaxakis, D., and Vlachakis, N. W. (2007). Exact solution for flow in a porous pipe with unsteady wall suction and/or injection. *Communication in Nonlinear Science and Numerical Simulation*, **12**(7):1181–1189.

Vafai, K. and Tien, C. L. (1982). Boundary and inertia effects on convective mass transfer in porous media. *International Journal of Heat and Mass Transfer*, **25**(8):1183–1190.

Wang, J., Zhu, J., Zhang, X., and Chen, Y. (2013). Heat transfer and pressure drop of nanofluids containing carbon nanotubes in laminar flows. *Experimental Thermal and Fluid Science*, **44**:716–721.

Wang, X., Xu, X., and Choi, S. S. U. (1999). Thermal conductivity of nanoparticle-fluid mixture. *Journal of Thermophysics and Heat Transfer*, **13**(4):474–480.

Wang, X. Q. and Mujumdar, A. S. (2007). Heat transfer characteristics of nanofluids: a review. *International Journal of Thermal Sciences*, **46**(1):277–284.

Wen, D. and Ding, Y. (2005). Experimental investigation into the pool boiling heat transfer of aqueous based γ-alumina nanofluids. *Journal of Nanoparticle Researsch*, **7**(2):265–274.

Xuan, Y. and Li, Q. (2003). Investigation on convective heat transfer and flow features of nanofluids. *Journel of Heat and mass Transfer*, **125**(1):151–165.

Yang, B. and Han, Z. H. (2003). Temperature-dependent thermal conductivity of nanorod-based nanofluids. *Applied Physics Letters*, **89**(8):083111.

You, S. M., Kim, J. H., and Kim, K. H. (2003). Effect of nanoparticles on critical heat flux of water in pool boiling heat transfer. *Applied Physics Letters*, **83**(16):3374–3376.

Yuan, S. W. (1956). Further investigation of laminar flow in channels with porous walls. *Journal of Applied Physics*, **27**(3):267–269.

Zaturska, M. B., Drazin, P. G., and Banks, W. H. H. (1988). On the flow of a viscous fluid driven along a channel by suction at porous walls. *Fluid Dynamics Research*, **4**(3):151–178.

APPENDICES

Appendix A: Published Articles

1. O. D. Makinde, S. Khamis, M. S. Tshehla and O. Franks (2014). Analysis of Heat Transfer in Berman Flow of Nanofluids with Navier Slip, Viscous Dissipation, and Convective Cooling, *Advances in Mathematical Physic*s, Article ID 809367, 13 pages.

2. Sara Khamis, Oluwole Daniel Makinde, Yaw Nkansah-Gyekye (2014). Modelling the effects of variable viscosity in unsteady flow of nanofluids in a pipe with permeable wall and convective Cooling, *Applied and Computational Mathematics*, 3(3): 75-84.

3. Sara Khamis Daniel Oluwole Makinde Yaw Nkansah-Gyekye (2015). Unsteady flow of variable viscosity Cu-water and Al2O3-water nanofluids in a porous pipe with buoyancy force, *International Journal of Numerical Methods for Heat & Fluid Flow*, 20 pages.

4. Sara Khamis, Oluwole Daniel Makinde & Yaw Nkansah-Gyekye (2015) Buoyancy-Driven Heat Transfer of Water-Based Nanofluid in a Permeable Cylindrical Pipe with Navier Slip through a Saturated Porous Medium, *Journal of Porous Media*, 18 (12): 1169-1180.

Appendix B

$$G_1 = 1 + m_4 Bi - 4m_4 Bib + 6m_4 Bib^2$$

$$\begin{aligned} G_2 &= -2m_1 m_4^2 Bi^4 - 3780 m_2 Prb + 5670 m_2 Prb^2 + 630 m_2 Pr \\ &+ 24 m_1 m_4^2 Bi^2 b + 232 m_2 m_4^2 PrBi^2 - 3294 m_2 m_4 PrBib \\ &+ 4536 m_2 m - 4 PrBib^2 - 1875 m_2 m_4^2 Bi^2 Prb + 580 m_2 m_4^2 Prb^2 Bi^2 \\ &- 8694 m_2 m_4^2 PrBi^2 b^3 + 5670 m_2 m_4^2 prBi^2 b^2 + 5670 m_2 m_4^2 PrBi^2 b^4 \\ &+ 54 m_1 m_4 Bib + 594 m_2 m_4 PrBi \end{aligned}$$

$$\begin{aligned} G_3 &= 6m_1 m_4 Bib + 70 m_2 Pr - 135 m_2 m_4 PrBib + 24 m_2 m_4 PrBi \\ &- 420 m_2 Prb + 630 m_2 Prb^2 + 189 m_2 m_4 PrBib^2 \end{aligned}$$

Appendix C: MATLAB Code for the model in chapter 3

```
%function file
function ds = ode_sys1(t,s,delta_eta,Pr,
             Ec,n,G,Nb,Nt,Re,Sc,eta,beta,Bi)
%input t the time variable (not used in this case)
% s the state vector
% k1,k2 model parameters
%output ds the derivative ds/dt at time t
w=zeros(1,n);
theta=w;
H=w;
dw=w;
dtheta=w;
dH=w;
for k=1:n
w(k) = s(k); %for clarity & readability, write the
theta(k) = s(n+k);
H(k)=s(2*n+k);
 end
for k=1:n
    if(k==1)
        W1=w(k);
        THETA1=theta(k);
        h1=H(k);
        W2=w(k+1);
        THETA2=theta(k+1);
        h2=H(k+1);
    elseif(k==n)
     W2=0;
  THETA2=theta(n)-delta_eta*Bi*(theta(n)-1);
  h2=H(n)-Nt/Nb*(theta(n)-delta_eta*Bi*(theta(n)-1)-theta(n));
  W1=w(k-1);
  THETA1=theta(k-1);
```

```
 h1=H(k-1);
    else
   W1=w(k-1);
   THETA1=theta(k-1);
   h1=H(k-1);
   W2=w(k+1);
   THETA2=theta(k+1);
   h2=H(k+1);
   end

dw(k)=G-Re*(W2-W1)/(2*delta_eta)
    +(W2-2*w(k)+W1)/(delta_eta)^2*exp(-beta*theta(k))
    +exp(-beta*theta(k))*(W2-W1)/(2*eta(k)*delta_eta)
   -beta*exp(-beta*theta(k))*(W2-W1)
   *(THETA2-THETA1)/(4*delta_eta^2);

dtheta(k)=-Re*(THETA2-THETA1)/(2*delta_eta)
        +(THETA2-2*theta(k)+THETA1)/(Pr*delta_eta^2)
         +(THETA2-THETA1)/(2*eta(k)*delta_eta)
         +Nb*(THETA2-THETA1)*(h2-h1)/(4*Pr*delta_eta^2)
         +Nt/Pr*((THETA2-THETA1)/(2*delta_eta))^2
         +Ec*exp(-beta*theta(k))*((W2-W1)/(2*delta_eta))^2;

dH(k)=-Re*(h2-h1)/(2*delta_eta)+(h2-2*H(k)
      +h1)/(Sc*(delta_eta)^2)
      +(h2-h1)/(2*eta(k)*Sc*delta_eta)
      + Nt*(THETA2-2*theta(k)
      +THETA1)/(Nb*(delta_eta)^2);
       end
ds = [dw';dtheta';dH']; %collect output in vector ds
%%%%%%%%%%%%%%%%%%%%%%%%%%%%%%%%%%%%%%%%%%%%%%%%%%%%
%SCRIPT file to run the ODE simulation for x->y->z->m
 %close all
 clear all
```

```
clc
%global c,global i;
%c=['k: ';'r  ';'k--';'k  '];
c=['k--';'r--';'b--';'g--'];
Pr = 6.2; %model parameter
Ec=1; %model parameter
Nb=0.1; %brownian motion parametr
Nt=0.1;%thermophorsis parametr
Sc=1;
Re=2;
G=1;
beta=0.1;
Bi=1;
%%%%%%%%%%%%%%%%%%%%%% loop for varying parameter
% Re1=linspace(1,2,3);
%   for i=1:length(Re1);
% Re=Re1(i);
tspan = 0:0.01:5;%time interval
 delta_eta=0.005;
 n=1/delta_eta-1;
eta=delta_eta:delta_eta:1-delta_eta;
 s0 =[zeros(1,n),zeros(1,n),ones(1,n)];%initial values
%%%%%%%%%%%%%%%%%%%%%%%%%%%%%%%%
[t,s] = ode15s(@ode_sys1,tspan,s0,[],delta_eta,Pr,
               Ec,n,G,Nb,Nt,Re,Sc,eta,beta,Bi);
 w1=s(:,1:n);
 theta1=s(:,n+1:2*n);
 H1=s(:,2*n+1:3*n);
 %%%%%%%%%%%%%%%%%%%%%%%%%%%%%%%%%%%%%%%%%%%%%%%%%%%%%
 %skin friction and Nusselt number
 Bi=linspace(1,10);
 sk=skin(Bi,beta,w1,theta1,delta_eta,t);
 plot(Bi,sk)
  figure
```

```
    Nu=nusselt(Bi,theta1,t);
    [ETA,T]=meshgrid(eta,t');
% % %%%%%%%%%%%%%%%%%%%%%%%%%%%%%%%%%%%%%%%
%velocity profiles against time
 figure
plot(t,w1(:,0.1*(n+1)),c(1),'LineWidth',2)
hold
plot(t,w1(:,0.3*(n+1)),c(2),'LineWidth',2)
plot(t,w1(:,0.5*(n+1)),c(3),'LineWidth',2)
plot(t,w1(:,0.7*(n+1)),c(4),'LineWidth',2)
% %title('Solution Curves for the Model')
 ylabel('Velocity ( W )')
 xlabel('Time ( t )')
 %Temperature profiles against time
figure
plot(t,theta1(:,0.1*(n+1)),c(1),'LineWidth',2)
hold
plot(t,theta1(:,0.3*(n+1)),c(2),'LineWidth',2)
plot(t,theta1(:,0.5*(n+1)),c(3),'LineWidth',2)
plot(t,theta1(:,0.7*(n+1)),c(4),'LineWidth',2)
 ylabel('Temperature ( \theta )')
 xlabel('Time ( t )')
%Nanoparticles Concentration profiles against time
figure
plot(t,H1(:,0.1*(n+1)),c(1),'LineWidth',2)
hold
plot(t,H1(:,0.3*(n+1)),c(2),'LineWidth',2)
plot(t,H1(:,0.5*(n+1)),c(3),'LineWidth',2)
plot(t,H1(:,0.7*(n+1)),c(4),'LineWidth',2)
%title('Solution Curves for the Model')
 ylabel('Concentration ( H )')
 xlabel('Time ( t )')
% % %%%%%%%%%%%%%%%%%%%%%%%%%%%%%%%%%%%%%%
%velocity profiles against radius
```

```
  figure
plot([eta,1],[w1(50,:),0],c(1),'LineWidth',2)
hold
plot([eta,1],[w1(100,:),0],c(2),'LineWidth',2)
plot([eta,1],[w1(150,:),0],c(3),'LineWidth',2)
plot([eta,1],[w1(200,:),0],c(4),'LineWidth',2)
% title('Solution Curves for the Model')
 ylabel('Velocity ( W )')
 xlabel('Distance ( \eta )')
%%%%%%%%%%%%%%%%%%%%%%%%%%%%%%%%%%%%%%%%%%%%%%%%%%%%
Temperature profiles against radius
figure
plot([eta],[theta1(50,:)],c(1),'LineWidth',2)
hold
plot([eta],[theta1(100,:)],c(2),'LineWidth',2)
plot([eta],[theta1(150,:)],c(3),'LineWidth',2)
plot([eta],[theta1(200,:)],c(4),'LineWidth',2)
 ylabel('Temperature ( \theta )')
 xlabel('Distance ( \eta )')

%%%%%%%%%%%%%%%%%%%%%%%%%%%%%%%%%%%%%%%%%%%%%%%%%%%%
%Nanoparticles concentration profiles against radius \eta
 figure
 plot(eta,H1(50,:),c(1),'LineWidth',2)
 hold
 plot(eta,H1(100,:),c(2),'LineWidth',2)
 plot(eta,H1(150,:),c(3),'LineWidth',2)
 plot(eta,H1(200,:),c(4),'LineWidth',2)
  %title('Solution Curves for the Model')
  ylabel('Concentration ( H )')
  xlabel('Distance ( \eta )')
%%%%%%%%%%%%%%%%%%%%%%%%%%%%%%%%%%%%%%%%%%%%%%%%%%%%
%plot([eta],[theta1(300,:)],c(i,:),'LineWidth',2)
%plot([eta],[w1(300,:)],c(i,:),'LineWidth',2)
```

```
% % % plot(t,H1(:,0.6*(n+1)),c(i:i),'LineWidth',2)
% plot(eta,H1(300,:),c(i,:),'LineWidth',2)
%   hold on
%pause
%   end
%   ylabel('Nanoparticles concentration (H)')
%   xlabel('Distance (\eta)')
```

Appendix D: MATLAB code for the model in chapter 5 (Method of line)

```
%function file
function ds = ode_sys1(t,s,delta_eta,Pr,Gr,n,A,Re,phi,Ec,
                       eta,beta,tau,b1,b2,b3,S,M,lambda)
% s the state vector
%output ds the derivative ds/dt at time t
w(1:n) = s(1:n); %for clarity & readability,
theta(1:n) = s(n+1:2*n);
for k=1:n
    if(k==1)
        W1=w(k);
        THETA1=theta(k);
              W2=w(k+1);
        THETA2=theta(k+1);
         elseif(k==n)
            W2= lambda*w(k)*exp(-beta)./(lambda*exp(-beta)
               -delta_eta*(1-phi)^(2.5));
   THETA2=1;
         W1=w(k-1);
        THETA1=theta(k-1);
          else
    W1=w(k-1);
    THETA1=theta(k-1);
       W2=w(k+1);
```

```
    THETA2=theta(k+1);
     end
dw(k)=-Re*(W2-W1)/(2*delta_eta)+
       b1*A+b1*exp(-beta*theta(k))/(1-phi)^(2.5)*((W2-2*w(k)
       +W1)/delta_eta^2+1/eta(k)*(W2-W1)/(2*delta_eta)
       -beta*(W2-W1)*(THETA2-THETA1)/(4*delta_eta^2))
       +b2*Gr*theta(k)-S*b1*(1-phi)^(-2.5)*exp(-beta*theta(k))*w(k)
       -M*Re*b1*(w(k))^2;

dtheta(k)=-Re*(THETA2-THETA1)/(2*delta_eta)
        +b3/(Pr*(1-phi+phi*tau))*((1/(eta(k)*2*delta_eta)
        *(THETA2-THETA1))+(THETA2-2*theta(k)+THETA1)/delta_eta^2)
         +Ec*exp(-beta*theta(k))/((1-phi)^(2.5)*(1-phi+phi*tau))
         *((W2-W1)/(2*delta_eta))^2
         +Ec*S*exp(-beta*theta(k))*((1-phi)^(2.5)
         *(1-phi+phi*tau))^(-1)*w(k)^2
         +M*Re*Ec*(1-phi+phi*tau)^(-1)*(w(k))^3;
end
ds = [dw';dtheta']; %collect the output in vector ds
%SCRIPT file to run the ODE simulation (chapter 5)
%  close all
%  clear all
% clc
c=['k';'r';'b';'g'];
%c=['k-.';'r-.';'b-.';'g-.'];
Pr = 6.2; %model parameter
A=1;
Gr=0.1;
beta=0.5;
Re=2;
phi=0.3;
Ec=1;
S=0.5;
M=10;
```

```
Bi=0;
lambda=0.5;
% copper
% ks=401; %thermal conductivity of copper
% rho_s=8933; %copper
% cp_s=385; %cu
%  gama_s=1.67e-5; %copper
%sigma_s=59.6e+6;-
%aluminium
% %%%%%%%%%%%%%%%%%%%%%%%%%Aluminium
ks=40; %thermal conductivity of Aluminium
rho_s= 3970; %aluminium
cp_s=765;%aluminium
gama_s=0.85e-5; %aluminium
sigma_s=35e+6;
% %%%%%%%%%%%%%%%%%%%%5
kf=0.613; %thermal conductivity of water
rho_f=997.1;%density of water
cp_f=4179;%water
gama_f=210e-6;%volumetric expansion coeffient/K
%sigma_f=5.5e-6;
tau=(rho_s*cp_s)/(rho_f*cp_f);
b1=rho_f/((1-phi)*rho_f+phi*rho_s);
b2=1-phi+phi*gama_s/gama_f;
b3=((ks+2*kf)-2*phi*(kf-ks))/((ks+2*kf)+phi*(kf-ks));
%b4=1-phi+phi*sigma_s/sigma_f;
% %%%%%%%%%%%%%%%%%%%%%%%%%%%%%%
tspan = 0:0.01:15; %time interval
% S1=linspace(1,4,4);
%  %Nu=zeros(length(tspan),length(S1));
%   for i=1:length(S1);
% S= S1(i);
  delta_eta=0.005;
 n=1/delta_eta-1;
```

```
eta=delta_eta:delta_eta:1-delta_eta;
 s0 = [zeros(1,n),zeros(1,n)]; %initial values
[t,s] = ode15s(@ode_sys1,tspan,s0,[],delta_eta,Pr,Gr,n,A,Re,phi,
              Ec,eta,beta,tau,b1,b2,b3,S,M,lambda);
 w1=s(:,1:n);
 theta1=s(:,n+1:2*n);
eta=[0 eta 1];
% w1=[w1(:,1) w1 zeros(size(w1,1),1)];
 w1=[w1(:,1) w1 lambda*w1(:,end-1).*exp(-beta*theta1(:,end))
  ./(lambda*exp(-beta*theta1(:,end))-delta_eta*(1-phi)^(2.5))];

theta1=[theta1(:,1) theta1 ones(length(t),1)];
%theta1=[theta1(:,1) theta1 (theta1(:,end)
         +Bi*delta_eta)/(1+Bi*delta_eta)];
% %%%%%%%%%%%%%%%%%%%%%%%%%%%%%%%%%%%%%%%%%%%%
 figure
   plot(t,w1(:,0.1*(n+1)),'c','LineWidth',2)
  hold on
 plot(t,w1(:,0.5*(n+1)),'y','LineWidth',2)
 plot(t,w1(:,0.6*(n+1)),'r','LineWidth',2)
 plot(t,w1(:,0.7*(n+1)),'b','LineWidth',2)
 plot(t,w1(:,0.8*(n+1)),'k','LineWidth',2)
  plot(t,w1(:,0.9*(n+1)),'g','LineWidth',2)
  ylabel('Velocity ( W )')
  xlabel('Time ( t )')
% figure
% plot(t,theta1(:,0.1*(n+1)),'c','LineWidth',2)
% hold on
% plot(t,theta1(:,0.5*(n+1)),'y','LineWidth',2)
% plot(t,theta1(:,0.6*(n+1)),'r','LineWidth',2)
% plot(t,theta1(:,0.7*(n+1)),'b','LineWidth',2)
% plot(t,theta1(:,0.8*(n+1)),'k','LineWidth',2)
% plot(t,theta1(:,0.9*(n+1)),'g','LineWidth',2)
%  ylabel('Temperature ( \theta )')
```

```
%  xlabel('Time ( t )')
%%%%%%%%%%%%%%%%%%%%%%%%%%%%%%%%%%%%%%%%
figure
plot(eta,w1(10,:),'k','LineWidth',2)%
 hold on
plot(eta,w1(50,:),'b','LineWidth',2)
plot(eta,w1(200,:),'r--','LineWidth',2)
plot(eta,w1(300,:),'y','LineWidth',2)
 plot(eta,w1(end,:),'r','LineWidth',2)
 ylabel('Velocity ( W )')
 xlabel('Distance ( \eta )')
%%%%%%%%%%%%%%%%%%%%%%%%%%%%%%%%%%%%%%%%
 figure
 plot(eta,theta1(100,:),'k--','LineWidth',2)
 hold on
 plot(eta,theta1(200,:),'b--','LineWidth',2)
 plot(eta,theta1(500,:),'c','LineWidth',2)
 plot(eta,theta1(1400,:),'y--','LineWidth',2)
 plot(eta,theta1(end,:),'r--','LineWidth',2)
%  ylabel('Temperature ( \theta )')
%  xlabel('Distance ( \eta )')
%%%%%%%%%%%%%%%%%%%%%%%%%%%%
% hold on
% plot(eta,theta1(end,:),c(i,:),'LineWidth',2.5)
% %plot(eta,w1(end,:),c(i,:),'LineWidth',2.5)
%
% % % % % % % % %pause
% ylabel('\theta ')
% %ylabel('W')
% xlabel('\eta')
%   end

     %legend('Re=-2','Re=0','Re=2')
Skin friction and Nusselt number
```

```
% sk(:,i)=-(1-phi)^-(2.5)*(w1(:,end)-w1(:,end-1))/delta_eta;
 Nu(:,i)=-b3*(theta1(:,end)-theta1(:,end-1))/delta_eta;
   % end
% hold on
% plot(lambda1,sk(end,:),'b')
% % %plot(t,sk(:,end),'r--')
%  xlim([0.5 1])
%  ylabel('C_f ')
% %  %xlabel('$\varphi$','Interpreter','Latex')
%  xlabel('\lambda')
%plot(t,sk(:,end),'k--')
% figure
% plot(lambda1,Nu(end,:),'k:')
% %   plot(t,Nu(:,end),'r--')
% xlim([0.5 1])
% % % % % % % % plot(Gr1,Nu,'k')
%  ylabel('Nu ')
% % xlabel('$\varphi$','Interpreter','Latex')

%plot(eta,w1(end,:),'LineWidth',2)
```